Politecnico di Torino

Corso di Laurea Magistrale in Ingegneria Civile

Tesi di Laurea Magistrale

Development of a Rheological Testing Protocol for the Cement Paste

Candidato:
Karina Mylena Lopes Rodrigues

Relatori:
Davide Dalmazzo
Ezio Santagata
Eldho Choorackal

Anno accademico 2019/2020

Acknowledgements

Firstly, I would like to thank my supervisor, Davide Dalmazzo, for his guidance through each stage of the process. I wish to express my sincere appreciation also to my co-supervisors Ezio Santagata and Eldho Choorackal for helping me and for inspiring my interest in the development of innovative technologies. Without all their persistent help, the goal of this project would not have been accomplished.

I would like to thank the whole Department of Environment, Land and Infrastructure Engineering for the opportunity to develop my master's thesis in the area I appreciate and with all the support, specially from Riccardo Rabezzana, which successful guided me during the laboratory experiments.

I would like to thank to the great classmates that became the greatest friends, Alexandre and Larissa, it was essential their presence and support both academically and personally, which was a blessing sharing this experience with and I do not imagine my graduate journey without them.

I would like to thank to the amazing people who became friends along the way in Turin, specially Marcos, Alessandra, Natália, Guilherme, Daria, Laura, Johnny, Rodrigo, Fabrizio, Felipe, Carolina, Tiago, Arthur, Victor, Rodrigo, Karen, Benedetta, Alberto, Luis, Matthias and Mateo. They supported, inspired, and taught me in many different ways. Studying abroad is not easy, but becomes definitely better when you have such great people by your side to share good memories with.

I would like to thank the support of my good friends Laura, Bruno, André, Vitória, and Bernardo that, even in different cities, were always a message away, proving me that no matter how far we are, true friendships never die.

I would like to thank to my grandparents, Valmir and Nancy that are actively present in my life encouraging me to pursuit my dreams, to my father Dirceu, my grandmother Maria Aparecida and my aunt Lucélia for cheering for my success with all their love.

Finally, but not last, I wish to acknowledge the physical and psychological support and great love of my family, that are the biggest blessing of God in my life, my mother Lucelene, my father Paulo, and my sisters Maria Eduarda and Sophia. They kept their presence and transmit their love even from far away, they taught me everything, specially to be strong, and it was crucial to keep me going. This work would not have been possible without their input, this achievement is dedicated to them.

Abstract

This work develops and analyzes the outcome of several practical experiments in order to propose a protocol to measure cement paste properties in a parallel plate rheometer. The observed parameters are: the shear rate, the shear stress, the viscosity and the density.

The protocol was developed considering preparation of the cement paste, preservation of the mixture, interval of measurement and shear rate sequence. The rheometer employed was an Anton-Paar rheometer model MCR301 pared with the cross-hatched stainless-steel parallel plates PP25 P2, the preparation protocol of the samples was based on the standard ASTM C305, and the density of the mixture was measured by the procedure UNI EN 1097-7: 2000.

The obtained result of each experiment was compared to the theoretical Bingham model for the confirmation of the cement paste as a Bingham fluid, taking into the consideration the relation among shear stress, dynamic yield stress, plastic viscosity, and shear rate. As the outcome of those experiments we propose a protocol that can be applied to measurement of cement paste rheology properties allowing the reproducibility of the measurements for virtually any cement paste mixture.

Acknowledgements 3
Abstract 4
List of Figures 7
List of Tables 9
1. Introduction 11
1.1. Objectives 11
1.2. Document Structure 11
2. Properties of Fresh Concrete and Cement Paste 13
2.1. Concepts related to rheology 14
2.2. Hypothesis adopted in the rheometric experiments 18
2.3. Thixotropic and structural build-up/breakdown behavior of cement-based materials 20
2.4. Literature review on rheometer testing protocols 22
3. Materials and Methods 25
3.1. Raw material 25
3.2. Preparation of samples 26
3.3. Test and measuring equipment 28
3.4. Measurement protocols 31
3.5. Summary of icons 38
4. Experimental Investigation 39
4.1. Experiment A 39
4.2. Experiment B 40
4.3. Experiment C 41
4.4. Experiment D 41
4.5. Experiment E 42
4.6. Experiment F 42
5. Results and Discussion 44
5.1. Experiment A 44
5.2. Experiment B 47
5.3. Experiment C 52
5.4. Experiment D 56
5.5. Experiment E 62
5.6. Experiment F 68

5.7.Comparison Between Preservation Methods 77
5.7.1.Experiments A and B 78
5.7.2.Experiments C and D 79
5.7.3.Experiments E and F 81
6. Proposed Standard Protocol 83
6.1.Raw material 83
6.2.Preparation of samples 83
6.3.Preservation technique 83
6.4.Time stamps 84
6.5.Test and measuring equipment 84
6.6.Measurement protocols 84
6.7.Footprint measurement 86
7. Conclusion 87
8. References 89
A. Annex - Numerical Results for Experiment A 91
B. Annex - Numerical Results for Experiment B 97
C. Annex - Numerical Results for Experiment C 103
D. Annex - Numerical Results for Experiment D 107
E. Annex - Numerical Results for Experiment E 112
F. Annex - Numerical Results for Experiment F 118

List of Figures

Fig. 2.1. Dispersion of compacted powder particles due to excess water (Sheinn et al., 2002). 13
Fig. 2.2. Rheometer parallel plate configuration compared to concrete (Ferraris & Gaidis, 1992). 15
Fig. 2.3. Rheometers configurations (Roussel, 2012, apud Coussot, 2005 and Rojas, 2013). 17
Fig. 2.4. Velocity profile with wall slip between parallel-plates. (Himmel & Wagner, 2013 apud Yoshimura and Prud'homme, 1988). 19
Fig. 2.5. Edge fracture in the parallel-plate rheometer. (Keentok & Xue, 1999). 19
Fig. 2.6. Coagulation by VT, (b) dispersion by agitation (c) re-coagulation by VT. (Wallevik, 2020, apud Wallevik, 2003). 21
Fig. 2.7. Tattersall & Banfill hypothesis of the mechanism of structural breakdown. (Wallevik, 2020, apud Wallevik, 2011). 21
Fig. 2.8. Hypothesis of the mechanism of structural breakdown. (Wallevik, 2020, apud Wallevik, 2011). 22
Fig. 3.1. Automatic sieve employed in the experiments (< 63 μm). 25
Fig. 3.2. Automatic mixing employed in the experiments. 26
Fig. 3.3. Sample preparation process. 27
Fig. 3.4. Rheometer employed in this work. 28
Fig. 3.5. Rheometer's cross-hatched stainless-steel parallel plates PP25 P2 with s = 1 mm and 29
d = 0.5 mm. 29
Fig. 3.6. Two different syringes employed in the experiments (5ml and 50ml). 30
Fig. 3.7. Batch isolated with wetted paper. 30
Fig. 3.8. Hood and closed switch for the air circulation of the hood. 31
Fig. 3.9. Shear sequence S1 strain rates variation. 32
Fig. 3.10. Shear sequence S2 strain rates variation. 33
Fig. 3.11. Shear sequence S3 strain rates variation. 34
Fig. 3.12. Piknometers used to cement paste density measures. 36
Fig. 3.13. Piknometers used to density measures of degassed cement pastes and the depressurizer equipment. 37
Fig. 3.14. Icons employed in this document to represent the options of experiment protocols. 38
Fig. 4.1. Timeline for Experiment A. 40
Fig. 4.2. Timelines for Experiment B. 40
Fig. 4.3. Timeline of Experiment C. 41
Fig. 4.4. Timeline of Experiment D. 42
Fig. 4.5. Timeline of Experiment E. 42
Fig. 4.6. Timeline of Experiment F. 43
Fig. 5.1. Shear stress for both runs of Experiment A. 44
Fig. 5.2. Flow curves (shear rate and shear stress ratio) for second run of Experiment A. 45
Fig. 5.3. Flow curve (shear rate and shear stress ratio) with Bingham model for second run of Experiment A at the 5 min time stamp. 46
Fig. 5.4. Shear stress for both runs of Experiment B. 47
Fig. 5.5. Flow curves (shear rate and shear stress ratio) for time stamps 5, 20, and 35 mins of the second run of Experiment B. 48
Fig. 5.6. Flow curve (shear rate and shear stress ratio) for time stamp 5 min of the second run of Experiment B and the Bingham model prediction. 49
Fig. 5.7. Flow curve (shear rate and shear stress ratio) for time stamp 50 min of the second run of Experiment B. 50
Fig. 5.8. Samples at the rheometer just after the testing. At left: at 5 min time stamp; At right: at 50 min time stamp. 50
Fig. 5.9. Shear rate and viscosity over time for both runs of Experiment B. 51
Fig. 5.10. Shear stress for Experiment C. 52
Fig. 5.11. Flow curves (shear rate and shear stress ratio) for Experiment C. 53
Fig. 5.12. Viscosity over shear rate for Experiment C. 54
Fig. 5.13. Shear rate and viscosity over time for Experiment C. 55

Fig. 5.14. Shear stress for Experiment D. 57
Fig. 5.15. Flow curves (shear rate and shear stress ratio) for Experiment D. 58
Fig. 5.16. Viscosity over shear rate for Experiment D. 59
Fig. 5.17. Shear rate and viscosity over time for Experiment D. 60
Fig. 5.18. Quantity of water paste footprint results for Experiment D. 61
Fig. 5.19. Shear stress for Experiment E. 62
Fig. 5.20. Flow curves (shear rate and shear stress ratio) for Experiment E. 63
Fig. 5.21. Viscosity over shear rate for Experiment E. 64
Fig. 5.22. Shear rate and viscosity over time for Experiment E. 65
Fig. 5.23. Quantity of water paste footprint results for Experiment E. 67
Fig. 5.24. Shear stress for both runs of Experiment F. 68
Fig. 5.25. Flow curves (shear rate and shear stress ratio) for both runs of Experiment F. 70
Fig. 5.26. Viscosity over shear rate for both runs of Experiment F. 71
Fig. 5.27. Shear rate and viscosity over time for both runs of Experiment F. 74
Fig. 5.28. Quantity of water paste footprint results for both runs of Experiment F. 76
Fig. 5.29. Shear stress for Experiments A and B at 5, 20, 35, and 50 mins time stamps. 79
Fig. 5.30. Shear stress for Experiments C and D at 5, 20, 40, and 60 mins time stamps. 80
Fig. 5.31. Shear stress for Experiment D at 80 mins time stamp. 80
Fig. 5.32. Shear stress for Experiments E and F at 5, 20, 40, and 60 mins time stamp. 81
Fig. 5.33. Shear stress for Experiments E and F at 80 mins time stamps. 82
Fig. 6.1. Procedure for sample preparation. 83
Fig. 6.2. Proposed shear sequence (S3) strain rates variation. 84
Fig. A.1. Shear stress for both runs of Experiment A. 91
Fig. A.2. Flow curves (shear rate and shear stress ratio) for both runs of Experiment A. 93
Fig. A.3. Viscosity over shear rate for both runs of Experiment A. 94
Fig. A.4. Shear rate and viscosity over time for both runs of Experiment A. 96
Fig. B.1. Shear stress for both runs of Experiment B. 97
Fig. B.2. Flow curves (shear rate and shear stress ratio) for both runs of Experiment B. 99
Fig. B.3. Viscosity over shear rate for both runs of Experiment B. 100
Fig. B.4. Shear rate and viscosity over time for both runs of Experiment B. 102
Fig. C.1. Shear stress for Experiment C. 103
Fig. C.2. Flow curves (shear rate and shear stress ratio) for Experiment C. 104
Fig. C.3. Viscosity over shear rate for Experiment C. 105
Fig. C.4. Shear rate and viscosity over time for Experiment C. 106
Fig. D.1. Shear stress for Experiment D. 107
Fig. D.2. Flow curves (shear rate and shear stress ratio) for Experiment D. 108
Fig. D.3. Viscosity over shear rate for Experiment D. 109
Fig. D.4. Shear rate and viscosity over time for Experiment D. 110
Fig. D.5. Paste footprint results for Experiment D. 111
Fig. E.1. Shear stress for Experiment E. 112
Fig. E.2. Flow curves (shear rate and shear stress ratio) for Experiment E. 113
Fig. E.3. Viscosity over shear rate for Experiment E. 114
Fig. E.4. Shear rate and viscosity over time for Experiment E. 115
Fig. E.5. Paste footprint results for Experiment E. 116
Fig. F.1. Shear stress for both runs of Experiment F. 118
Fig. F.2. Flow curves (shear rate and shear stress ratio) for both runs of Experiment F. 120
Fig. F.3. Viscosity over shear rate for both runs of Experiment F. 122
Fig. F.4. Shear rate and viscosity over time for both runs of Experiment F. 123
Fig. F.5. Paste footprint results for both runs of Experiment F. 126

List of Tables

Tab. 2.1. Summary of literature similar experimental works. 23
Tab. 3.1. Shear sequence S1 timeline and values - 360 seconds. 33
Tab. 3.2. Shear sequence S2 timeline and values - 225 seconds. 34
Tab. 3.3. Shear sequence S3 timeline and values - 555 seconds. 35
Tab. 4.1. Summary of experiments executed. 39
Tab. 5.1. Shear stress steady state for both runs of Experiment A. 45
Tab. 5.2. Numerical values of Bingham model for both runs of Experiment A. 46
Tab. 5.3. Shear stress steady state for both runs of Experiment B. 48
Tab. 5.4. Numerical values of Bingham model for both runs of Experiment B. 49
Tab. 5.5. Shear stress steady state for Experiment C. 53
Tab. 5.6. Numerical values of Bingham model for Experiment C. 54
Tab. 5.7. Viscosity over shear rate values for Experiment C. 54
Tab. 5.8. Shear rate and apparent viscosity over time values for Experiment C. 56
Tab. 5.9. Shear stress steady state for Experiment D. 57
Tab. 5.10. Numerical values of Bingham model for Experiment D. 58
Tab. 5.11. Viscosity over shear rate values for Experiment D. 59
Tab. 5.12. Shear rate and apparent viscosity over time values for Experiment D. 60
Tab. 5.13. Paste footprint values for Experiment D. 61
Tab. 5.14. Shear stress steady state for Experiment E. 63
Tab. 5.15. Numerical values of Bingham model for Experiment E. 64
Tab. 5.16. Viscosity over shear rate values for Experiment E. 64
Tab. 5.17. Shear rate and apparent viscosity over time values for Experiment E. 65
Tab. 5.18. Paste footprint values for Experiment E. 67
Tab. 5.19. Shear stress steady state for both runs of Experiment F. 69
Tab. 5.20. Numerical values of Bingham model for both runs of Experiment F. 69
Tab. 5.21. Viscosity over shear rate values for both runs of Experiment F. 72
Tab. 5.22. Shear rate and apparent viscosity over time values for both runs of Experiment F. 72
Tab. 5.23. Paste footprint values for both runs of Experiment F. 75
Tab. 5.24. Shear stress steady state for Experiments A to F. 78
Tab. 6.1. Proposed shear sequence (S3) timeline and values - 555 seconds. 85
Tab. A1. Shear stress steady state for both runs of Experiment A. 92
Tab. A.2. Numerical values of Bingham model for both runs of Experiment A. 92
Tab. A.3. Viscosity over shear rate values for both runs of Experiment A. 94
Tab. A.4. Shear rate and apparent viscosity over time values for both runs of Experiment A. 95
Tab. B.1. Shear stress steady state for both runs of Experiment B. 98
Tab. B.2. Numerical values of Bingham model for both runs of Experiment B. 98
Tab. B.3. Viscosity over shear rate values for both runs of Experiment B. 100
Tab. B.4. Shear rate and apparent viscosity over time values for both runs of Experiment B. 101
Tab. C.1. Shear stress steady state for Experiment C. 103
Tab. C.2. Numerical values of Bingham model for Experiment C. 104
Tab. C.3. Viscosity over shear rate values for Experiment C. 105
Tab. C.4. Shear rate and apparent viscosity over time values for Experiment C. 106
Tab. D.1. Shear stress steady state for Experiment D. 107
Tab. D.2. Numerical values of Bingham model for Experiment D. 108
Tab. D.3. Viscosity over shear rate values for Experiment D. 109
Tab. D.4. Shear rate and apparent viscosity over time values for Experiment D. 110
Tab. D.5. Paste footprint values for Experiment D. 111
Tab. E.1. Shear stress steady state for Experiment E. 112
Tab. E.2. Numerical values of Bingham model for Experiment E. 113
Tab. E.3. Viscosity over shear rate values for Experiment E. 114
Tab. E.4. Shear rate and apparent viscosity over time values for Experiment E. 115

Tab. E.5. Paste footprint values for Experiment E. 117
Tab. F.1. Shear stress steady state for both runs of Experiment F. 119
Tab. F.2. Numerical values of Bingham model for both runs of Experiment F. 121
Tab. F.3. Viscosity over shear rate values for both runs of Experiment F. 121
Tab. F.4. Shear rate and apparent viscosity over time values for both runs of Experiment F. 123
Tab. F.5. Paste footprint values for both runs of Experiment F. 125

1. Introduction

Rheological measurements on cement pastes are influenced by intrinsic factors such as the raw materials, water/cement ratio, presence of admixtures, air void content, and also by external conditions such as mixing procedure, stress history and environmental conditions. On the mixing procedure the velocity of shear mixing and time taking for the mixing are included in the influencing factors. For the environmental conditions we can also cite humidity, temperature and air circulation. Besides, chemical reactions that occurs on the cement paste associated with the drying and curing phase of such filler pastes and wall slip effects also deserves attention.

Such variability often prevents the appropriate rheological measurement of cement paste in laboratory. In fact, the use of rheometers becomes challenging because of a lack of proper testing protocol. It is primordial to reduce the variability in test results, and for this goal a primary importance has to be given to the definition of a standard protocol that take into account all these factors.

1.1. Objectives

Given the importance of appropriate rheological measurement of cement paste in laboratory, this thesis main objective is the definition of standard protocol for our lab to test cement paste materials (selection of the measuring system as a function of the material's consistency). In order to achieve such main objective, this thesis intermediate objectives are:

1. To propose and compare a series of sample preparation and preservation techniques;
2. To propose a series of measurement techniques to get information about rheological behavior and physical properties;
3. To perform a series of practical experiments combining sample preparation and preservation techniques, with measurement techniques in order to discover the appropriate way to perform reliable and reproducible tests.

In order to go from the intermediate objectives towards the main objective it is also necessary to evaluate the effect of air voids, density of the sample and water content in the rheological response by testing specimens measuring this properties. However, the more important step is to propose a standard protocol through the comparison of the results obtained in each experiment with theoretical models, and performing successive experiments.

1.2. Document Structure

This thesis is organized as follows:

- Chapter 2 presents basic definitions on the domain of fresh concrete and cement paste, as well as its rheological properties, including related works;
- Chapter 3 presents the common definitions employed in this work concerning equipments, procedures, and techniques to the preparation, preservation, measurement, and analysis of rheological properties of cement paste mixtures;
- Chapter 4 presents the detailed description of the six experiments of rheological properties measurement conducted in this thesis;

- Chapter 5 presents the more relevant results for the conducted experiments, as well as the analysis of each experiment leading to the proposition of new experiments (full results are attached in the annexes);
- Chapter 6 details the proposed standard protocol to perform the measurement of rheological properties of cement paste samples considering the more successful experiment steps analyzed in Chapter 5;
- The conclusion, Chapter 7, summarizes this thesis contribution and proposes future works to the advances already obtained by the experiments and analysis conducted in this thesis.

2. Properties of Fresh Concrete and Cement Paste

This chapter presents basic concepts for properties of fresh concrete and cement paste, including rheology. Those concepts are necessary to fully understand the scientific contribution of this work.

The concrete is made up of the components: cement, fine aggregates, coarse aggregates and water. It is a worldwide material used in the construction due to its structural properties. Concrete is a concentrated suspension of solid particles, the aggregates, in a viscous non-homogeneous liquid, the cement paste.

The concrete's fresh state is characterized by its workability since the concrete industry has recognized the need to monitor concrete workability to ensure that concrete can be properly placed and can achieve adequate hardened strength (after setting) (Koehler and Fowler, 2003).

This recognition were made by Abrams in the 1920s, when he established the eponymous rule that the strength of hardened concrete is inversely proportional to the water/cement ratio, thus showing that the higher water contents needed to give more easily workable concrete had a negative effect on strength. This is a result of the pore space left behind by the consumption of water during hydration of the cement: the higher the water content the higher the porosity and the lower the strength (Figure 2.1). Controlling workability therefore helps to control strength and other hardened properties. Without satisfactory fresh properties it is unlikely that the desirable properties of the hardened materials can be achieved (Banfill, 1991).

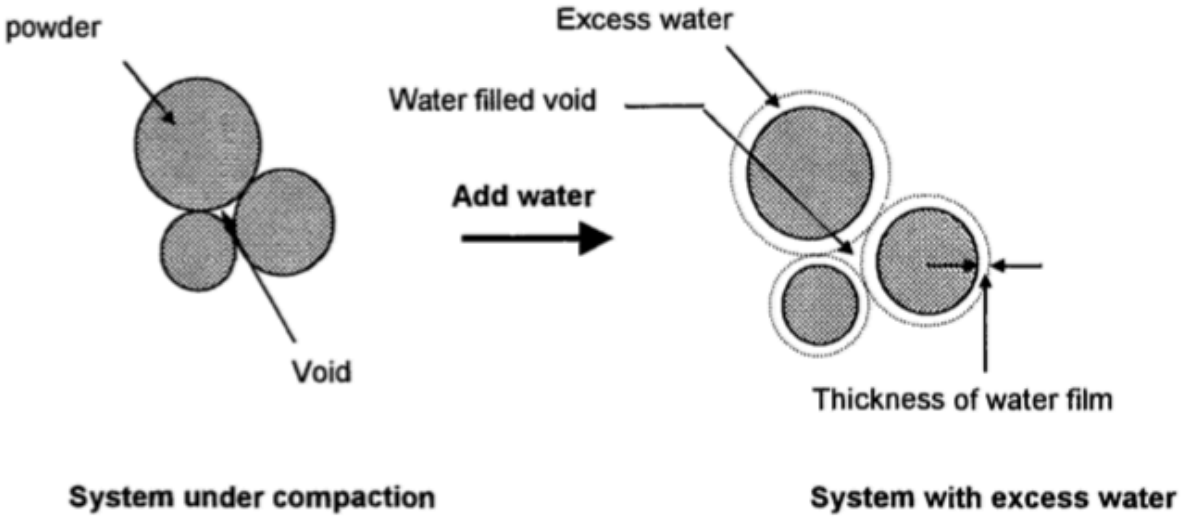

Fig. 2.1. Dispersion of compacted powder particles due to excess water (Sheinn et al., 2002).

The high-performance concrete mixes, the Flowable cement-based mixtures such as Self Compacting Concrete (SCC) and Controlled Low Strength Materials (CLSM) are gaining popularity in the construction sector. They are susceptible to small changes in mix proportions, which makes the monitoring of the workability even more important.

Institutes and associations around the world have described the term “workability" as follows:

- The American Concrete Institute (ACI 116R-00, 73) considers workability “that property of freshly mixed concrete or mortar that determines the ease with which it can be mixed, placed, consolidated, and finished to a homogenous condition.”.
- The Japanese Association of Concrete Engineers defines workability as “that property of freshly mixed concrete or mortar that determines the ease and homogeneity with which it can be mixed, placed, and compacted due to its consistency, the homogeneity with which it can be made into concrete, and the degree with which it can resist separation of materials.”.
- The American Society for Testing and Materials (ASTM) describes workability as "that property determining the effort required to manipulate a freshly mixed quantity of concrete with minimum loss of homogeneity.”.

The Slump test is widely used for the check of the workability of concrete in its plastic state, seeking to measure its consistency by the indication of the water content and evaluate if the sequent hardened strength of the concrete is suitable for the application destination.

Still, the concrete industry quickly realized the slump test’s inability to represent workability fully, and, within several years of the introduction of the slump test, several attempts were made to develop better, more complete tests (Powers,1968, apud Koehler and Fowler, 2003).

The rheological (flow) properties of concrete are important for the construction industry because concrete is usually put into place in its plastic form and, aside from measuring the flow of concrete, rheology is concerned with the prediction of the flow from the properties of the components or from the mix design (Ferraris, 1999).

Sant et al. (2008), showed that not only the rheological properties of fresh concrete are dependent of the cement paste’s chemical interactions and cement hydration, but also of the shape and gradation of the aggregates contained in the mixture. On the other hand, the evolution of the concrete's properties at early ages depends strongly on the cement paste, and this evolution starts from the time the cement enters in contact with the water.

2.1. Concepts related to rheology

The rheological approach is a microstructure approach that has as main objective the formulation of mixes with adequate performance after its setting, at the hardened state, whose fresh rheological behavior be compatible with the application method employed.

This approach takes into account on how intrinsic and extrinsic factors, such as particle size, chemical composition, water content, incorporated air, additives, mixing condition, temperature, relative humidity, particle dispersion and phase separation influence on the rheology and on the performance of the concrete on its hardening state.

Ferraris & Gaidis (1992), studied the connection between the rheology of fresh concrete and of the cement paste, where they stated that the distance between the aggregate on the concrete depends on the cement paste volume content.

The cement paste acts as a lubricant between aggregates in concrete and affects strongly the concrete flow/workability as changes its w/c (water-cement ratio), presence of admixtures, or by the simply change in the paste volume, without changing its composition.

With that, they had defined that the measurement of paste rheology as a function of the gap between rotational parallel plates rheometer, that simulates the gap between aggregates (Figure 2.2), is a refined approach to predict concrete flow. They also pointed to the importance of the conditions of the experiment (as for example, the temperature, the shear rate and the mixing energy) for the rheological behavior of a material.

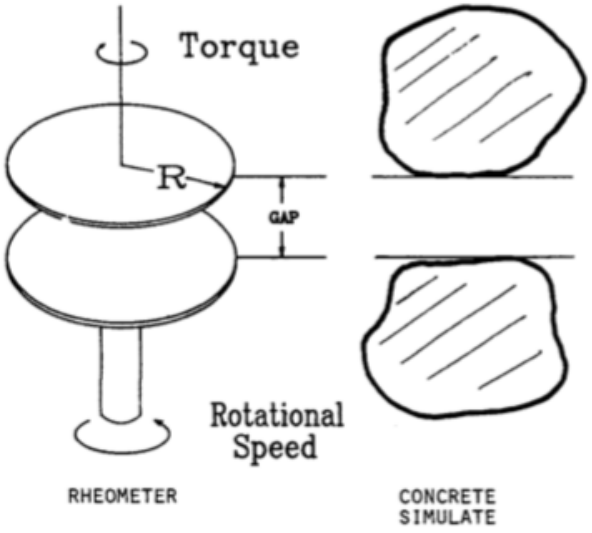

Fig. 2.2. Rheometer parallel plate configuration compared to concrete (Ferraris & Gaidis, 1992).

The cement-based materials were established as a Bingham fluid (Eq. 1), a material that can support shear stress without flowing, but flows at higher stresses. So, concrete flow curves have started to be measured in terms of shear stress and shear rate emerge in order to obtain yield stress and plastic viscosity. For a liquid, the plastic viscosity is the slope of the shear stress-shear rate plot and the yield stress is equal to the intersection point on the stress axis.

$$\text{Bingham: } \tau = \tau_0 + \mu\,\gamma \qquad \text{(Eq. 1)}$$

Where,

τ = shear stress (Pa)
τ_0 = dynamic yield stress (Pa)
μ = plastic viscosity (Pa.s)
γ = shear rate (1/s)

While the yield stress indicates the minimum stress that must be applied to deform fresh concrete immediately after shear, the stress needed to be applied for the material starts to flow. The plastic viscosity expresses the increase in stress required to provide a given shear rate, it is important, for example, to control the pumping rate and the ease of finishing of the concrete surface. At least, the shear rate describes the shearing effect the liquid experiences, it is the velocity gradient, dV/dH, a measure of the speed at which the intermediate layers move with respect to each other.

Banfill in 1991 has defined that the cement systems are yield stress fluid and the yield stress is a consequence of the inter particle forces, and links between particles are broken by shearing so the measured yield stress depends upon time and previous shear history.

Nevertheless, Banfill, in 1991, also stated that the self-compacting concrete, characterized by a very low yield stress has a change in the flow curve from Bingham to Herschel-Bulkley (Equation 2) type behavior, due to the use of the thickeners applied to prevent segregation that raise the viscosity of the water.

$$\text{Herschel-Bulkley} : \tau = \tau_0 + K\,\gamma^n \qquad \text{(Eq. 2)}$$

Where,

τ = shear stress (Pa)
τ_0 = dynamic yield stress (Pa)
K and n = material parameters
γ = shear rate (1/s)

Banfill, in 1991, also described that, however, in more highly engineered concrete, such as self-compacting concrete, rheology is paramount and the challenge is to design concrete mixes with a low yield stress and the difficulty with it is that the concrete is prone to segregation, with the fine matrix filtering through the coarse particles, and it is necessary to thicken the fine matrix. Various solutions have been tried, such as: very high powder contents using inert powders to minimize the cost and the generation of heat during hydration; water soluble thickeners to raise the viscosity of the water; entrained air bubbles; or a combination of these.

Seeking to establish a uniform and widely accepted nomenclature for concrete rheology, the National Institute of Standards and Technology (NIST) divided existing rheology test methods into four broad categories in terms of the type of flow produced during the test, tests that directly measure the flow properties of concrete (Hackley and Ferraris 2001):

- Confined Flow Tests: The material flows under its own weight or under an applied pressure through a narrow orifice.
- Free Flow Tests: The material either flows under its own weight, without any confinement or an object penetrates the material by gravitational settling.
- Vibration Tests: The material flows under the influence of applied vibration. The vibration is applied by using a vibrating table, dropping the base supporting the material, and external vibrator, or an internal vibrator.
- Rotational Rheometers: The material is sheared between two parallel surfaces, one or both which are rotating.

Rheometers are equipment used for the evaluation of rheological properties of fluids and suspensions, allowing the study of the viscosity and yield stress as function of, for example, time and temperature. While confined flow, free flow, and vibration test methods generally attempt to simulate field placement flow conditions, rotational rheometers attempt to apply the concepts of traditional rheometers to concrete and cement paste.

Generally, commercial rheometers are not suitable for materials with large particle size, such as concrete and mortar. The reason is that coarse granular materials pose difficulties in measurement. There are well-established rules for the sizes of apparatus and sample to ensure that rheological measurements are reliable, chiefly that any gap must be 10 times the size of the

largest particles and that in coaxial cylinders the ratio of outer to inner cylinder radius must be as near 1.0 as possible. Cement pastes are of course well within the capability of any of the wide range of laboratory bench top instruments available commercially. (Banfill, 1991).

On the cement-based rheometers, only a small sample is needed to perform the shear testing, which has simplified the assessment of the workability. Another positive point is to detect the origin of workability losses (structural build-up). Among various geometries of rheometers, the most used for cement pastes are parallel plate, cone and plate, and couette cell (coaxial cylinder and vane-in-cup) (Figure 2.3).

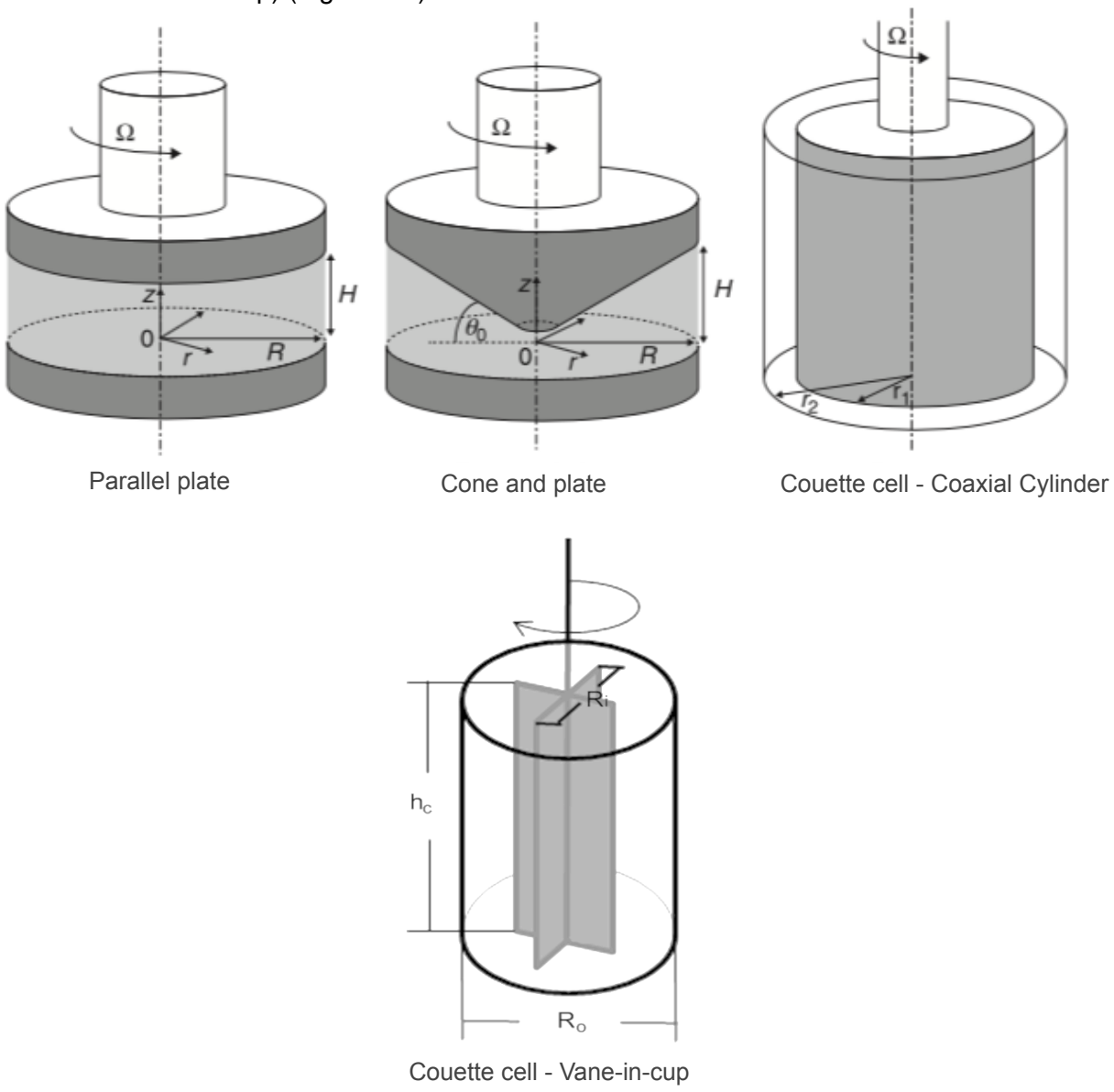

Fig. 2.3. Rheometers configurations (Roussel, 2012, apud Coussot, 2005 and Rojas, 2013).

Basically, the suspension rheometers are based or in torque or in shear. In the first case the torque, which is proportional to tension, is controlled and the resulting shear rate is evaluated; in the second case, the shear rate applied is controlled and the force required to achieve to this shear is recorded. Torque rheometers are suitable for evaluations where stress requirements

control material flow, while shear devices are best suited for evaluating rheological behavior at various flow rates.

The parallel plate geometry consists of two parallel plates separated by a gap, in which the sample is contained by surface tension (Feys et al., 2017 apud Macosko, 1994). The measurement consists of the upper plate rotating at a certain velocity and creating a torque, this way a shear is imposed. The cone and plate geometry is an alternative to the parallel plate, with a cone virtual tip touching the bottom plate, which is fixed. In these cases, the shear rate is heterogeneous and controlled and the shear stress is unknown (Roussel, 2012).

The couette cell - coaxial cylinder often consists of a static cylindrical cup and a concentric rotatable cylinder, or vice-versa (Feys et al., 2017 apud Macosko, 1994). Rotation and torque measurement are possible in this geometry. In the couette cell - vane-in-cup geometry, the vane replaces the coaxial cylinder inside of the cylindrical cup. As the number of the vane's blades increase, the circumferential polygon approaches the circle of the inner cylinder (Feys et al., 2017). These both cases have the shear rate is unknown and the shear stress is heterogeneous and controlled (Roussel, 2012).

2.2. Hypothesis adopted in the rheometric experiments

There are a large variety of configurations for cement rheometer experiments. These configurations include different geometries as concentric cylinder arrangements, parallel plate arrangements, and also different vane geometries were used by different researchers.

In order to avoid problems with the rheometric experiments, we have to pay attention to the hypothesis made computing the relation between shear rate and shear stress. It is important to ensure the cement paste to be homogenized before performing the flow curve tests to find out rheological parameters. Additionally, it is assumed a no-slip boundary condition and rough surfaces are usually employed to guarantee no wall slip in the experiments.

The wall slip in rheology experiments is a common problem encountered while testing highly concentrated emulsions or suspensions on a rheometer and this effects the measured viscosity, that can be significantly lower than the actual viscosity of the sample. The wall slip is an apparent discontinuity of the fluid velocity in proximity to a solid surface, the macroscopic velocity profile at a still solid surface attains a nonzero value, thus invalidating the no-slip boundary condition that is used when deriving the typical working equations in rheometry (Carotenuto et al, 2015).

A method to determine wall slip in rotational measurements between parallel-plates was presented by Yoshimura and Prud'homme in 1988, the scheme in Figure 2.4 shows the velocity profile between parallel-plates.

The parallel plates are separated by a distance H and the upper plate is moving with the angular velocity Ω. Considering wall slip, it is characterized by a velocity u_{slip} and the apparent shear rate $\dot{\gamma}_{app}$ at any radial position r is higher than the true shear rate $\dot{\gamma}$ applied to the sample.

To overcome wall slip effects in rotational rheometry, it is used to alter the sample gap, or apply a chemical or physical change on the surface properties of the geometry, as employs a roughed surface geometry which improve the contact between the sample and the geometry to reduce

slip. According to Catotenuto et al, the use of the roughed surface geometries intent to trap the particles of the material within the roughness, ensuring their constant concentration in the measurement cell and a true zero velocity at the “solid” surface.

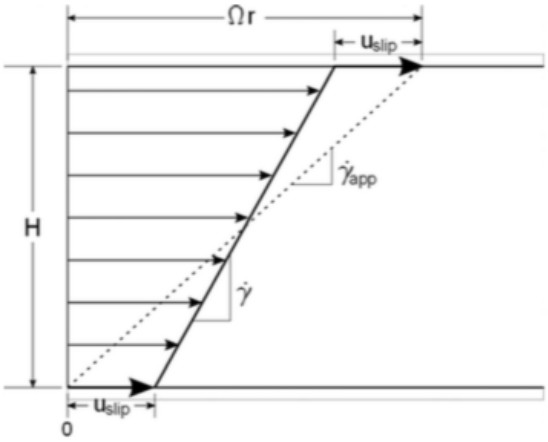

Fig. 2.4. Velocity profile with wall slip between parallel-plates. (Himmel & Wagner, 2013 apud Yoshimura and Prud’homme, 1988).

Another point we have to take into account to avoid wrong rheological measurements is the edge fracture, an instability that can occur on the parallel plate flow measurements of suspensions and viscoelastic liquids, which makes a limitation on the ability of making measurements with high shear rates.

The edge failure is characterized by the formation of a “crack" or indentation at a critical shear rate on the free surface of the liquid (Keentok & Xue, 1999). This phenomenon occurs on parallel plate during shearing, where at a critical rate of shear (function of the surface tension of the liquid and the fracture diameter), a crack or a surface distortion occurs at the free surface and this propagates into the interior of the sample.

The edge failure can be illustrated by Figure 2.5, where h is the gap width and R is the radius of the parallel plate rheometer, the upper plate is moving with the angular velocity/rate of rotation Ω and 2a is the edge fracture diameter.

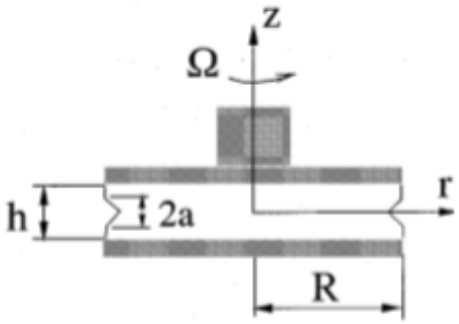

Fig. 2.5. Edge fracture in the parallel-plate rheometer. (Keentok & Xue, 1999).

Experiments show that the edge failure is dependent of the physical dimensions of the parallel plate, and there is a maximum gap width beyond which the sample flows out of the gap. Therefore, it may be possible to avoid edge fracture using narrower gap.

2.3. Thixotropic and structural build-up/breakdown behavior of cement-based materials

The cement paste is a thixotropic yield stress fluid, which means that its behavior depends on its flow history and the material flow starts when the applied stress exceed the yield stress. Depending on the applied shear rate or shear stress and the mixture proportioning, cement pastes can display shear thickening or shear thinning behavior.

This type of fluid requires a rigorous procedure to ensure reproducibility and to allow the prediction of the behavior at complex situations. Important characteristics of thixotropic materials are: dynamic yield stress, critical shear rate, steady state behavior, and characteristic time to reach steady state at simple situations.

In the liquid regime, thixotropy is observable by a progressive decrease of apparent viscosity in time while it is imposed a change on the level of shear rate. Furthermore, starting from the material at rest, the shear stress decreases when a fixed shear rate is imposed. These effects are due to the association of each shear rate level corresponding to a specific steady state structure, and it takes some time to be reached (Ovarlez, 2012).

According to Feys et al 2017, thixotropy is generally associated with a physicochemical phenomenon causing changes in shear stress at constant shear rate, or vice versa. Besides, if the build-up is reversible, a thixotropic behavior is observed. However, flocculation and hydration occur simultaneously, so the build-up or breakdown of the material is not a straightforward phenomena. Permanent changes in rheological properties with time are defined as workability loss and techniques and strategies may be employed to determine the thixotropy or structural build-up, combining thixotropy with workability loss.

The reversible effects, related to thixotropy (and so to colloidal interactions), would dominate the irreversible effects (permanent changes), related to the ridification of the C-S-H bridges, for the first hour of cement hydration time, while after one hour, the reversible and irreversible effects would co-contribute to the structural build-up of the cement paste.

There is an intrinsic physical rheological model called Particle Flow Interaction Theory (PFI theory) that indicates the combined process of thixotropic behavior and structural breakdown. These concepts were proposed by Hattori and Izumi and by Tattersall and Banfill. According to Wallevik (2020), the thixotropy behavior in this theory is related to the coagulation (flocculation), dispersion (de-flocculation) and re-coagulation of the cement particles. Figure 2.6 depicts the coagulation and dispersion processes considering the potential energy interaction (V_T) and the distance between particles (D_s). The flocculation/coagulation occurs when two or more cement particles are in contact for a certain time and a work is required to separate them. During the contact, the particles are glued together as a result of the total potential energy interaction (V_T) , as, for example, van der Waals attraction, electrostatic repulsion, and steric hindrance. The thixotropic breakdown is caused by agitation of the mixture defining the dispersion/de-flocculation.

The term structural breakdown was introduced by Tattersall in the 50's when it was realized that in a rheological experiment no recovery torque was measured and Tattersal and Banfill (Wallevik, 2020) attributed the structural breakdown to the process of breaking connections

formed by the hydration process between the cement particles. For Tattersal and Banfill, when cement particles came into contact with water, hydration products form around them like a membrane, making the cement particles to link together. When the build-up of the structure due to hydration of cement minerals has a slower growth rate, the structural build-up process takes more time than the thixotropic build-up.

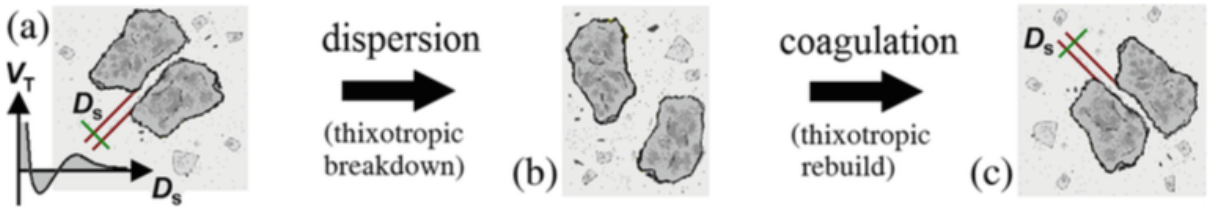

Fig. 2.6. Coagulation by V_T, (b) dispersion by agitation (c) re-coagulation by V_T. (Wallevik, 2020, apud Wallevik, 2003).

As the cement paste is submitted to shear, the bridging membrane is ruptured, which means that the formed links break and the cement particles separate (Figure 2.7). It is also a considered hypothesis that the structural breakdown is related to the breaking of breakable connections made by chemical products, as for example, early C-S-H, syngenite and ettringite (Figure 2.8).

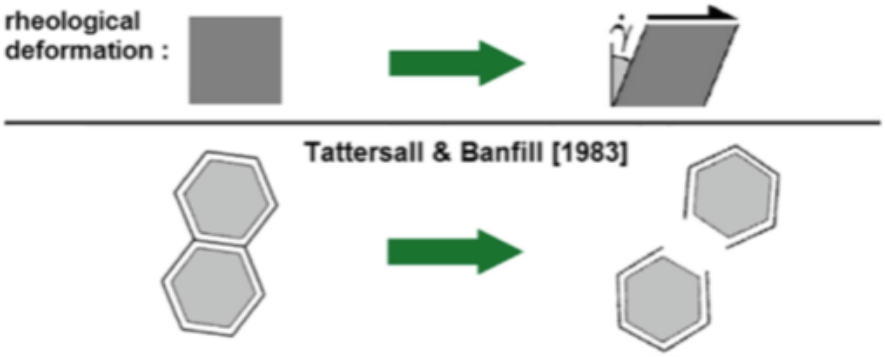

Fig. 2.7. Tattersall & Banfill hypothesis of the mechanism of structural breakdown. (Wallevik, 2020, apud Wallevik, 2011).

According to Russel 2012, apud. Tatersall & Banfill, the macroscopic flow is achieved as soon as the stress applied to the system overcomes what can be supported by the network of particles in interaction. This critical value is called yield stress and it is the dominant parameter of the workability of the cement-based materials.

According to Struble and Lei (1995), the early hydration products cause the cement particles to be bonded more strongly together and/or increase the number of inter particle bonds, it provokes an increasing of yield stress and the set of the cement paste corresponds to the development of such yield stress. This statement is explained by the fact that the setting is related to the flow of cement paste, so it is characterized by its yield stress and its plastic viscosity. When the cement paste is below the yield stress it displays solid-like behavior, but when it is above the yield stress it shows shear thinning, an indication that the micro-structure is progressively breaking down under shear.

The yield stress increases slowly at first, then more rapidly. The rapid increase in yield stress occurs at the end of the induction period (change in chemical kinetics) and corresponds to initial setting (changes in microstructure). The transition from the initial slow increase of yield stress to the more rapid increase occurs at about the same time as the increase of hydration rate. So, in order to setting to occur it is necessary, but not sufficient, that hydration takes place. Struble and Lei also stated that the setting time measured using the yield stress decreased when w/c ratio was reduced. Therefore, a paste with a lower w/c ratio has a shorter initial setting time.

For a normal cement, setting is generally attributed to the formation of C-S-H bridges (a product of hydration). It is important because, at initial set, the concrete can no longer be properly handled and be placed, while at final set, it begins to develop a useful strength.

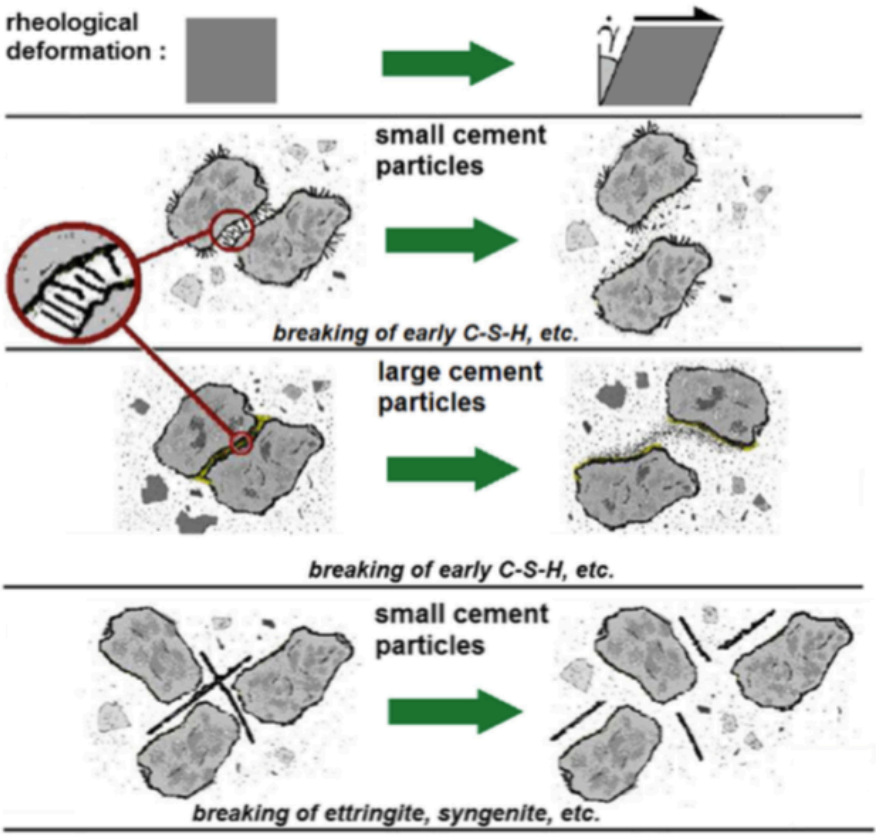

Fig. 2.8. Hypothesis of the mechanism of structural breakdown. (Wallevik, 2020, apud Wallevik, 2011).

2.4. Literature review on rheometer testing protocols

The measurement protocol has to take into account the highly thixotropic nature of cement paste. According to Roussel (2012): “At rest, thixotropic materials become structured in time”. Therefore, the measurement protocol is designed by setting a shear sequence on the rheometer in order to correctly collect the shear rate and shear stress, in order to compute the values to estimate the rheology of the cement paste.

According to Yuang (2017), static yield stress test is commonly used to monitor the structural build-up of cement-based materials and the development of static yield stress with time can be

used to characterize the evolution of the structural build-up of cement-based materials with time at early age. The static yield test is sensitive to the shear history, the mixing regime, and resting time, so a comparison between shear rates using different batches of sample could be overshadowed by the difference between the samples. This reinforces the need of having a standard protocol that encompass a reproducible preservation method and a shear sequence.

The static yield test is often performed by shearing the sample at a constant very low shear rate, and a critical peak value is obtained before the flow and used to calculate the static yield stress. At very low shear rate it allows the cement past to built up, and this is directly dependent of the material. A standard protocol has to take that into account, so in order to guarantee reproducibility we have to employ a pre-shear with high constant shear rate for a certain time, ensuring that all materials tested arrive to a steady state structure.

Normally, cement paste is pre sheared at high shear rate/shear stress for a fixed time, long enough to attain its equilibrium stage (steady state). Generally all observed literature reports for testing such materials follows the sequence:

- Perform the preconditioning with the application of a high shear rate or stress for a fixed time, achieving a reference state in order to start the tests always with the destructed state of the material;
- Allow some rest;
- Start the flow curve experiments in time intervals (time stamp measurements);
- Determine the yield stress and plastic viscosity by adopting rheological models like the Bingham model.

The Table 2.1 summarizes the test parameters and rheometer arrangements for six literature similar experimental works.

Tab. 2.1. Summary of literature similar experimental works.

Similar work	Test parameters	Rheometer arrangement
(Schankoski et al. 2017)	Pre shearing - 50 s^{-1} for 60 s, followed by a 30 s rest period Shear rate for flow curve - (0–50–0 s^{-1}) in 9 consecutive steps of 30 s each one.	Vane geometry.
(Han and Ferron 2016)	Pre shearing - 50 s^{-1} until an equilibrium state was achieved (typically within 120 s) 30 s rest period Shear rate for flow curve - step-up approach from 0 to 50 s^{-1} in increments of 10 s^{-1} .	Concentric cylinder geometry.

(Ferraris et al. 2001)	Shear rate for flow curve slowly increasing shear rate from 0 to 70 s in 160 s. As soon as the highest shear rate was reached, the plate stopped rotating. After this first phase (needed to homogenize the specimen), a full cycle of increasing shear rate by 10 steps from 3 to 50 s^{-1} and back to 0 shear rate with another 10 steps was performed.	Parallel plate rheometer. The gap (distance between the plates) was arbitrarily fixed at 0.4 mm.
(Sant et al. 2008)		Parallel plate rheometer, The gap between the plates was fixed at 1 mm.
(Corinaldesi and Moriconi 2011)	Shear rate, ranging from 1 to 100 s^{-1}.	Rotating rheometer based on coaxial rotary cylinders with a slowly increasing.
(Ferraris et al. 2014)	About fitting of Bingham model, yield stress, plastic viscosity by plotting shear rate vs shear stress of the sample.	

Thereby, the first important consideration is to consider a pre-shear step required to set similar initial conditions among all the testings. Consequently, on the same sample it is possible to perform different measurements:

- Yield stress by monitoring the shear stress during the transient phase at a constant shear rate;
- Yield stress and dynamic viscosity (Bingham model or similar) from shear rate ramps;
- Stiffness by oscillatory tests to monitor the structure development.

3. Materials and Methods

This chapter describes the key points of the experimental investigation conducted in this thesis. Specifically, this chapter presents the raw materials used, the techniques for sample preparation, as well as, both the measuring systems employed and the measuring protocol alternatives applied during this thesis' experiments.

3.1. Raw material

The raw materials considered in this thesis are those necessary to produce cement paste. Essentially, it is Cement (CEM V) dully sieved and plain (tap) water. The cement is sieved at size < 63 µm with an automatic sieve. Figure 3.1 presents a photo of the automatic sieve employed in the raw material preparation. This automatic sieve is ruled by the UNI EN 933-1, where it indicates the quantity of material that can be placed for sieve each time.

Fig. 3.1. Automatic sieve employed in the experiments (< 63 µm).

The importance of the sieved material is justified by Banfill (1991) as follows:

"Gap should be an order of magnitude larger than the size of the largest characteristic inclusion phase in the suspension" (Banfill, 1991, Rheology of fresh cement and concrete apud Vance, Sant & Neithalath, 2015).

3.2. Preparation of samples

The literature states the importance of a standard preparation procedure while conducting the experiments. Vance, Sant & Neithalath (2015) affirm that “Maintaining a consistent mixing procedure is critical when comparing rheological experiments.”. Han & Ferron (2016) also noticed conducting similar experiments that “Although the composition of the sample did not change, the changing in the mixing process affected the microstructure arrangement of the paste.”. Therefore, we decided to fix a standard procedure to prepare the samples for all experiments of this thesis.

It is important to recall the effects of the mixing procedure in producing a paste Vance, Sant & Neithalath (2015) also concluded about the different intensity in mixing procedures: "The shear history imparted to the paste through mixing was found to significantly influence the yield stress and plastic viscosity. With increasing mixing intensity, the plastic viscosity was noted to decrease due to the effectiveness of the mixing procedure in reducing the tendency of agglomeration in the paste.”.

The procedure was defined assuming the use of an automatic mixing with Heidolph RZR 2041 LAISS, match with blade BR 11 Straight Blade Impeller (shaft Ø 8 mm, blade size 50 × 12 mm) for the mixing procedure. Figure 3.2 presents two photos of the automatic mixing equipment, one focusing on the engine unit (left-hand side) and another focusing on the blade (right-hand side).

Fig. 3.2. Automatic mixing employed in the experiments.

Each of the samples was made following a procedure inspired on the ASTM C305 standard (www.astm.org). The ASTM C305 standard defines three steps called Initial mixing, Resting, and Final mixing. We decided to extended this standard procedure with three additional steps. Figure 3.3 describes the general procedure employed that comprises six steps. Steps 2, 3, and 4 of our procedure are the same as the ones defined on ASTM C305 standard.

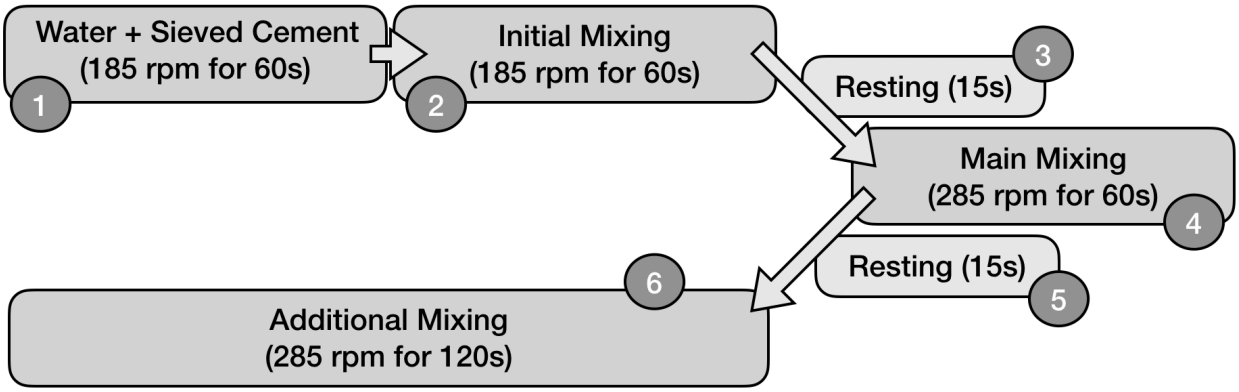

Fig. 3.3. Sample preparation process.

The first step is adding the sieved cement to the water. Following the recommendations of (Struble & Jiang, 2004 and Ferraris & Gaidis, 1992) the rate water cement (w/c) is 0.5. Because of the type of blade employed for the mixing procedure (blade BR 11 Straight Blade Impeller), the minimal quantity of material is 50g. Therefore, the produced material is composed by 100g of cement and 50g of water. The mixing starts with the 50g of water, then the 100g of cement is added in small amounts during 60 seconds with a slow rotation of 185 rpm.

The second step, called here Initial Mixing, is the same as the first step of the ASTM C305 standard, and it consists of a slow mixing for another 60 seconds at 185 rpm, which is the slowest speed of the employed mixing equipment.

The third step is a simple resting time of 15 seconds, that corresponds to the second step of ASTM C305 standard.

The fourth step is called here Main Mixing, but it corresponds to the third step of ASTM C305 standard where it is called Final mixing. We changed the step name here because it is no longer the last step to be performed. The fourth step is a mixing performed at a faster speed (285 rpm) than the Initial Mixing, but it runs for the same period of time of 60 seconds.

Han & Ferron (2016) proposed an extension to ASTM C305 with another resting step, and finally an additional mixing. Our two last steps corresponds to this extension edited by Han & Ferron (2016) over ASTM C305 standard. The fifth step, therefore, is another rest for 15 seconds.

The sixth and last step is the additional mixing performed at 285 rpm for 120 seconds as recommended by ASTM C305 standard edited by Han & Ferron (2016). After this final step the cement paste is prepared, but it has to be conserved from the external environment without separation of the mixture or hardened in order to be measured in the rheometer.

3.3. Test and measuring equipment

After the six mixing steps, the paste was ready to proceed with the measurements in Anton-Paar rheometer, model MCR301. Figure 3.4 presents two photos of the rotational rheometer employed in the experiments of this thesis. This rheometer allows us to measure the paste's viscosity, shear stress and yield stress. The same paste is proceeded to a measure the paste's density, water content and air content. The idea is to measure the paste footprint, to analyze it in terms of density, water content and air voids the paste that went to the testing on the rheometer.

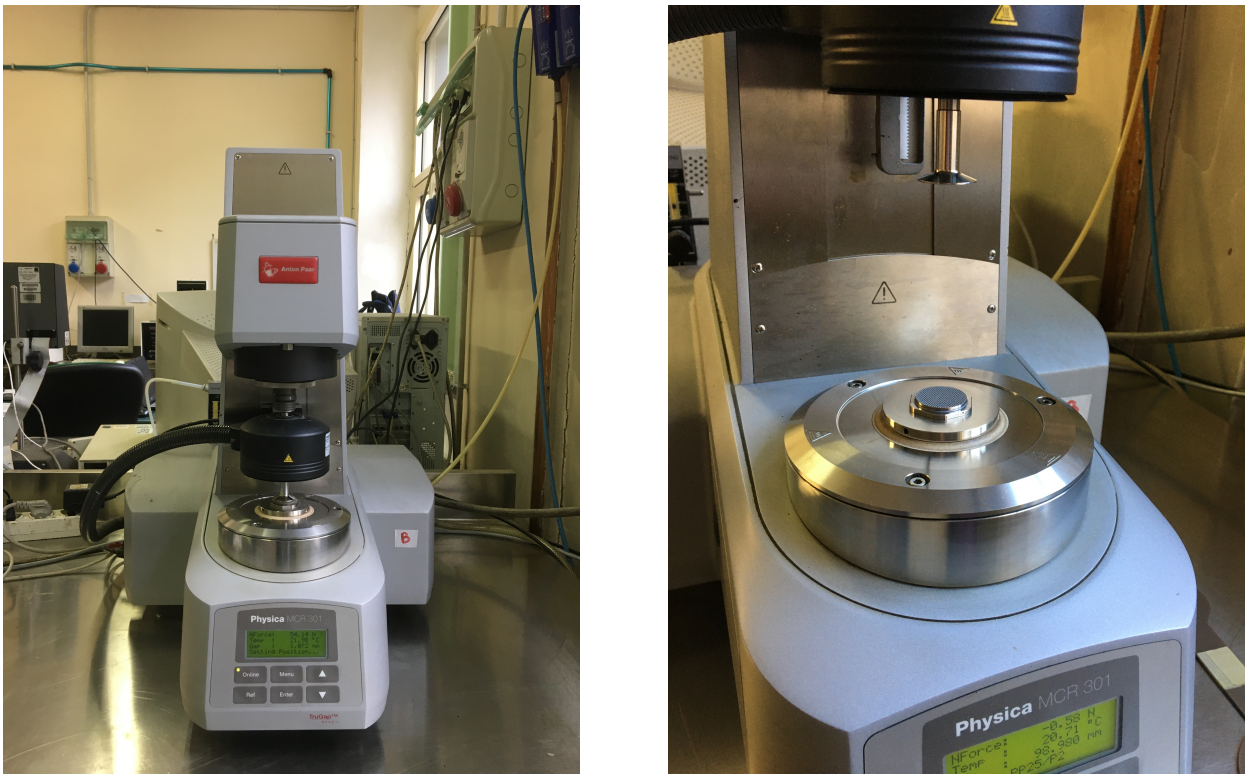

Fig. 3.4. Rheometer employed in this work.

The rotational rheometer works placing the cement mixture between two cross-hatched stainless-steel parallel plates with a rough dented surface. Specifically, for our experiments a pair of PP25 P2 plates were used (left-hand side of Figure 3.5). Those plates are represented schematically in the right-hand side of Figure 3.5 that shows the profile of a PP25 P2 plate, a plate with a diameter of 25 mm with dents of .5 mm depth and distance of 1 mm. Once the mixture was inside the rheometer, the tests were performed using those PP25/P2 plates. According to Ferraz et al. (2020), this rough geometry guarantees shear without slipping during the tests.

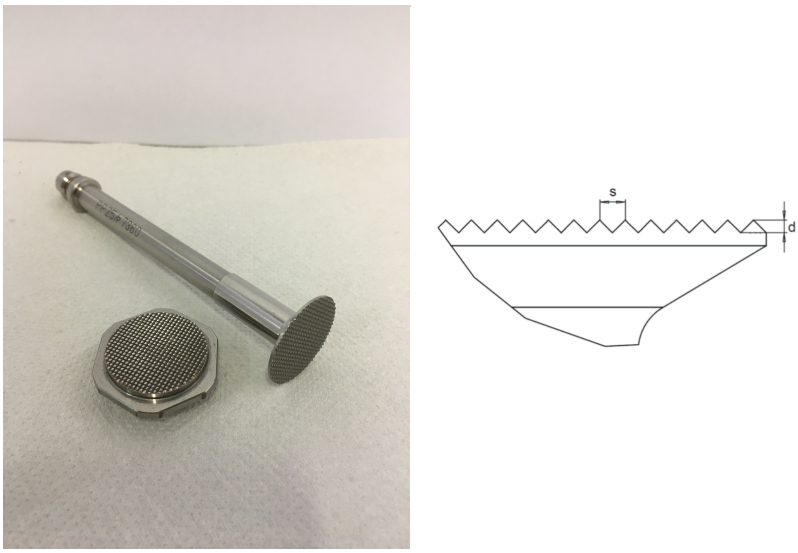

Fig. 3.5. Rheometer's cross-hatched stainless-steel parallel plates PP25 P2 with s = 1 mm and d = 0.5 mm.

Struble & Jiang (2004), analyzed the effects of air entrainment on rheological parameters in cement paste. According to their work: "With increasing air content, the yield stress increased and the plastic viscosity decreased. The increase in yield stress was an unexpected result because increasing air is well known to cause an increase in slump, and yield stress and slump are known to be negatively correlated (as yield stress increases, slump decreases). Two competing effects are proposed to explain the effects of entrained air voids on rheological parameters: the attraction of cement particles and voids to form bubble bridges, and a fluid response of air voids due to their deformability. Bubble bridges are proposed to dominate in the yield stress and the fluid response is proposed to dominate when the sample is flowing.".

Once the cement mixture is prepared, the paste have to be placed at the parallel plate rheometer with rough surface. According to Ley-Hernandez & Feys (2020), as the sample has a small volume required, the surface roughness and the variable gap can simulate the distance between the aggregates when testing. Therefore, four different methodologies were tested to evaluate the best way to conserve the paste from the external environment, and to each of those methodologies we create an icon to indicate which one was employed. The description of each methodology and the corresponding icon are indicated here below:

- **Preservation technique P1** - the cement paste is prepared before each experiment step and the paste sample is directly placed in the rheometer's parallel plates;
- **Preservation technique P2** - the cement paste is stored after preparation in a small syringe of 5 ml to prevent contact with the outside environment, and consequently preventing loss of water and hardening (such syringe is depicted in the left-hand side of Figure 3.6);
- **Preservation technique P3** - the cement paste is stored in a larger syringe of 50 ml, also to prevent contact with the outside environment (such syringe is depicted in the right-hand side of Figure 3.6);
- **Preservation technique P4** - the cement paste is stored in a batch isolated with wetted paper, as show in Figure 3.7.

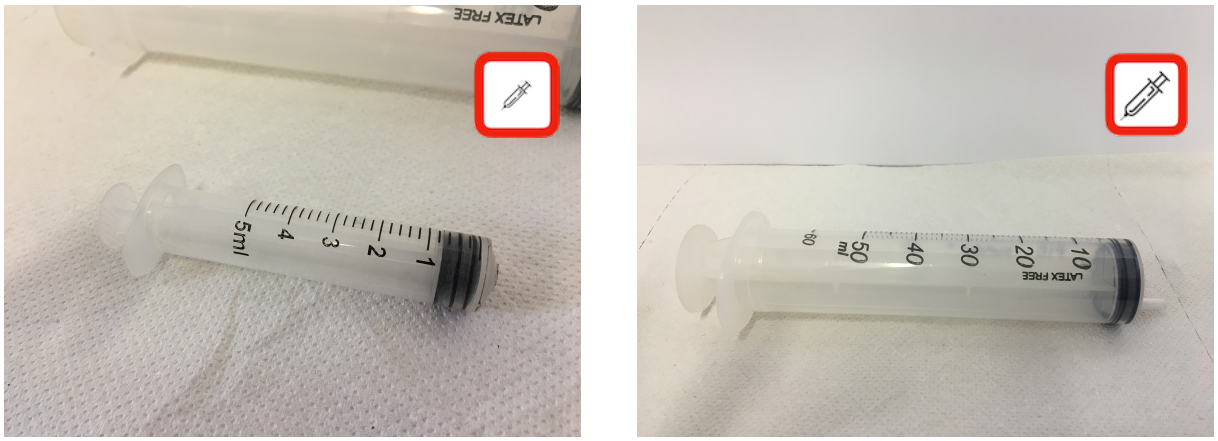

Fig. 3.6. Two different syringes employed in the experiments (5ml and 50ml).

Fig. 3.7. Batch isolated with wetted paper.

Furthermore, to prevent evaporation of water from the sample during the rheometer operation, according to the Ley-Hernandez & Feys it is enough to have a temperature-controlled hood placed on the top of the measuring system. For this work, the machine is set to a constant temperature of 20 ºC. For this work we tested options using the hood in the open and closed positions of the air circulation, respectively denoted as **H1** and **H2**. Figure 3.8 presents a photo of the hood in place over the rheometer plates, as well as another photo of the air circulation of the hood switch in the closed position. Once again, we create to icons to represent the open and closed positions of the hood.

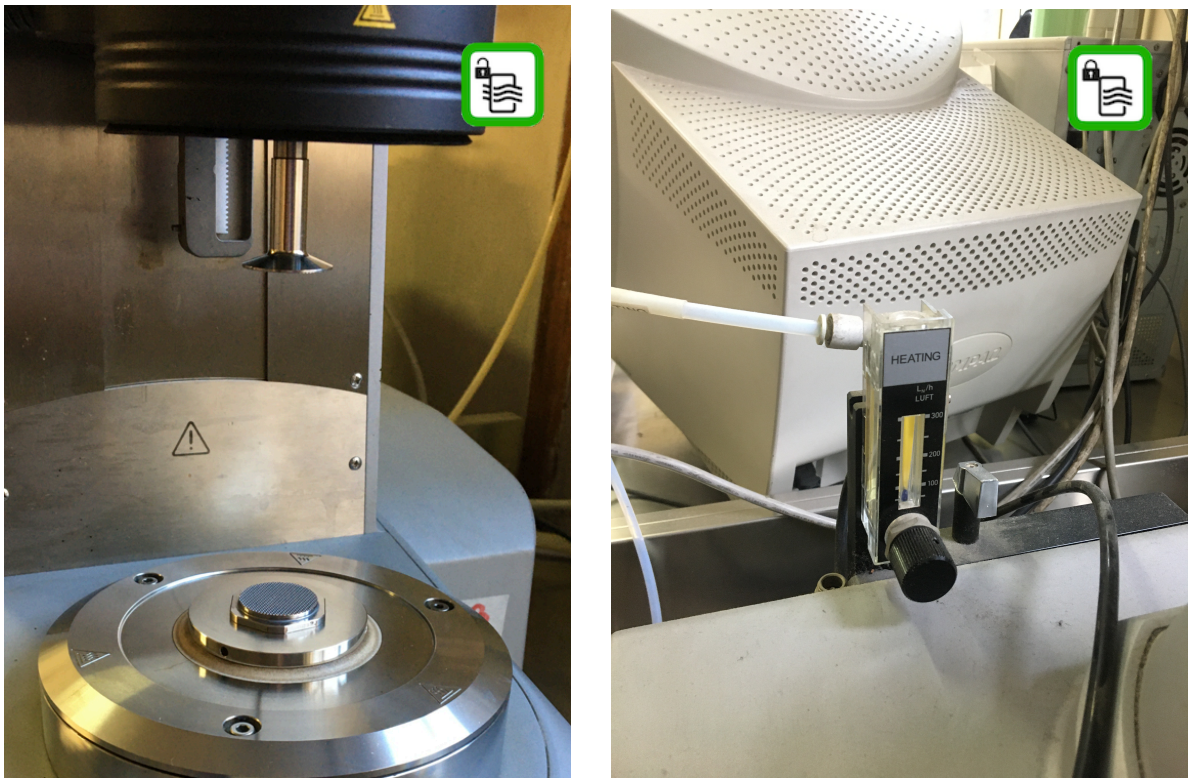

Fig. 3.8. Hood and closed switch for the air circulation of the hood.

3.4. Measurement protocols

The measurement protocol has to take into account the highly thixotropic nature of cement paste. According to Roussel (2012): “At rest, thixotropic materials become structured in time”. Therefore, the measurement protocol is designed by setting a shear sequence on the rheometer in order to correctly collect the shear rate and shear stress and to compute the values to estimate the rheology of the cement paste.

It is important to remember that we are interested in discover the more adequate form to evaluate the rheology of the cement paste. As mentioned in Chapter 2, having the shear rate and the shear stress it is possible to apply one of the models (Bingham or Herschel-Bulkley) to compute the interesting measures as the plastic viscosity and dynamic yield stress.

The first important consideration is to consider a pre-shear step required to set similar initial conditions among all the testings. Consequently, on the same sample it is possible to perform different measurements:

- Yield stress by monitoring the shear stress during the transient phase at a constant shear rate;
- Yield stress and dynamic viscosity (Bingham model or similar) from shear rate ramps;
- Stiffness by oscillatory tests to monitoring the structure development or something similar.

Conversely, we consider each experiment composed by a two steps, the initial one is the pre-shear, and the second one the sweep test step or shear rate steps test. Formally, the overall protocol is set as the definition of a shear sequence, and for this thesis we consider three possible sequences (and their respective icons):

- **Shear sequence S1** that defines strain rates changed logarithmically from 50 s^{-1} to 0.05 preceded by a 60 seconds fixed strain value and followed by a 60 seconds fixed strain value (13 shear rates with 20 s each for a total of around 6 minutes - 360 seconds) - Figure 3.9 depicts the variation of strain rates, and Table 3.1 shows the timeline details for Shear sequence S1;
- **Shear sequence S2** that defines strain rates alternating the highest value (50 s^{-1}) with intervals with lower values each time slower until the end of the experiment (6 lower value intervals: 30, 10, 3, 1, 0.3, and 0.1 for a total of nearly 4 minutes - 225 seconds) - Figure 3.10 depicts these variation of strain rates, and Table 3.2 shows the timeline details for Shear sequence S2;
- **Shear sequence S3** that also defines strain rates alternating the highest value (50 s^{-1}) with intervals with lower values, but unlike S2, it decreases the slower rates until the middle of experiment, and then it increase the slower values symmetrically (lower value intervals: 30, 10, 3, 1, 0.3, 0.1, 0.3, 1, 3, 10, 30 for a total a little more than 9 minutes - 555 seconds) - Figure 3.11 depicts these variation of strain rates, and Table 3.3 shows the timeline details for Shear sequence S3.

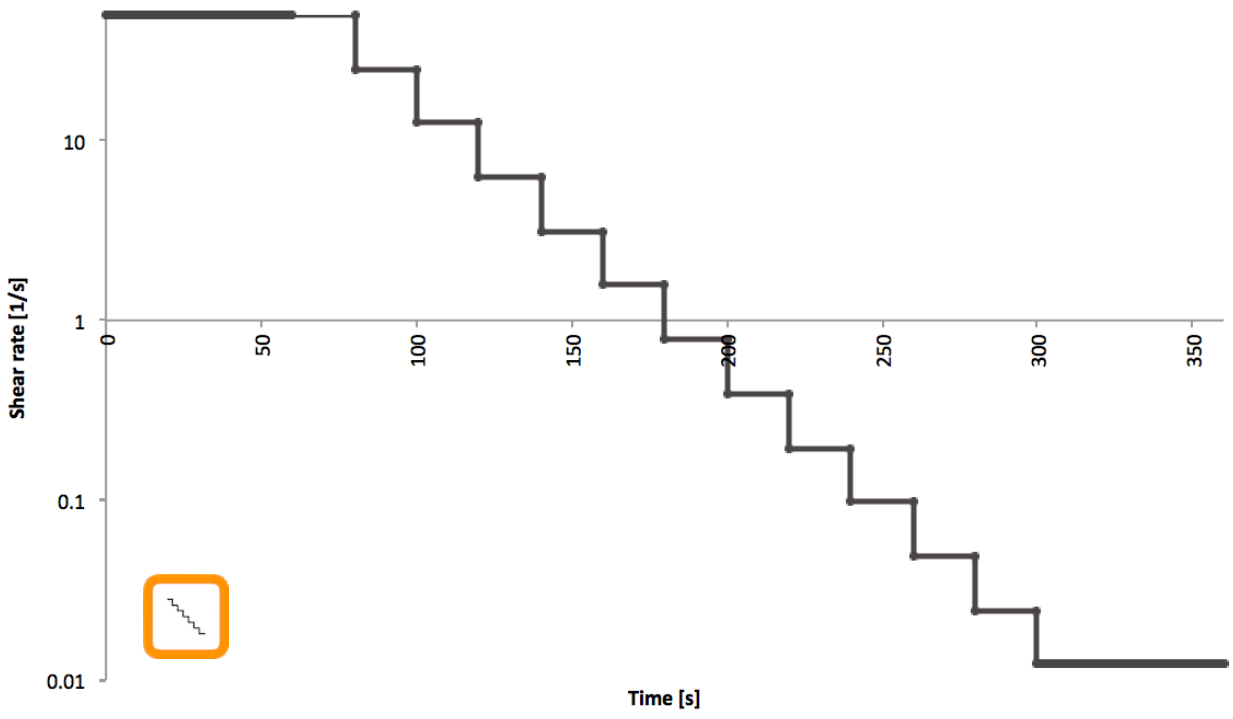

Fig. 3.9. Shear sequence S1 strain rates variation.

Tab. 3.1. Shear sequence S1 timeline and values - 360 seconds.

time (s)	duration (s)	measure points	Shear Sequence S1
0	60	120	50.00 s^{-1}
60	20	1	50.00 s-1
80	20	1	25.00 s^{-1}
100	20	1	12.50 s^{-1}
120	20	1	6.25 s^{-1}
140	20	1	3.13 s^{-1}
160	20	1	1.56 s^{-1}
180	20	1	0.78 s^{-1}
200	20	1	0.39 s^{-1}
220	20	1	0.20 s^{-1}
240	20	1	0.10 s^{-1}
260	20	1	0.05 s^{-1}
280	20	1	0.01 s^{-1}
300	60	120	0.01 s^{-1}

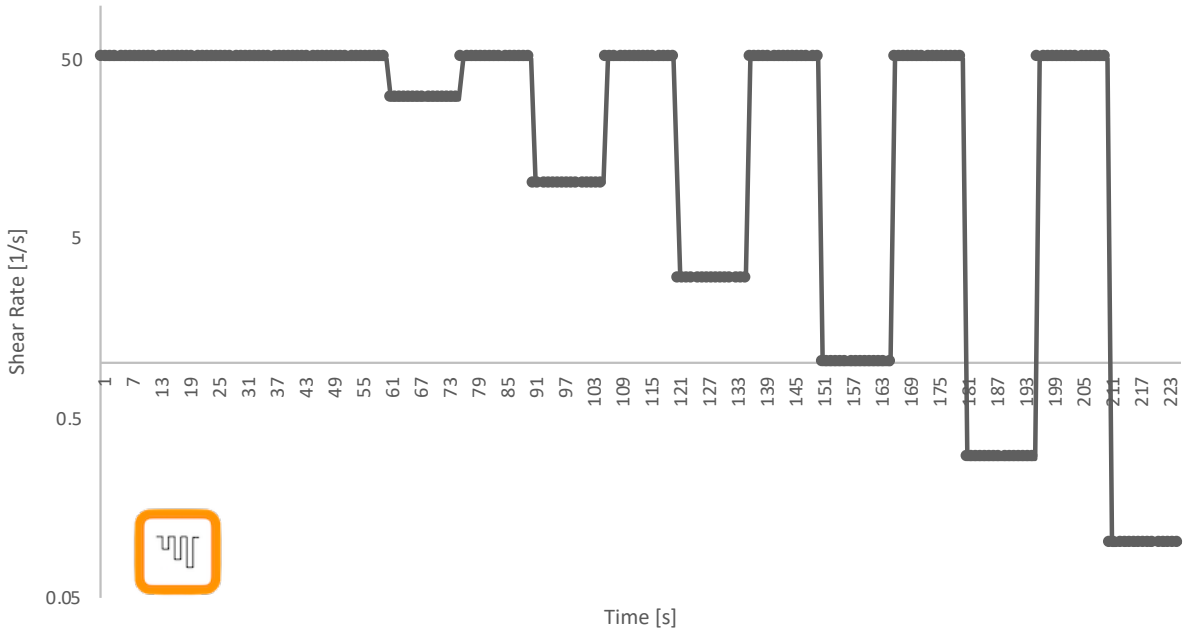

Fig. 3.10. Shear sequence S2 strain rates variation.

Tab. 3.2. Shear sequence S2 timeline and values - 225 seconds.

time (s)	duration (s)	measure points	Shear Sequence S2
0	60	120	50 s^{-1}
60	15	15	30 s^{-1}
75	15	15	50 s^{-1}
90	15	15	10 s^{-1}
105	15	15	50 s^{-1}
120	15	15	3 s^{-1}
135	15	15	50 s^{-1}
150	15	15	1 s^{-1}
165	15	15	50 s^{-1}
180	15	15	0.3 s^{-1}
195	15	15	50 s^{-1}
210	15	15	0.1 s^{-1}

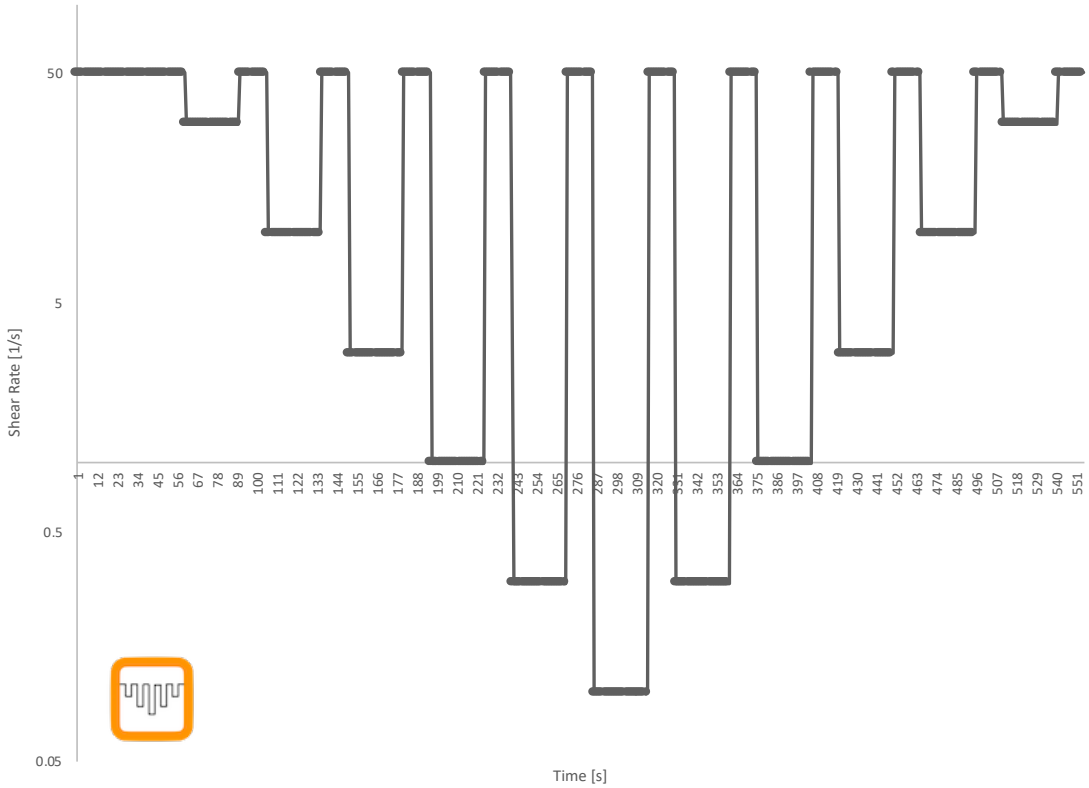

Fig. 3.11. Shear sequence S3 strain rates variation.

Tab. 3.3. Shear sequence S3 timeline and values - 555 seconds.

time (s)	duration (s)	measure points	Shear Sequence S3
0	60	120	50 s^{-1}
60	30	15	30 s^{-1}
90	15	15	50 s^{-1}
105	30	15	10 s^{-1}
135	15	15	50 s^{-1}
150	30	15	3 s^{-1}
180	15	15	50 s^{-1}
195	30	15	1 s^{-1}
225	15	15	50 s^{-1}
240	30	15	0.3 s^{-1}
270	15	15	50 s^{-1}
285	30	15	0.1 s^{-1}
315	15	15	50 s^{-1}
330	30	15	0.3 s^{-1}
360	15	15	50 s^{-1}
375	30	15	1 s^{-1}
405	15	15	50 s^{-1}
420	30	15	3 s^{-1}
450	15	15	50 s^{-1}
465	30	15	10 s^{-1}
495	15	15	50 s^{-1}
510	30	15	30 s^{-1}
540	15	15	50 s^{-1}

Additionally, to the rheometer measurements (shear rate and shear stress), the cement paste footprint is analyzed using a small piknometer with alcohol at given time stamps. Figure 3.12 presents in the left-hand side empty piknometers and at the right-hand side the piknometers filled with alcohol and cement paste.

Fig. 3.12. Piknometers used to cement paste density measures.

Specifically, the density of the mixture is measured by the procedure UNI EN 1097-7: 2000, which takes approximately 15 minutes to be undertaken. In fact, two density measures are taken, one as it is, and another submitting the sample to a depressurizer engine. Figure 3.13 presents the piknometers for density measure for degassed cement paste samples on the left-hand side (empty and full of samples) and the depressurizer equipment in the right-hand side.

The UNI EN 1097-7: 2000 describes tests for mechanical and physical properties of aggregates, the determination of the particle density of filler by the pyknometer method. This is a method for determining the volume of irregularly formed samples, when the mass of the sample is known, the density can be calculated. For the calculation we need to carry out all weighing with an accuracy of 0,001 g.

The principle is based on the replacement of a certain amount of liquid of known density with the test portion, so a pyknometer with known volume, containing the test portion, is topped up with the liquid. The suitable liquid, must be one in which the cement paste does not dissolve or react, therefore we have used alcohol. Basically, the volume of this liquid is calculated by dividing the mass of the liquid added by the liquid density. The volume of the test portion is then calculated by subtraction of this volume from the pyknometer volume.

Fig. 3.13. Piknometers used to density measures of degassed cement pastes and the depressurizer equipment.

Therefore, the method consists in weigh the clean and dry pyknometer with stopper (m_0), fill the pyknometer with (10 ± 1) g of cement paste taken from the test portion and weigh it again (m_1), add sufficient liquid to completely submerge the test specimen and weigh it again (m_2).

Then, the particle density of the cement paste and of the degassed cement paste, in megagrams per cubic meter, can calculated by the following equation:

$$\rho_f = \frac{m_1 - m_0}{V - \frac{m_2 - m_1}{\rho_l}}$$

Where:
ρ_f : density of the particle density of the cement paste at the room temperature, in megagrams per cubic meter
ρ_l : density of the alcohol at the room temperature, in megagrams per cubic meter
V : volume of the pyknometer, in millimeters;
m_0 : mass of the empty pyknometer with stopper, in grams;
m_1 : mass of the pyknometer with the cement paste test portion, in grams;
m_2 : mass of the pyknometer with the filler test portion, topped up with the alcohol, in grams;
for the degassed sample degassed cement paste sample it is measured after submitting the sample to the depressurizer engine.

Finally, the paste footprint include the quantity of water that is present in the sample and this is made heating a small 5g sample into an oven up to 110º celsius until it dries.

The cement paste footprint analysis was made with two different protocols (and corresponding icons):

- **F1** where the water quantity measures were performed to all time stamps, the density measures were performed to all time stamps but the first, and the degased density at the second time stamps; and
- **F2** where the density and the degased density were performed only at the second time stamps and the water quantity measures were performed to all time stamps.

Additionally, for the cases where no footprint analysis is performed, we will use the following empty icon.

3.5. Summary of icons

Figure 3.14 presents all icons employed in this document to represent the options of experiment protocols.

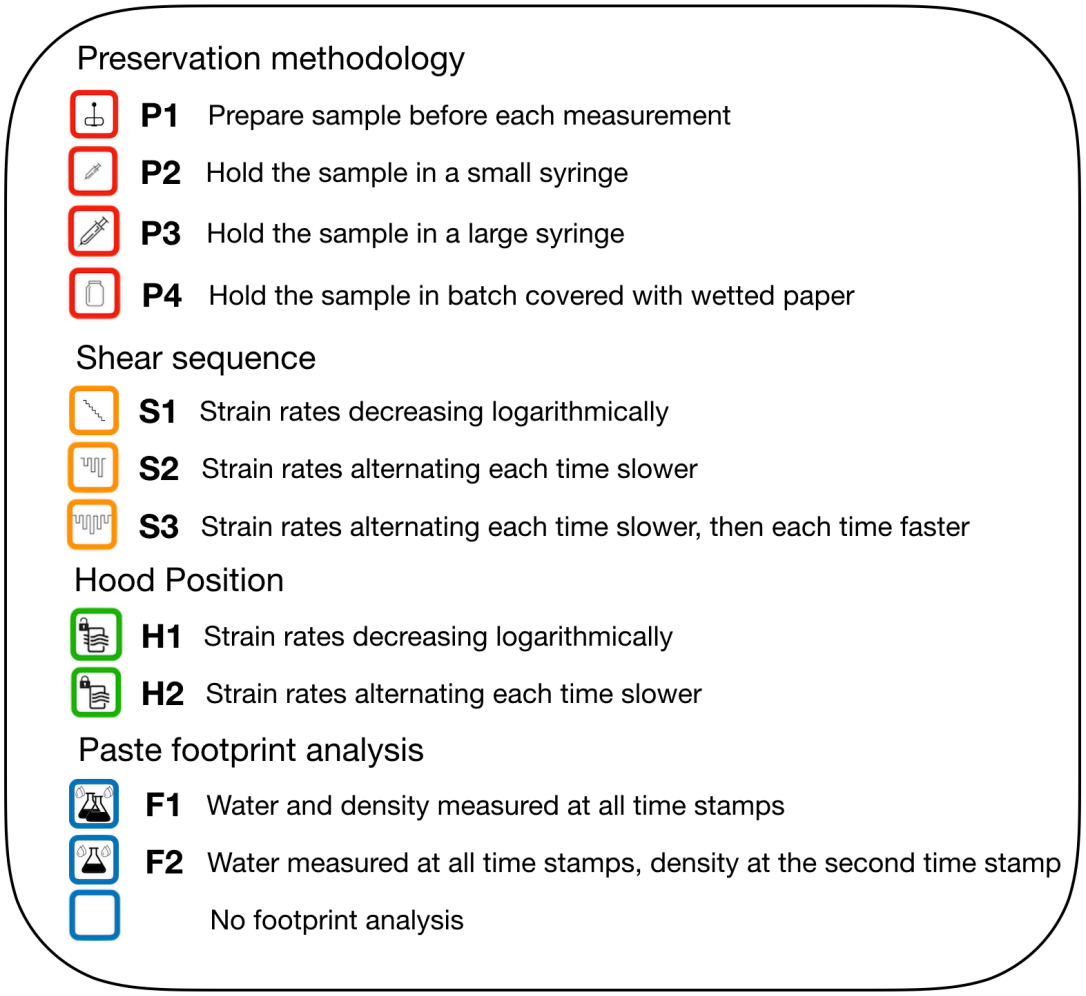

Fig. 3.14. Icons employed in this document to represent the options of experiment protocols.

4. Experimental Investigation

For this study, six different experiments were performed combining techniques to preserve the cement paste from outside contact (P1, P2, P3, and P4), shear strain sequences in the rheometer (S1, S2, and S3), and position of the hood open or closed (H1 and H2).

Associated with the cement paste preservation method, we also define the intervals in which the rheometer observations were made to each experiment. Specifically, for methods P1 and P2, the time stamps for rheometer observations is 5, 20, 35, and 50 minutes. For methods P3 and P4, the time stamps for rheometer observations is 5, 20, 40, 60, and 80 minutes.

The experiments were named from A to F, actually, the evolution from one experiment to the next was an attempt to improve the measurement quality with the new experiment. The assessment of each experiment quality was made by analyzing the results of the previous experiment. Table 4.1 summarizes the characteristics of the six experiments stating which cement paste preservation method was employed, which shear strain sequence was applied, the hood position, the time stamps where the rheometer values were observed, and finally, the kind of cement paste footprint was performed.

Tab. 4.1. Summary of experiments executed.

Experiment	Preservation	Sequence	Hood	Time stamps [min]	Footprint	Iconic code
A	P2	S1	H1	5, 20, 35, 50	-	
B	P1	S1	H1	5, 20, 35, 50	-	
C	P2	S2	H1	5, 20, 40, 60	-	
D	P3	S2	H2	5, 20, 40 ,60, 80	F1	
E	P3	S3	H2	5, 20, 40 ,60, 80	F2	
F	P4	S3	H2	5, 20, 40 ,60, 80	F2	

4.1. Experiment A

This experiment consists in the preservation method P2, shear strain sequence S1, time stamps of 5, 20, 35, and 50 minutes, and no cement paste footprint analysis. Figure 4.1 depicts the timeline for this experiment steps to carry it out. In this picture:

- Step 1 stands for the end of the mixing procedure;
- Step 2 stands for the placement of the sample on the rheometer plates;
- Step 3 stands for submitting the sample to shear strain sequence S1.

It is important to stress that according to preservation method P2, after the cement paste is ready it is hold in a small 5ml syringe and applied at each Step 2 into the rheometer. Likewise, the shear strain sequence S1 is applied at each Step 3, having the rheometer hood kept open. Finally, the shear rate and the shear stress values are taken from the rheometer readings.

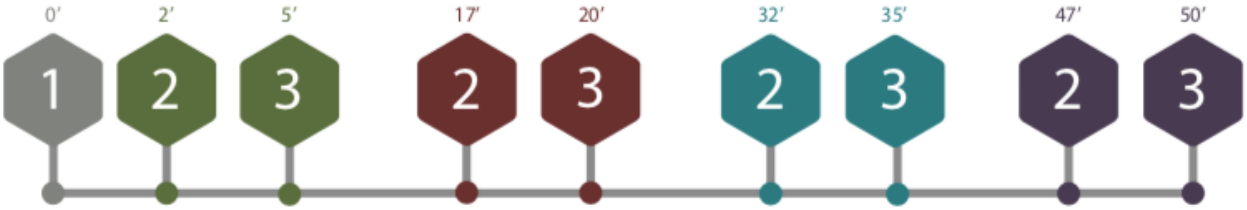

Fig. 4.1. Timeline for Experiment A.

4.2. Experiment B

This experiment consists in the preservation method P1, shear strain sequence S1, time stamps of 5, 20, 35, and 50 minutes, and no cement paste footprint analysis. Figure 4.2 depicts the four timelines for this experiment steps to carry it out. In this picture:

- Step 1 stands for the end of the mixing procedure;
- Step 2 stands for the placement of the sample on the rheometer plates;
- Step 3 stands for submitting the sample to shear strain sequence S1.

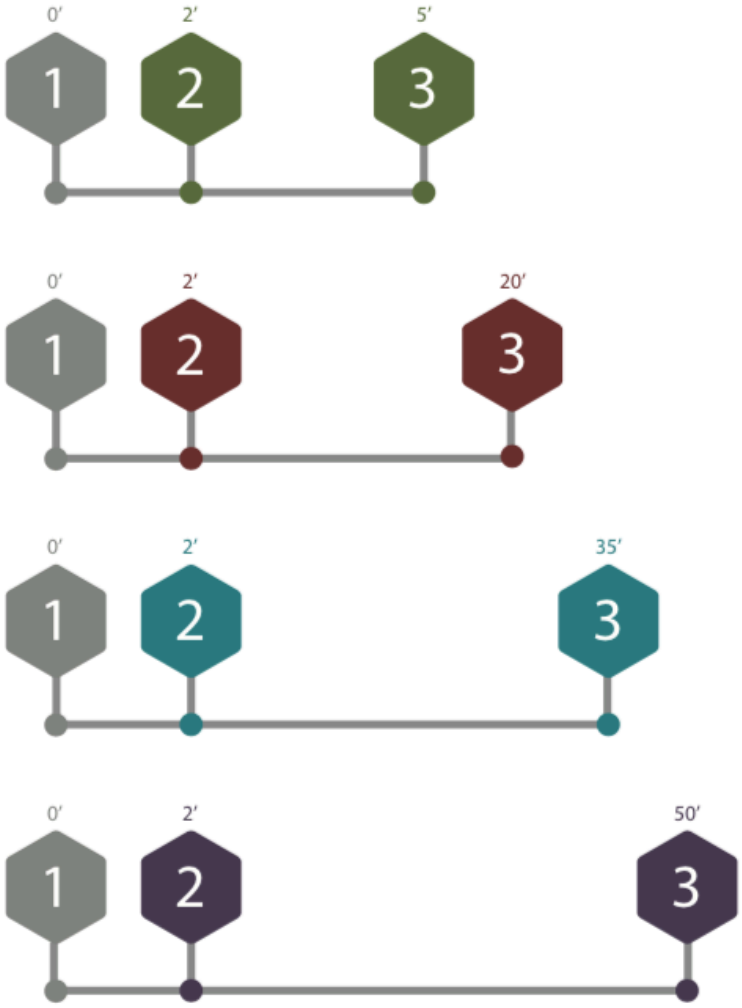

Fig. 4.2. Timelines for Experiment B.

It is important to stress that according to preservation method P1, the cement paste is prepared for each of the four applications of each Step 2 and left to rest into the rheometer. The shear strain sequence S1 is applied at each Step 3, having the rheometer hood kept open. Finally, the shear rate and the shear stress values are taken from the rheometer readings.

4.3.Experiment C

This experiment consists in the preservation method P2, shear strain sequence S2, time stamps of 5, 20, 40, and 60 minutes, and cement paste footprint analysis at the last three time stamps. Figure 4.3 depicts the timeline for this experiment steps to carry it out. In this picture:

- Step 1 stands for the end of the mixing procedure;
- Step 2 stands for the placement of the sample on the rheometer plates;
- Step 3 stands for submitting the sample to shear strain sequence S2.

It is important to stress that according to preservation method P2, after the cement paste is ready it is hold in a small 5ml syringe and applied at each Step 2 into the rheometer. Likewise, the shear strain sequence S2 is applied at each Step 3, having the rheometer hood kept open. Finally, the shear rate and the shear stress values are taken from the rheometer readings.

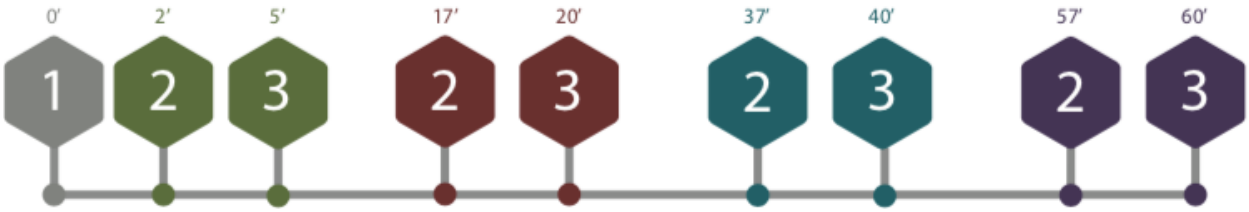

Fig. 4.3. Timeline of Experiment C.

4.4. Experiment D

This experiment consists in the preservation method P3, shear strain sequence S2, time stamps of 5, 20, 40, 60, and 80 minutes, and cement paste footprint analysis at the last four time stamps for the density and degased density and for all time stamps for quantity of water. Figure 4.4 depicts the timeline for this experiment steps to carry it out. In this picture:

- Step 1 stands for the end of the mixing procedure;
- Step 2 stands for the placement of the sample on the rheometer plates;
- Step 3 stands for submitting the sample to shear strain sequence S2.

It is important to stress that according to preservation method P3, after the cement paste is ready it is hold in a large 50ml syringe and applied at each Step 2 into the rheometer. Likewise, the shear strain sequence S2 is applied at each Step 3, having the rheometer hood kept closed. Finally, the shear rate and the shear stress values are taken from the rheometer readings, followed by a paste footprint analysis at time stamps 20, 40, 60, and 80.

Fig. 4.4. Timeline of Experiment D.

4.5. Experiment E

This experiment consists in the preservation method P3, shear strain sequence S3, time stamps of 5, 20, 40, 60, and 80 minutes, and cement paste footprint analysis, at the second time stamp for the density and degased density and for all time stamps for quantity of water. Figure 4.5 depicts the timeline for this experiment steps to carry it out. In this picture:

- Step 1 stands for the end of the mixing procedure;
- Step 2 stands for the placement of the sample on the rheometer plates;
- Step 3 stands for submitting the sample to shear strain sequence S3.

It is important to stress that according to preservation method P3, after the cement paste is ready it is hold in a large 50ml syringe and applied at each Step 2 into the rheometer. Likewise, the shear strain sequence S3 is applied at each Step 3, having the rheometer hood kept closed. Finally, the shear rate and the shear stress values are taken from the rheometer readings, followed by a paste footprint analysis.

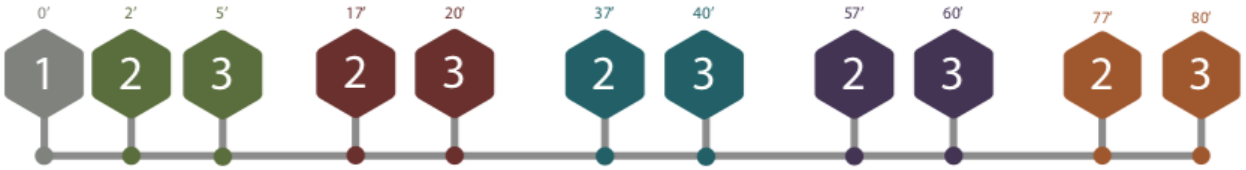

Fig. 4.5. Timeline of Experiment E.

4.6. Experiment F

This experiment consists in the preservation method P4, shear strain sequence S3, time stamps of 5, 20, 40, 60, and 80 minutes, and cement paste footprint analysis, at the second time stamp for the density and degased density and for all time stamps for quantity of water. Figure 4.6 depicts the timeline for this experiment steps to carry it out. In this picture:

- Step 1 stands for the end of the mixing procedure;
- Step 2 stands for the placement of the sample on the rheometer plates;
- Step 3 stands for submitting the sample to shear strain sequence S3.

It is important to stress that according to preservation method P3, after the cement paste is ready it is hold in a batch covered by wetted paper and applied at each Step 2 into the rheometer. Before the sample is placed on the rheometer, a hand-mixing with a small spoon is performed for 30s to guarantee homogeneity of the mixture, the sample is putted with the spoon inside a big syringe (by its barrel) with the spoon and, finally, placed on the rheometer plates.

Likewise, the shear strain sequence S3 is applied at each Step 3, having the rheometer hood kept closed. Finally, the shear rate and the shear stress values are taken from the rheometer readings, followed by a paste footprint analysis.

Fig. 4.6. Timeline of Experiment F.

5. Results and Discussion

This chapter presents some relevant numerical results obtained from the conducted experiments (A, B, C, D, E, and F) and their discussion in order to establish an appropriated way to evaluate the rheology properties of cement paste. The full numerical results are presented in detail in the Annexes A to F at the end of this document. This chapter is organized with the summary of each experiment, the presentation of the key numerical results and the discussion leading to the proposition to the next experiment.

5.1. Experiment A

This experiment consists in the preservation method P2, shear strain sequence S1, time stamps of 5, 20, 35, and 50 minutes, rheometer hood open, and no cement paste footprint analysis. Experiment A was performed twice, therefore the results are presented for both runs. Figure 5.1 shows the shear stress curves obtained for the first 60 seconds after the shear strain sequence was started.

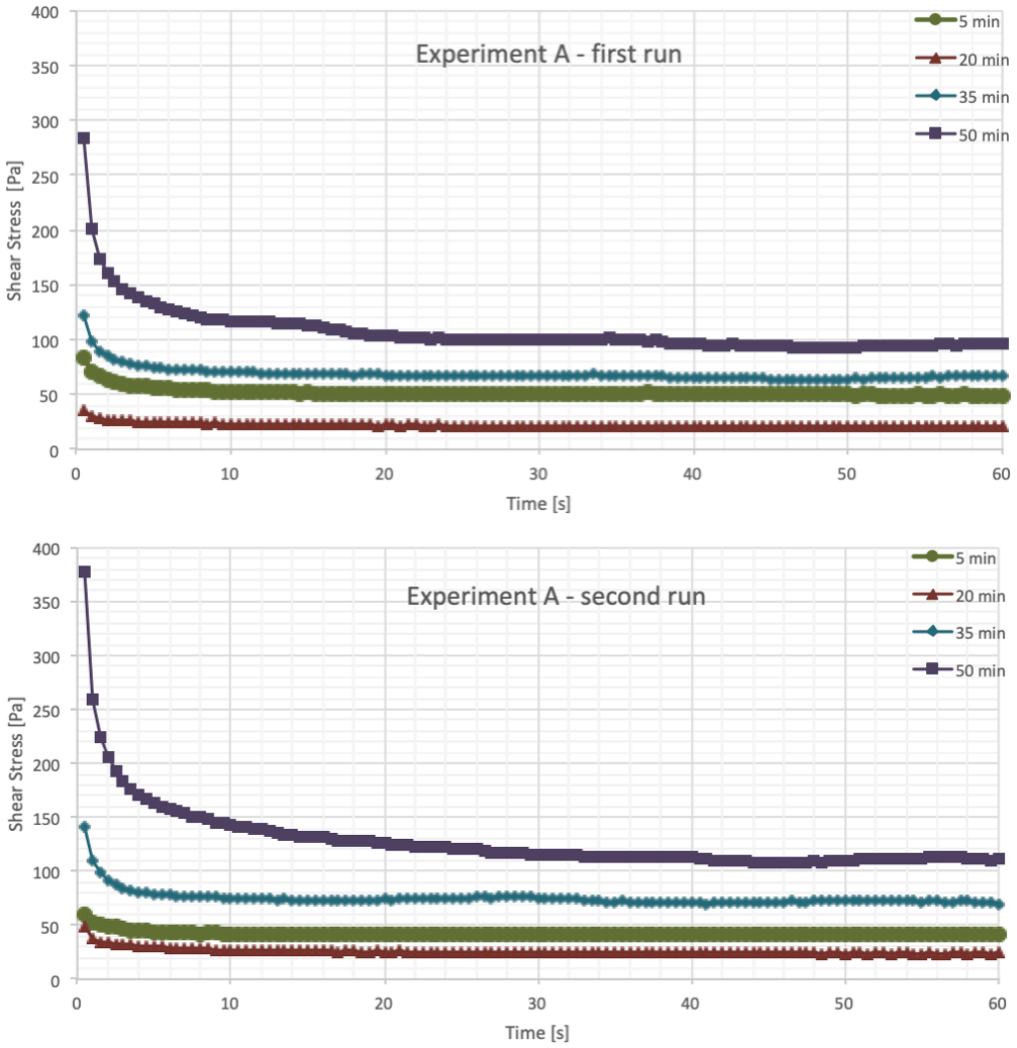

Fig. 5.1. Shear stress for both runs of Experiment A.

It is noticeable that all curves in Figure 5.1 show a steady state convergence, this convergence can also be observed by the average values of the last four results, as well as the standard deviation shown in Table 5.1. To reach the steady state convergence is important to guarantee that the transitional phase at the beginning passes and the samples achieve a reference state, so that the next measurements at various shear rates can be assumed to be done at the destructed state of the material. It is also noticeable that the shear rate curve for the time stamp 20 minutes is the lowest, which seems surprising, since a lower shear stress was expected for the 5 minutes time stamp curve.

Tab. 5.1. Shear stress steady state for both runs of Experiment A.

run	time stamp	shear stress last four values average	std dev	run	time stamp	shear stress last four values average	std dev
1st	5	49.15	0.20	2nd	5	41.84	0.29
	20	21.01	0.20		20	23.97	0.21
	35	66.81	0.24		35	71.05	0.66
	50	96.27	0.48		50	111.53	0.22

Analyzing the obtained results for experiment A we obtain the flow curves presented in Figure 5.2. These curves represent the ratio between the shear stress measured in the rheometer at each time stamp by the shear rate imposed in a set of curves. We can see that the lower values of shear stresses from all time stamps are reached at different shear rates, and that illustrates how the Experiment A's results are not reliable.

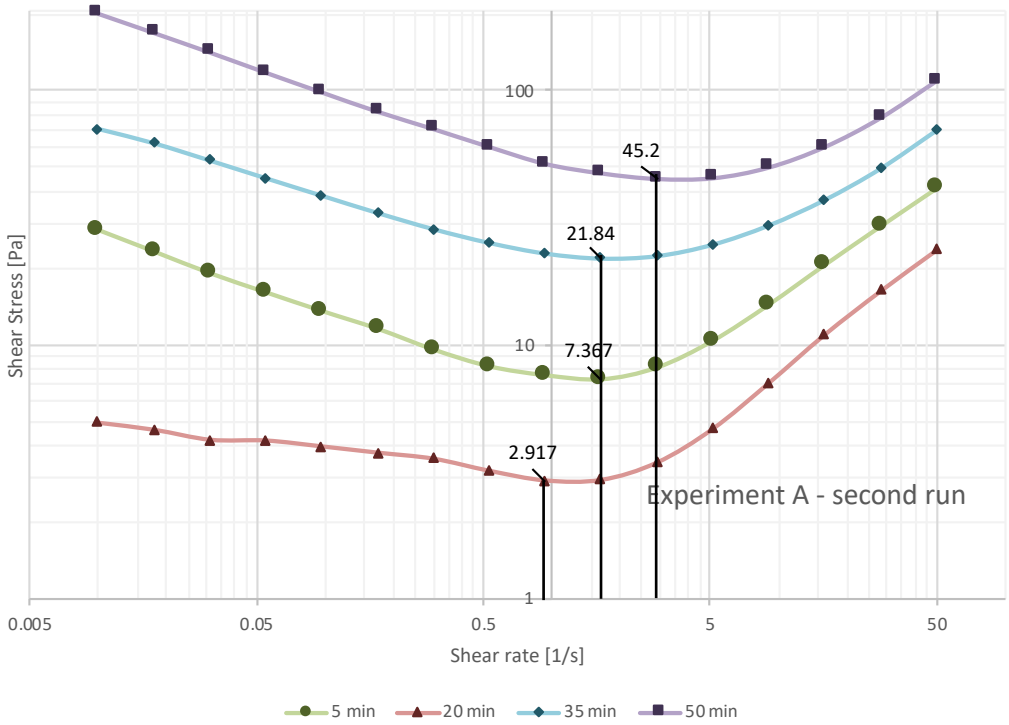

Fig. 5.2. Flow curves (shear rate and shear stress ratio) for second run of Experiment A.

Applying the Bingham model to the obtained results for Experiment A we obtain Table 5.2, the numerical values for the Bingham model computation. Focusing on the 5 min time stamp, we obtain in Figure 5.3 the flow curve representing the ratio between the shear stress computed using the Bingham model at each time stamp by the shear rate imposed.

Tab. 5.2. Numerical values of Bingham model for both runs of Experiment A.

time stamp	1st run dynamic yield stress (τ_0)	2nd run dynamic yield stress (τ_0)	1st run plastic viscosity (μ)	2nd run plastic viscosity (μ)
5	18.599	13.013	0.562	0.536
20	3.323	3.544	0.363	0.414
35	18.386	35.894	0.894	0.512
50	46.928	89.659	0.686	0.000

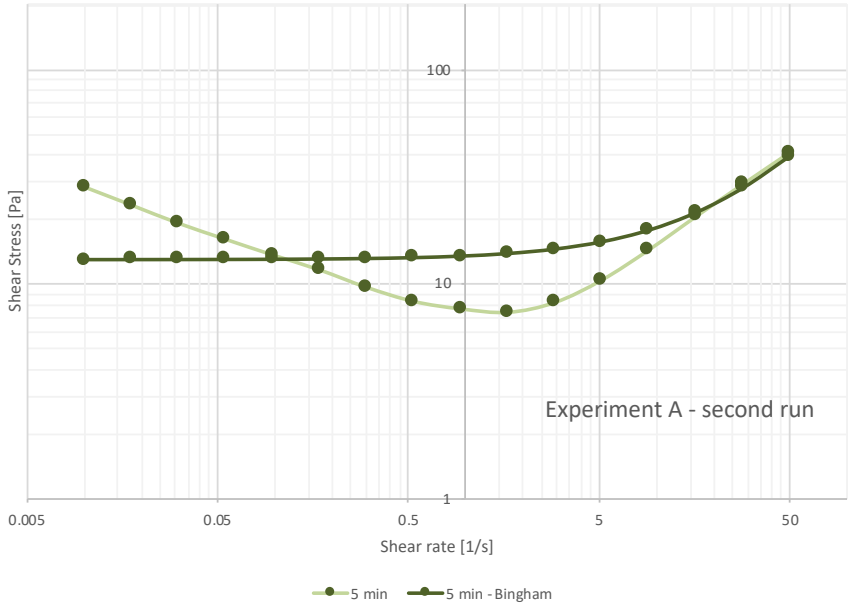

Fig. 5.3. Flow curve (shear rate and shear stress ratio) with Bingham model for second run of Experiment A at the 5 min time stamp.

Observing these results, both in Table 5.2 and Figure 5.3, it possible to notice the inadequacy of the rheology measures for Experiment A. In fact, for both runs the Bingham model computation of the plastic viscosity does not match the measured values (more detailed information can be found in Annex A). This is the main reason that motivated us to abandon Experiment A, and to try Experiment B. Analyzing Figure 5.2 we can highlight that the inadequacy occurs by the fact that we have the measured shear stress decreasing and then increasing again as the shear rate increases. In contrast, the Bingham model results shows the shear stress increasing as the shear rate increases. This also happened for the other time stamps, and, therefore, we conclude that the behavior does not fit with Bingham model, that is suitable to describe steady state behavior of fresh cement paste. Consequently, we concluded that Experiment A protocol is not suitable for rheology measures.

Furthermore, we believed the use of a small syringe was inadequate because it limited the overall time of experiment, due to the limitation of amount of material. Therefore, we propose to change the preservation method replacing the preservation in the small syringe for placing the cement paste directly over the rheometer plates, which led us to Experiment B.

5.2. Experiment B

This experiment consists in the preservation method P1, shear strain sequence S1, time stamps of 5, 20, 35, and 50 minutes, rheometer hood open, and no cement paste footprint analysis. Experiment B was performed twice, therefore the results are always presented for both runs. Figure 5.4 shows the shear stress curves obtained for the first 60 seconds after the shear strain sequence was started.

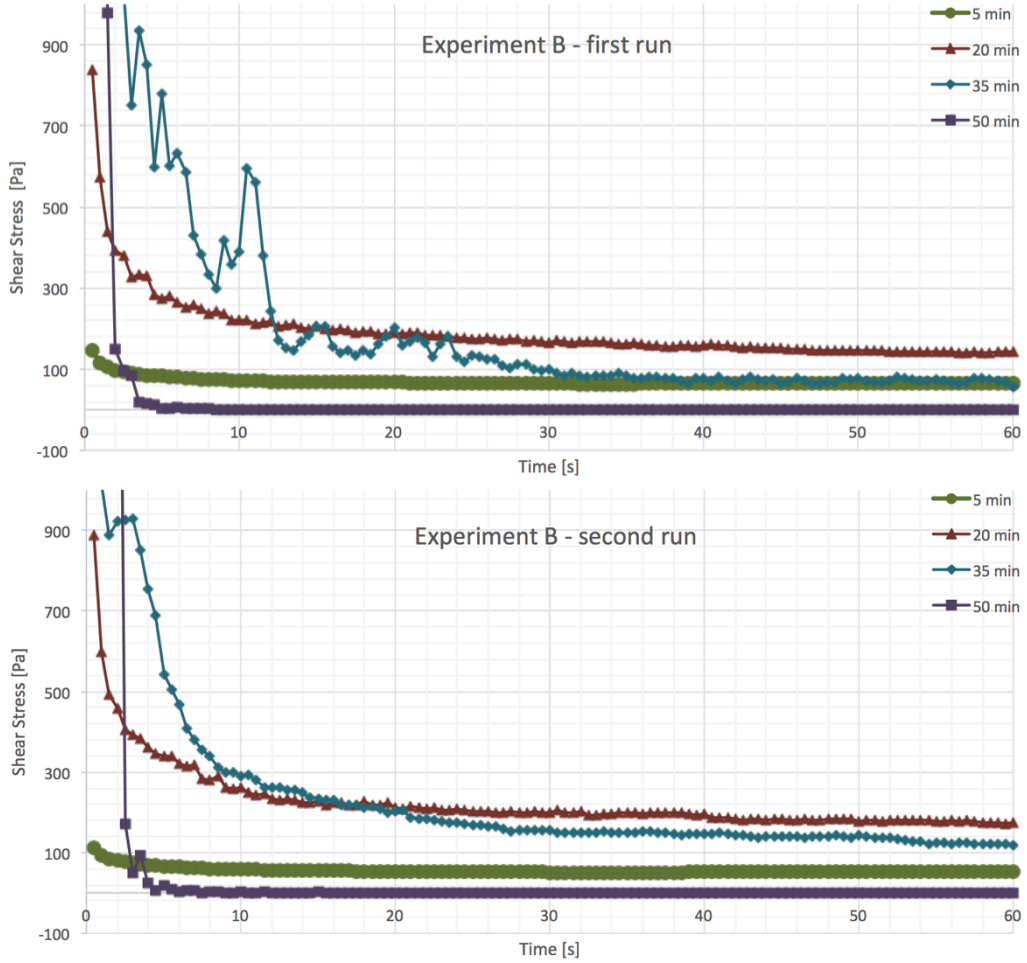

Fig. 5.4. Shear stress for both runs of Experiment B.

It is noticeable that all curves in Figure 5.4 show a steady state convergence, this convergence can also be observed by the average values of the last four results, as well as the standard deviation shown in Table 5.3. To reach the steady state convergence is important to guarantee that the transitional phase at the beginning passes and the samples achieve a reference state, so that the next measurements at various shear rates can be assumed to be done at the destructed state of the material.

Tab. 5.3. Shear stress steady state for both runs of Experiment B.

run	time stamp	shear stress last four values average	std dev	run	time stamp	shear stress last four values average	std dev
1st	5	64.54	0.13	2nd	5	53.85	0.22
	20	141.90	0.80		20	173.83	1.39
	35	66.85	7.81		35	121.53	1.35
	50	38.23	0.00		50	0.01	0.19

It is also noticeable that the shear rate curves do not follow the expected order of the time stamps. For instance, the 50 mins time stamp values are the lowest ones, which differs considerably from Experiment A, and the second lowest results are the ones for the 5 mins stamp.

Analyzing the obtained results for experiment B we obtain the flow curves presented in Figure 5.5. Analogously to Experiment A results, these curves represent the ratio between the shear stress measured in the rheometer at each time stamp by the shear rate imposed in a set of curves. We can see that the lower values of shear stresses from all time time stamps are reached at different shear rates, and that illustrates how the Experiment B results are not reliable.

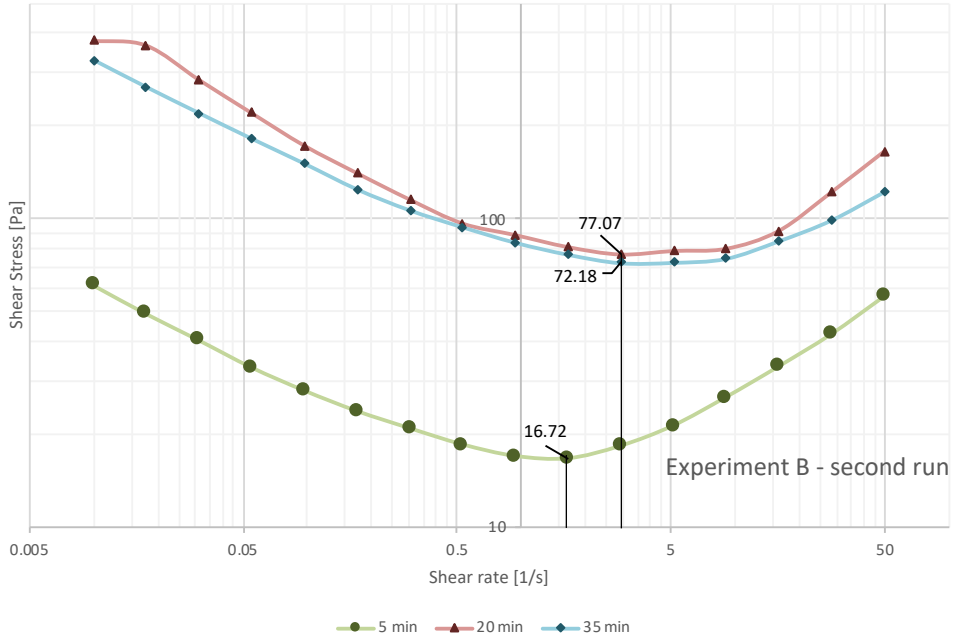

Fig. 5.5. Flow curves (shear rate and shear stress ratio) for time stamps 5, 20, and 35 mins of the second run of Experiment B.

Applying the Bingham model to the obtained results for experiment B we obtain Table 5.4, the numerical values for the Bingham model computation. Focusing on the 5 min time stamp, we obtain in Figure 5.6 the flow curve representing the ratio between the shear stress computed using the Bingham model at each time stamp by the shear rate imposed.

Tab. 5.4. Numerical values of Bingham model for both runs of Experiment B.

time stamp	1st run dynamic yeld stress (τ_0)	2nd run dynamic yeld stress (τ_0)	1st run plastic viscosity (μ)	2nd run plastic viscosity (μ)
5	48.153	28.203	0.128	0.479
20	132.817	160.031	0.000	0.000
35	68.189	134.886	0.000	0.000
50	0.005	0.095	0.000	0.000

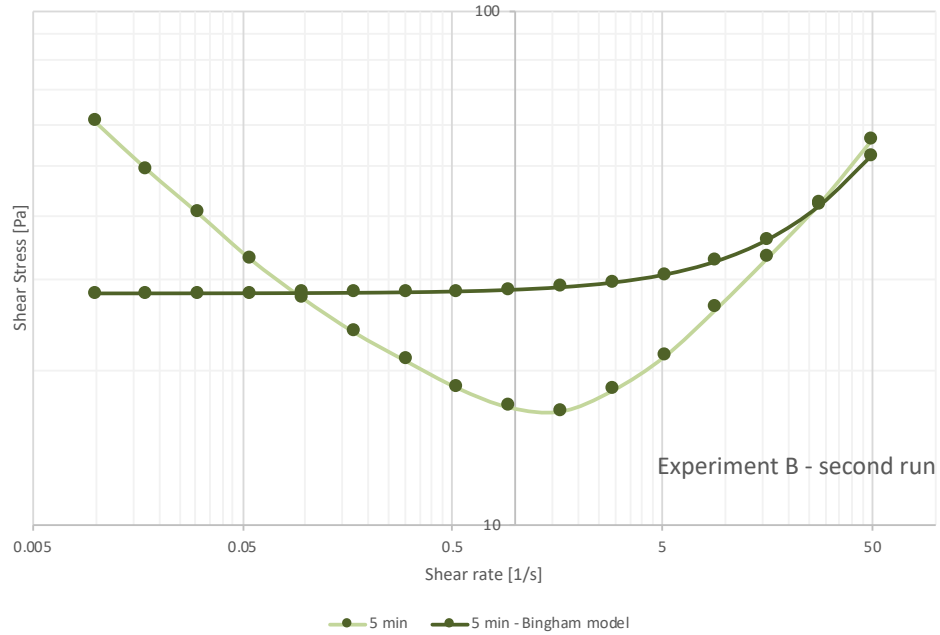

Fig. 5.6. Flow curve (shear rate and shear stress ratio) for time stamp 5 min of the second run of Experiment B and the Bingham model prediction.

Observing these results, both in Table 5.4 and Figures 5.5 and 5.6 it is possible to notice the inadequacy of the rheology measures also for Experiment B. In fact, for both runs the Bingham model computation of the plastic viscosity does not match the measured values, with a particularly strange result for the 50 minutes time stamp showed in Figure 5.7. The strange result is probably due to the hardening of the cement paste, which makes the rheometer measures the friction at the interface, giving us, therefore, a meaningless result. This is the main reason that motivated us to abandon Experiment B and to try Experiment C.

Once again we have for time stamps 5, 20, and 35 the measured shear stress fluctuation as the shear rate increases (Figure 5.5). The Bingham model mismatch for Experiment B is similar to what happened for Experiment A as can be seen for the time stamp 5 minutes depicted in Figure 5.6. For time stamp 50, however, the variation was very erratic demonstrating the total corruption of the samples after 50 minutes, as depicted in Figure 5.7.

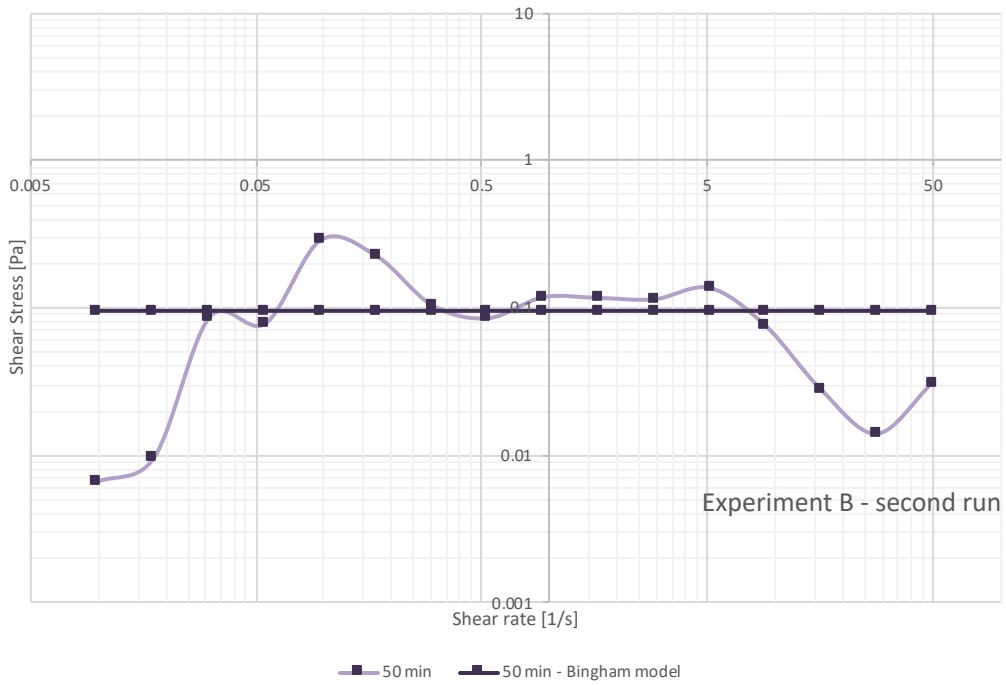

Fig. 5.7. Flow curve (shear rate and shear stress ratio) for time stamp 50 min of the second run of Experiment B.

The detached low values for the 50 minutes time stamp presented very low viscosity, and that could also be seen visually by the condition of the sample after the end of the test, and explained by the not-welcomed hardening of the paste. At Figure 5.8 we can notice the difference from the sample after testing at 5 and 50 min time stamps.

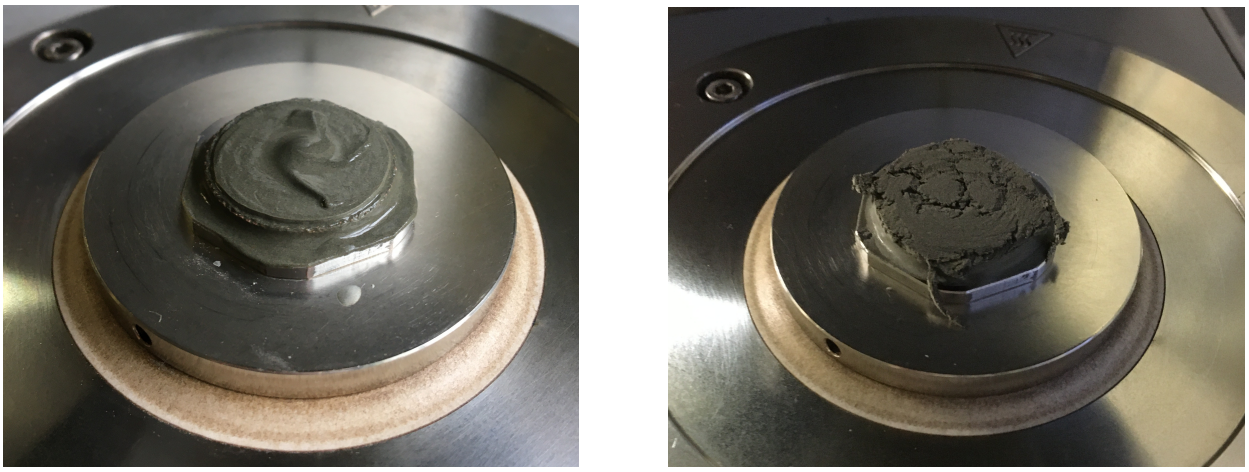

Fig. 5.8. Samples at the rheometer just after the testing. At left: at 5 min time stamp; At right: at 50 min time stamp.

In Figure 5.9 is presented the shear rate applied for six minutes (360 seconds) and the resulting viscosity at each time stamp for both runs of Experiment B. It is once again noticeable the detached and erratic lowest values for the 50 minutes time stamp values and a non convergence of its viscosity values, but as general rule for the other time stamps, as expected, the viscosity increases as the shear rate drops.

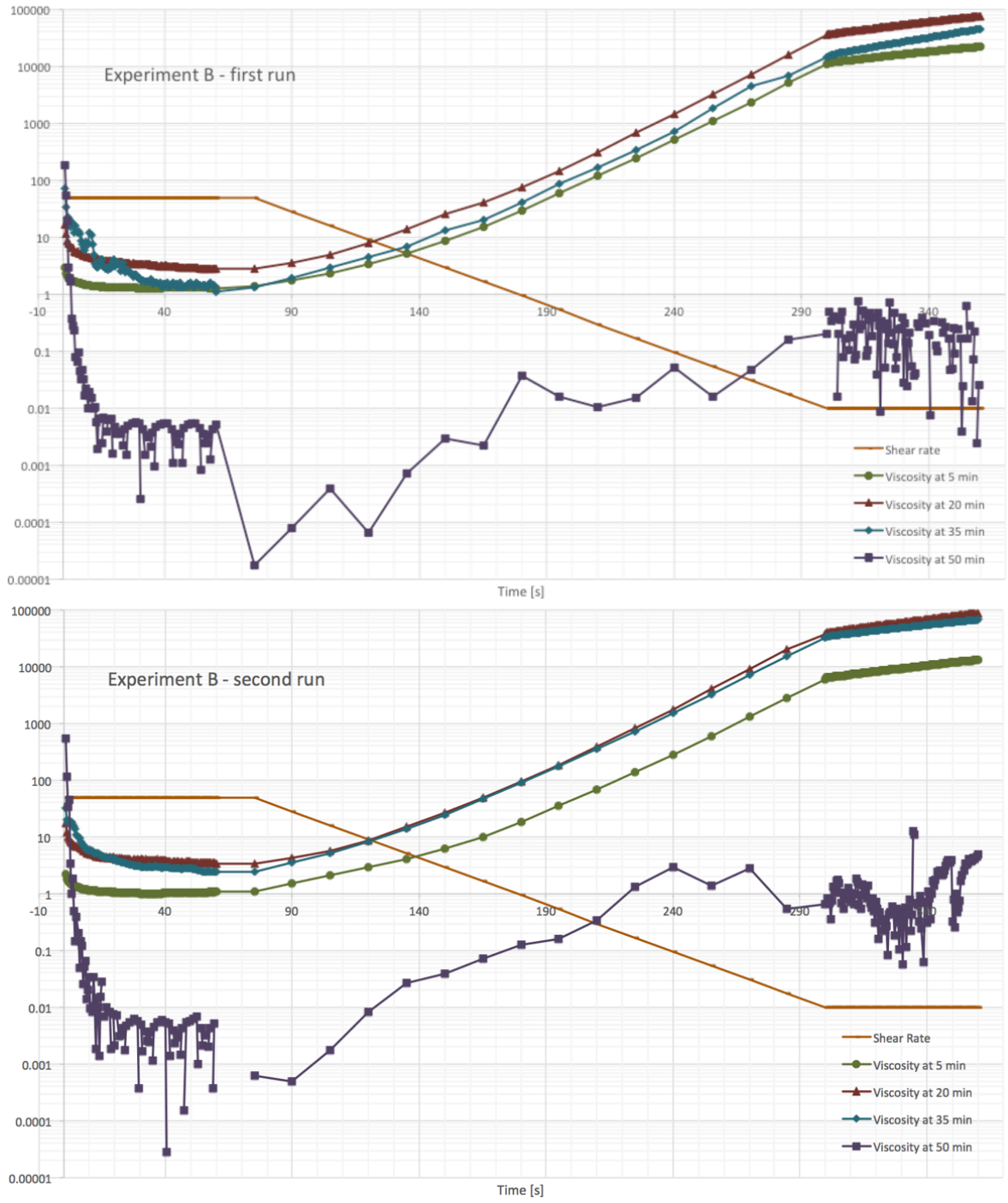

Fig. 5.9. Shear rate and viscosity over time for both runs of Experiment B.

We can notice a non-linear behavior presented in the viscosity measurement resulted in Figure 5.9 when we have the strain rates changing logarithmically from 50 to 0.05 s-1, specially at the 35 min time stamp of Experiment B first run. The reason for this anomaly is probably due to a stress history affecting the sample. After that, the strain rate decreases logarithmically until reach the rate of 0.05 s-1 and we have a step with a constant shear rate. The very low shear rate allows the cement paste to built up, therefore consistent with the increase of the viscosity and the shear stress.

After observing all numerical results from Experiment B we concluded for the inadequacy of the experiment because of the discrepancy in the flow curves and the weird shear rate and viscosity measures. Furthermore, to prepare the cement paste repeatedly at each time stamp is a procedure prone to error and even the literature observation have some reservations about this preparation method, as stated by Ivanova and Mechtcherine (2020): “A comparison between single- and multi-batch approaches showed that the structural build-up rate of both cement paste and mortar did not undergo significant changes. Therefore, single batch of material can be used for its evaluation, ensuring both time efficiency of experiments and reliable results.”.

In consequence, we return to the use of a small syringe as preservation method, but we changed the shear strain sequence from the logarithmic decreasing (S1) to the sequence alternating high and low strains (S2). We decide to do that seeking a better match of the Bingham model with the measured flow curve and the ratio between the shear stresses measured by the shear rates imposed.

5.3. Experiment C

This experiment consists in the preservation method P2, shear strain sequence S2, time stamps of 5, 20, 40, and 60 minutes, rheometer hood open H1, and no cement paste footprint analysis. Unlike Experiments A and B, Experiment C was performed only once. Figure 5.10 shows the shear stress curves obtained for the first 60 seconds after the shear strain sequence started.

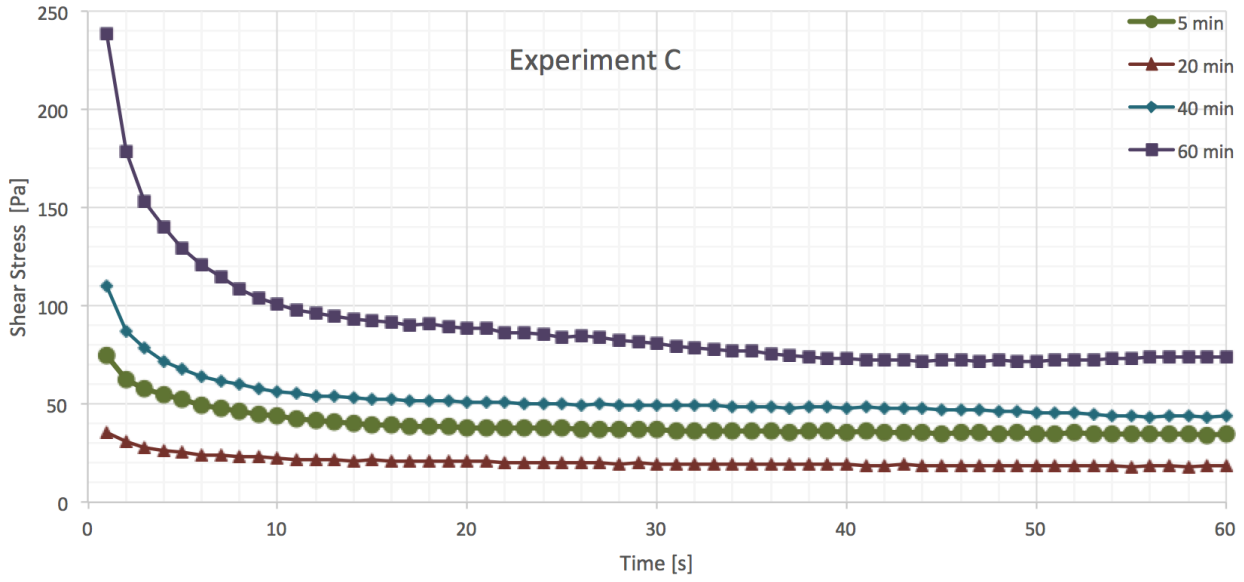

Fig. 5.10. Shear stress for Experiment C.

It is noticeable that all curves in Figure 5.10 show a steady state convergence, this convergence can also be observed by the average values of the last four results, as well as the standard deviation shown in Table 5.5. To reach the steady state convergence is important to guarantee that the transitional phase at the beginning passes and the samples achieve a reference state, so that the next measurements at various shear rates can be assumed to be done at the destructed state of the material.

It is also noticeable that the shear rate curve for the time stamp 20 minutes is the lowest, which seems surprising, since a lower shear stress was expected for the 5 minutes time stamp curve.

Tab. 5.5. Shear stress steady state for Experiment C.

time stamp	shear stress last four values average	std dev
5	34.60	0.21
20	38.23	0.00
40	43.67	0.20
60	74.20	0.30

Applying the Bingham model to the obtained results for experiment C we obtain the flow curves presented in Figure 5.11. These curves represent the ratio between the shear stress measured in the rheometer at each time stamp by the shear rate imposed in a set of curves, and by the shear stress computed using the Bingham model. Table 5.6 presents the numerical values for the Bingham model computation.

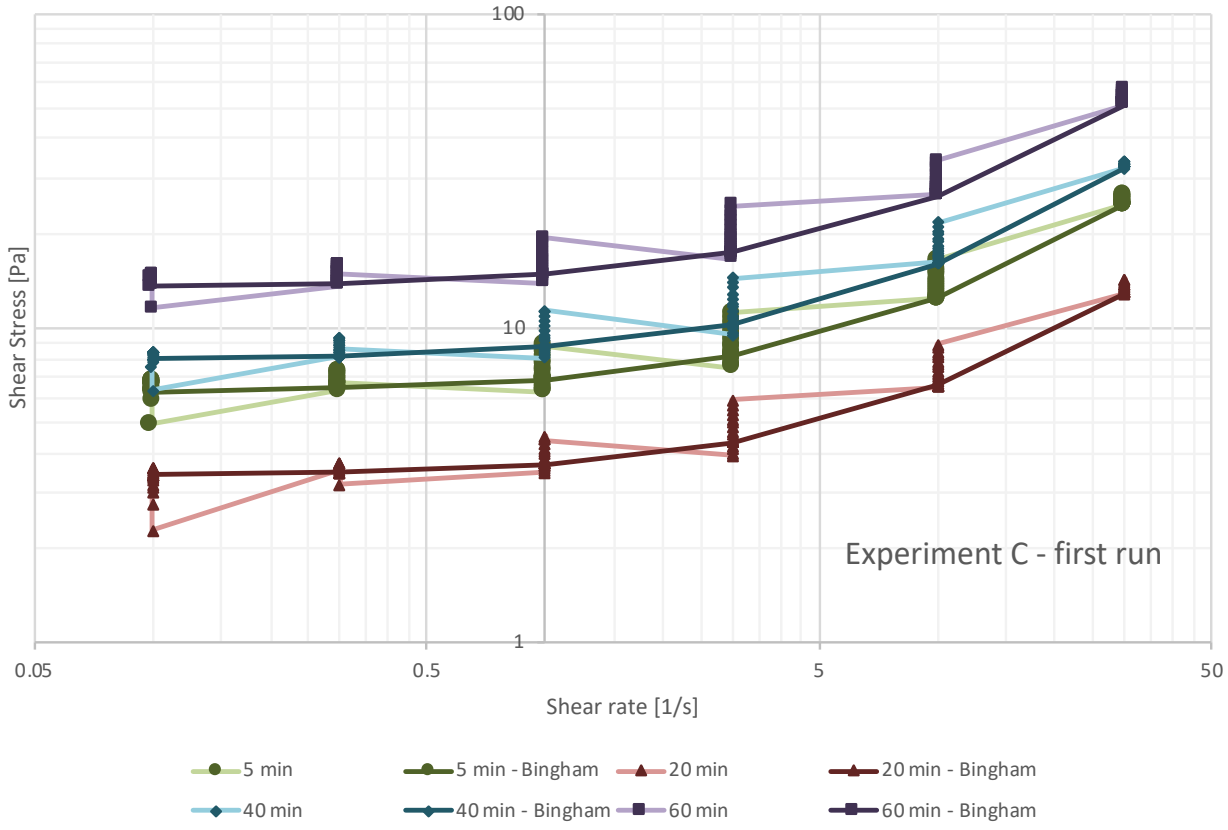

Fig. 5.11. Flow curves (shear rate and shear stress ratio) for Experiment C.

Tab. 5.6. Numerical values of Bingham model for Experiment C.

time stamp	dynamic yield stress (τ_0)	plastic viscosity (μ)
5	6.234	0.614
20	3.368	0.320
40	7.859	0.822
60	13.579	1.267

Observing the results both in Table 5.6 and Figure 5.11 we notice a better adequacy than the one for Experiments A and B. In fact, there was a welcomed coincidence on the obtained values, as we can notice that the Bingham model fits well with the measured values. With the sequence alternating high and low strains (S2) we get, as expected, the increase of the shear rate corresponding to the increase of the shear stress, and we are also able to monitor it at each shear rate step.

Carrying on the gathering of numerical results for Experiment C, Figure 5.12 shows the viscosity versus the shear rate. Table 5.7 presents the numeric values plotted in Figure 5.12. In those results we can see a thixotropy behavior as the apparent viscosity of the cement paste shows a progressive decrease in time, while the change of level of shear rate is imposed.

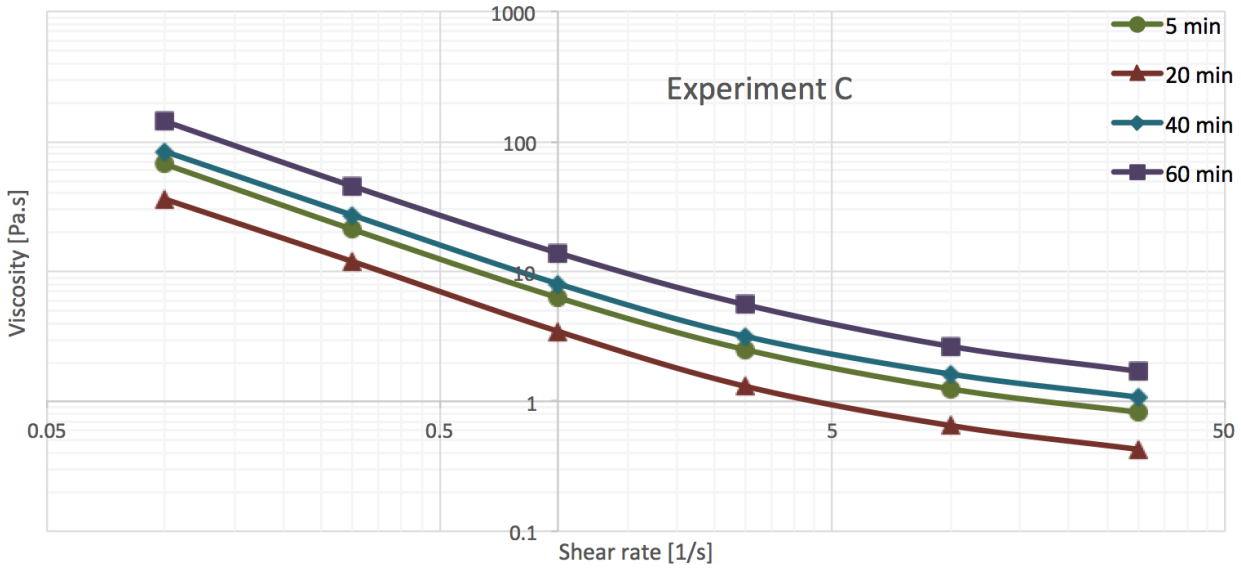

Fig. 5.12. Viscosity over shear rate for Experiment C.

Tab. 5.7. Viscosity over shear rate values for Experiment C.

Shear rate	5 min	20 min	40 min	60 min
30.0	0.8	0.4	1.1	1.7
10.0	1.2	0.7	1.6	2.7
3.0	2.5	1.3	3.2	5.6

Shear rate	5 min	20 min	40 min	60 min
1.0	6.3	3.5	8.0	13.9
0.3	21.1	11.9	27.1	45.3
0.1	66.8	36.0	83.7	142.9

In Figure 5.13, it is presented the shear rate applied for almost four minutes (225 seconds) and the resulting viscosity at each time stamp for Experiment C. As expected, the viscosity increases as the shear rate drops for all time stamps. Table 5.8 presents the numerical values shown in Figure 5.13.

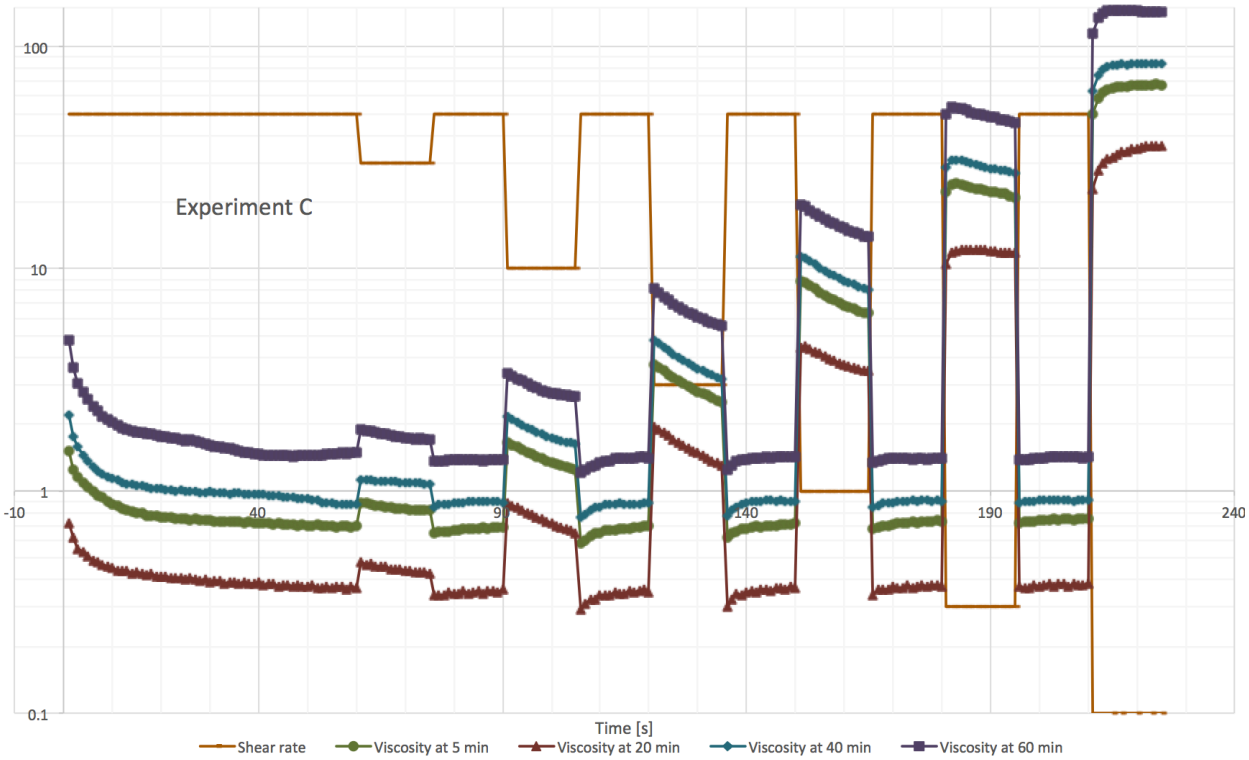

Fig. 5.13. Shear rate and viscosity over time for Experiment C.

As the steady state viscosity of cement pastes depends on strain rate, Bingham model is a suitable model to evaluate this behavior. Applying shear rate step tests we noticed a better match between Experiment C measures and the Bingham model results. We can notice the structure breakdown (destructuration), with small values of viscosity, when we have constant high shear rate of 50 s-1, and a structure built-up (structuration), with bigger values of viscosity, when we have constant lower values at each step of the shear rate.

The alternation between the constant high shear rate of 50 s-1 to constant lower values at each step of the shear rate are important for two main reasons. The first reason is that the application of the high shear rate for long enough ensure that all steps of lower shear rates start from a steady state of the material. The second reason is that with the values of apparent viscosity results at each step of high shear rate allow us to verify if the sample is changing in time. As we

can observe at Table 5.8, the results kept at a small range of variation, which is positive, guaranteeing the good preservation of the sample inside the rheometer.

Tab. 5.8. Shear rate and apparent viscosity over time values for Experiment C.

time	shear rate	apparent viscosity 5 min	apparent viscosity 20 min	apparent viscosity 40 min	apparent viscosity 60 min
60	50.0	0.69	0.37	0.88	1.49
75	30.0	0.82	0.43	1.08	1.71
90	50.0	0.68	0.36	0.89	1.39
105	10.0	1.25	0.65	1.62	2.65
120	50.0	0.70	0.35	0.88	1.41
135	3.0	2.50	1.31	3.17	5.55
150	50.0	0.72	0.37	0.90	1.42
165	1.0	6.29	3.46	8.04	13.89
180	50.0	0.73	0.37	0.90	1.40
195	0.3	21.07	11.93	27.09	45.34
210	50.0	0.75	0.38	0.90	1.43
225	0.1	66.84	35.97	83.70	142.90

Observing all numerical results from Experiment C we concluded that there was a considerably better adequacy verified in the flow curves, but still the cement paste hardening, due to preservation method P2, prevents us to carry on the measures to larger time stamps. This can be noticed for example for the high values of viscosity for all time stamps. Illustrates that the fact that for the 60 mins time stamp the viscosity reached the impressive value of 142. Motivated by this, we decided to change the preservation method to a large syringe (50ml) and to keep the hood closed during the testing, to ensure no air circulation, and so to prevent the hardening of the paste. This brought us to Experiment D where we also started performing a footprint analysis of the cement paste.

5.4. Experiment D

This experiment consists in the preservation method P3, shear strain sequence S2, time stamps of 5, 20, 40, 60, and 80 minutes, rheometer hood closed H2, and cement paste footprint F1, with density analysis starting at time stamp 20, and quantity of water at all time stamps. As Experiment C, Experiment D was performed only once. Figure 5.14 shows the shear stress curves obtained for the first 60 seconds after the shear strain sequence was started.

It is noticeable that all curves in Figure 5.14 show a steady state convergence, this convergence can also be observed by the average values of the last four results, as well as the standard deviation shown in Table 5.9. To reach the steady state convergence is important to guarantee that the transitional phase at the beginning passes and the samples achieve a reference state,

so that the next measurements at various shear rates can be assumed to be done at the destructed state of the material. It is also noticeable that the shear rate curve for the time stamp 20 mins is the lowest, followed by the 60 mins one, which seems surprising, since a lower shear stress was expected for the 5 minutes time stamp curve.

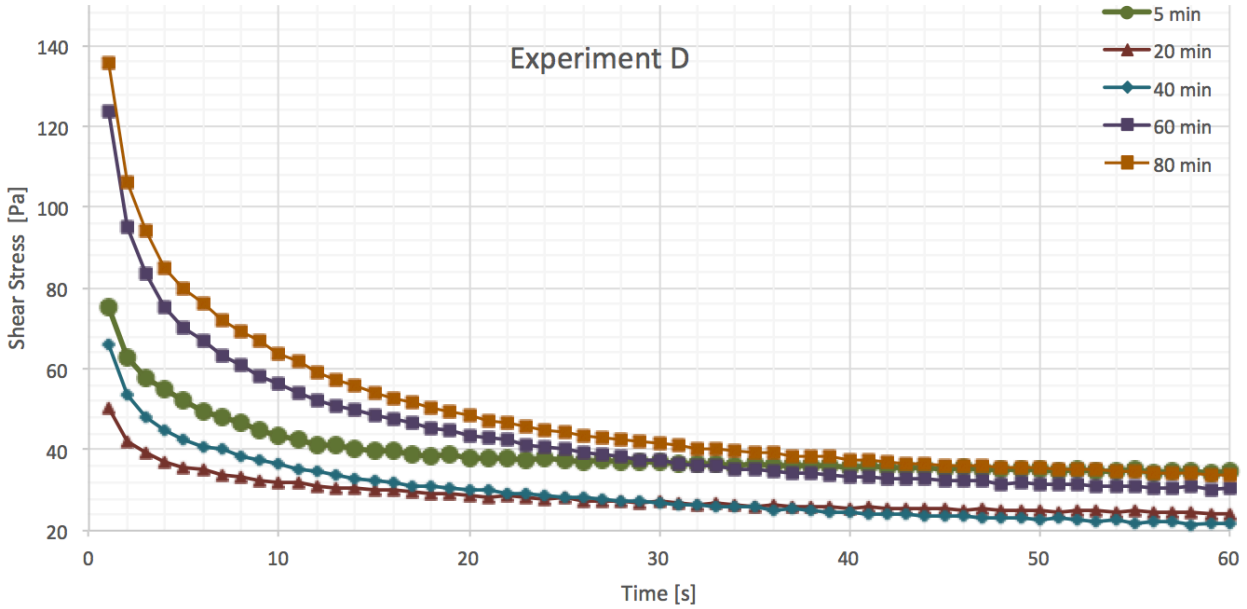

Fig. 5.14. Shear stress for Experiment D.

Tab. 5.9. Shear stress steady state for Experiment D.

time stamp	shear stress last four values average	std dev
5	39.30	0.29
20	24.35	0.20
40	38.23	0.00
60	30.55	0.26
80	33.89	0.29

Applying the Bingham model to Experiment D's results we obtain the flow curves presented in Figure 5.15. These curves represent the ratio between the shear stress measured in the rheometer at each time stamp and by the shear stress computed using the Bingham model. Table 5.10 presents the corresponding numerical values for the Bingham model computation.

Observing these results, both in Table 5.10 and Figure 5.15, we notice an adequacy similar to the one of Experiment C for 5 and 20 min. Again, there was a welcomed coincidence on the obtained values fitting with the Bingham model, as it is happening the model's expected behavior, since while the shear rate is decreasing, also the shear stress decreases. With the sequence alternating high and low strains (S2) we also are able to monitor what is happening at each shear rate step.

Tab. 5.10. Numerical values of Bingham model for Experiment D.

time stamp	dynamic yield stress (τ_0)	plastic viscosity (μ)
5	6.704	0.711
20	4.269	0.428
40	3.367	0.381
60	4.452	0.547
80	4.949	0.595

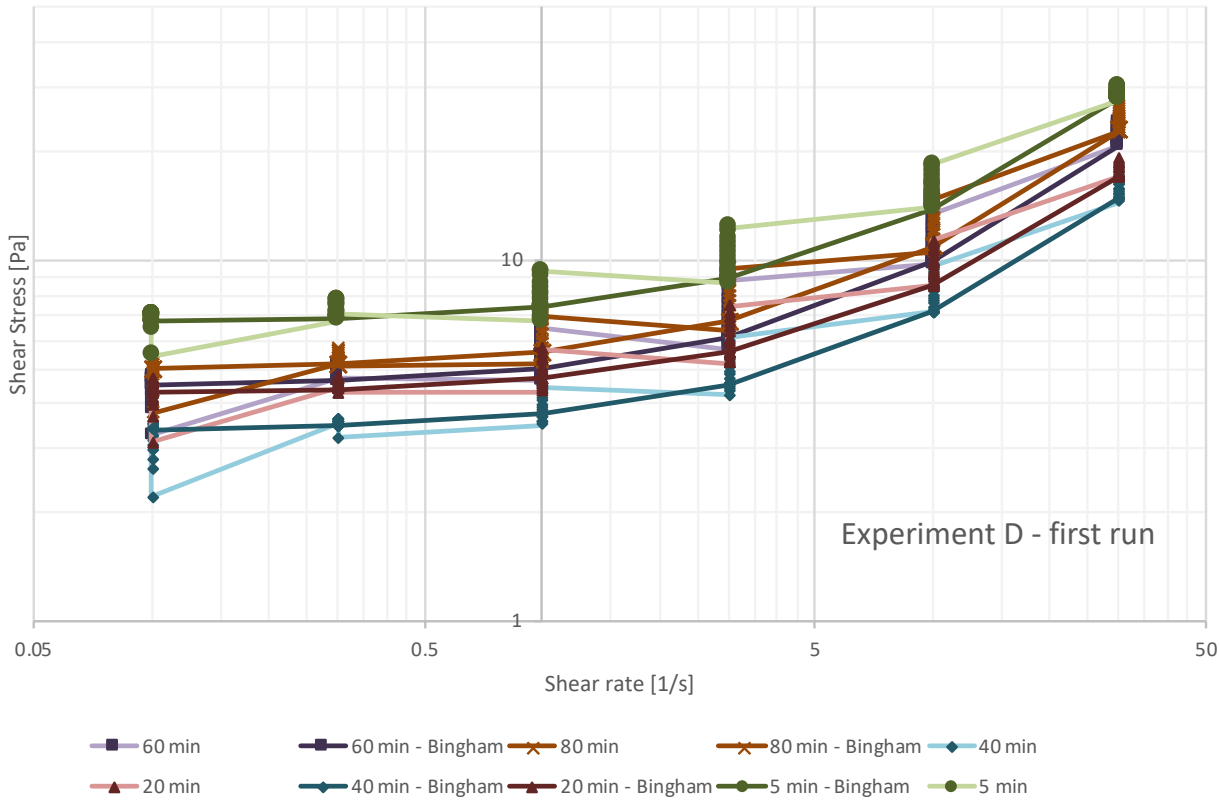

Fig. 5.15. Flow curves (shear rate and shear stress ratio) for Experiment D.

Carrying on the gathering of numerical results for Experiment D, Figure 5.16 shows the viscosity versus the shear rate. Table 5.11 presents the numeric values plotted in Figure 5.16. In fact, these results show a coincidence with Experiment C for 5 and 20 min time stamps. We can also see a thixotropy behavior as the apparent viscosity of the cement paste has a progressive decrease in time while the change of level of shear rate is imposed.

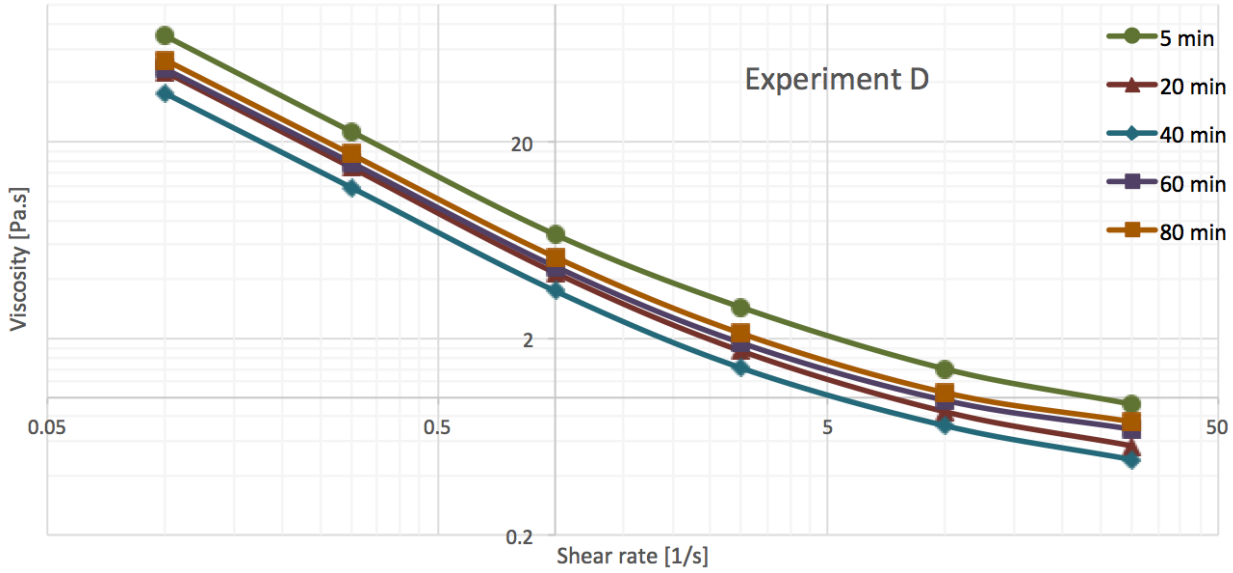

Fig. 5.16. Viscosity over shear rate for Experiment D.

Tab. 5.11. Viscosity over shear rate values for Experiment D.

Shear rate	5 min	20 min	40 min	60 min	80 min
30	0.9265	0.5686	0.4841	0.6907	0.7539
10	1.398	0.8463	0.7188	0.9679	1.059
3	2.877	1.725	1.414	1.897	2.119
1	6.76	4.315	3.49	4.643	5.187
0.3	22.63	14.85	11.74	15.71	17.33
0.1	69.49	45.53	35.44	47.18	52.43

In Figure 5.17 it is presented the shear rate applied for almost four minutes (225 seconds) and the resulting viscosity at each time stamp for Experiment D. As expected, the viscosity increases as the shear rate drops for all time stamps. Table 5.12 presents the numerical values shown in Figure 5.17. We notice the structure breakdown and built-up as we saw for Experiment C due to the shear rate steps tests, but we also noticed the lesser viscosity values that seemed to justify our changes from Experiment C to Experiment D.

Analyzing Table 5.12, again we can notice the importance of the alternation between the constant high shear rate (50 s-1) and the constant lower values at each step of the shear rate. The application of the high shear rate is sustained long enough to ensure that all steps of lower shear rates start from a steady state of the material. Following this pattern we can see that the sample always reach more or less the same viscosity value at shear rate of 50 s-1, guaranteeing that the sample is not changing in time due to the good preservation inside the rheometer, and, therefore, confirming that the hood position closed (H2) is effective.

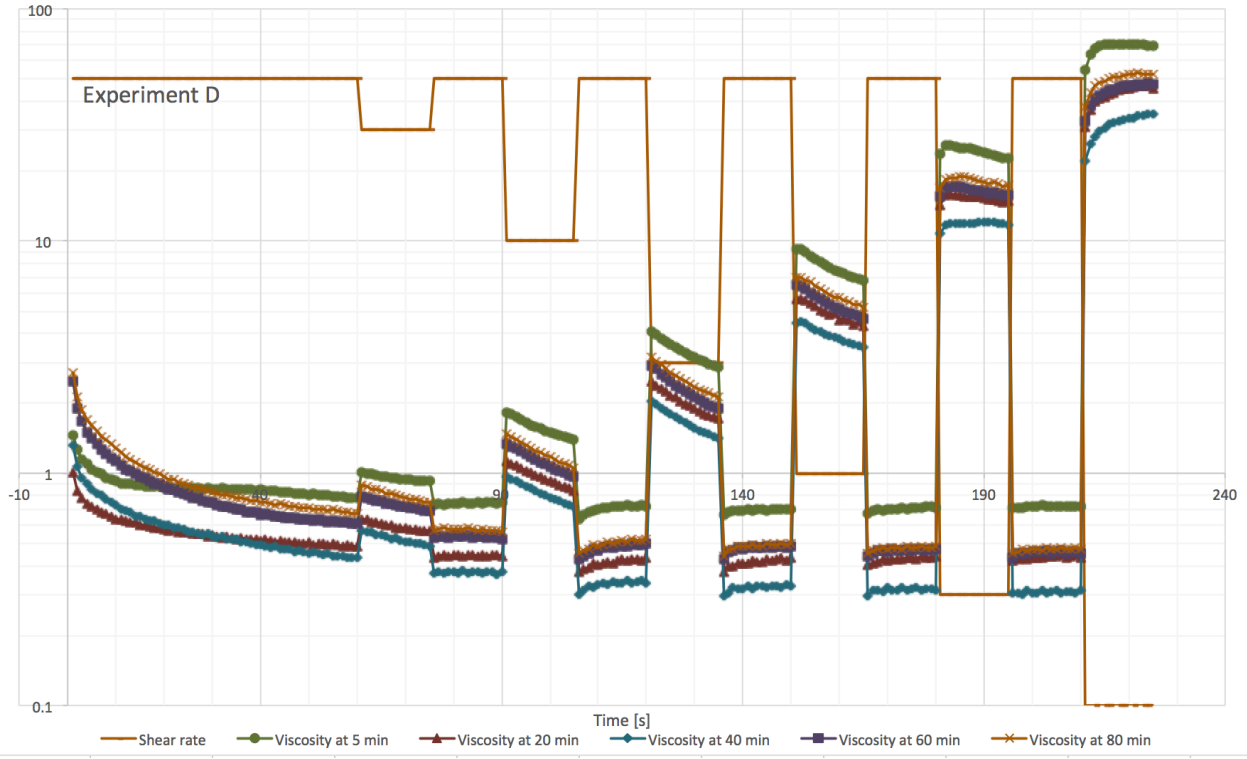

Fig. 5.17. Shear rate and viscosity over time for Experiment D.

Tab. 5.12. Shear rate and apparent viscosity over time values for Experiment D.

time	shear rate	apparent viscosity 5 min	apparent viscosity 20 min	apparent viscosity 40 min	apparent viscosity 60 min	apparent viscosity 80 min
60	50.0	0.78	0.49	0.43	0.61	0.67
75	30.0	0.93	0.57	0.48	0.69	0.75
90	50.0	0.75	0.44	0.38	0.52	0.56
105	10.0	1.40	0.85	0.72	0.97	1.06
120	50.0	0.72	0.43	0.34	0.50	0.52
135	3.0	2.88	1.73	1.41	1.90	2.12
150	50.0	0.70	0.43	0.32	0.48	0.50
165	1.0	6.76	4.32	3.49	4.64	5.19
180	50.0	0.71	0.44	0.31	0.47	0.49
195	0.3	22.63	14.85	11.74	15.71	17.33
210	50.0	0.72	0.44	0.31	0.45	0.47
225	0.1	69.49	45.53	35.44	47.18	52.43

For Experiment D the paste footprint was analyzed by the measurement of quantity of water and density of the sample. In such way, it was measured the quantity of water in all time stamps (5 to 80 mins). It was also analyzed the density of the sample at time stamps 20, 40, 60, and 80 mins. Finally, an analysis of the degased sample was performed one single time at the 20 time stamp. Figure 5.18 depicts the results of the quantity of water analysis and in Table 5.13 the numerical values for all footprint analysis are informed.

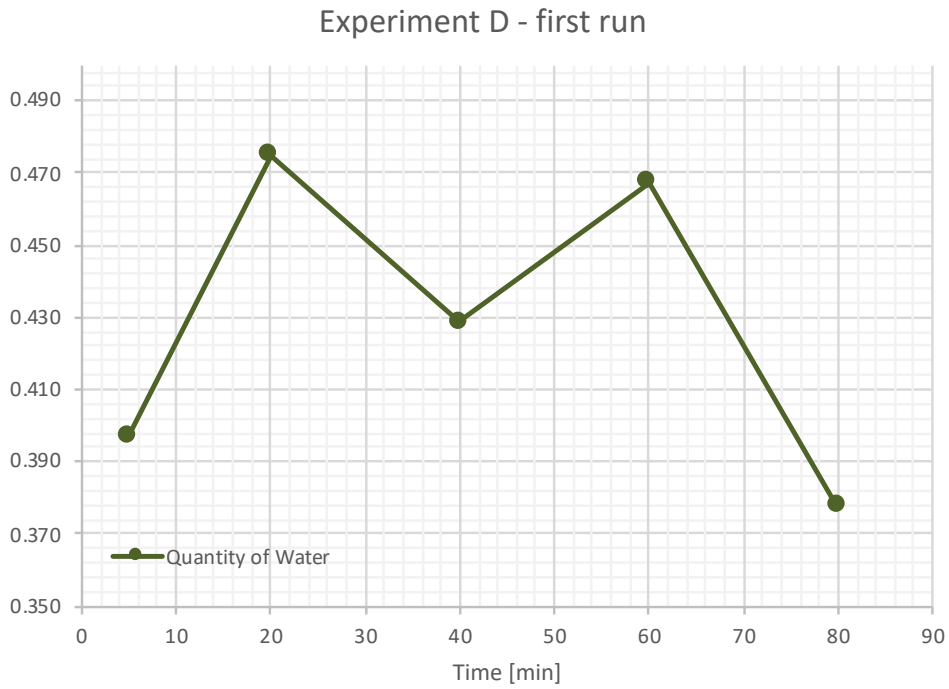

Fig. 5.18. Quantity of water paste footprint results for Experiment D.

Tab. 5.13. Paste footprint values for Experiment D.

measure	5 min	20 min	40 min	60 min	80 min
Quantity of water %	40%	47%	43%	47%	38%
Density of Degased Sample [Mg/m3]		1.905			
Density Sample [Mg/m3]		1.938	1.920	2.459	2.863

Observing all the numerical results for Experiment D it is possible to notice an improvement from the previous experiments (A, B, and C). However, analyzing the results from Table 5.13, we notice inconsistent values of quantity of water, that fluctuates between 38% and 47%. Even if we hypothesized that the densities of the sample were increasing as the water percentage decreases, the hypothesis does not hold as true because the density of the degased sample is lower than all the values of density of the original sample. It is important to mention that it is expected to have a degased sample with a higher density than the original sample.

These inconsistencies in terms of paste footprint were seen by the numerical values and by physical observation as we perceived some segregation of the mixture during the experiment. Those facts led us to believe that, despite the benefits of using a larger syringe, the preservation

method P3 could not prevent the segregation of the material well enough. Therefore, the results are not reliable as we cannot guarantee that these values come from a homogenized mixture, but due to different phases, either more watery or more hardened mixture.

To confirm that hypothesis, we tried to change the shear strain sequence again, from S2 to S3 for Experiment E. Shear sequence S2 goes from an initial high shear value to a final low value, characterizing an overall built up of the structure. Sequence S3, on the contrary, does not stop at the final low value, but performs an inverse procedure going from the last low value to the initial high value, characterizing also an overall structure breakdown. Therefore, with S3 we intent to confirm also the thixotropy of the structure. If the build up is reversible, we confirm a thixotropic behavior related to colloidal interactions, otherwise, we have permanent changes contributing to the structural build up, occurring due to the ridification of the C-S-H bridges created by the hydration of the cement paste, provoking a workability loss.

5.5. Experiment E

This experiment consists in the preservation method P3, shear strain sequence S3, time stamps of 5, 20, 40, 60, and 80 minutes, rheometer hood closed, and cement paste footprint F2, with density analysis at time stamp 20, and quantity of water at all time stamps. As Experiments C and D, Experiment E was performed only once. Figure 5.19 shows the shear stress curves obtained for the first 60 seconds after the shear strain sequence was started.

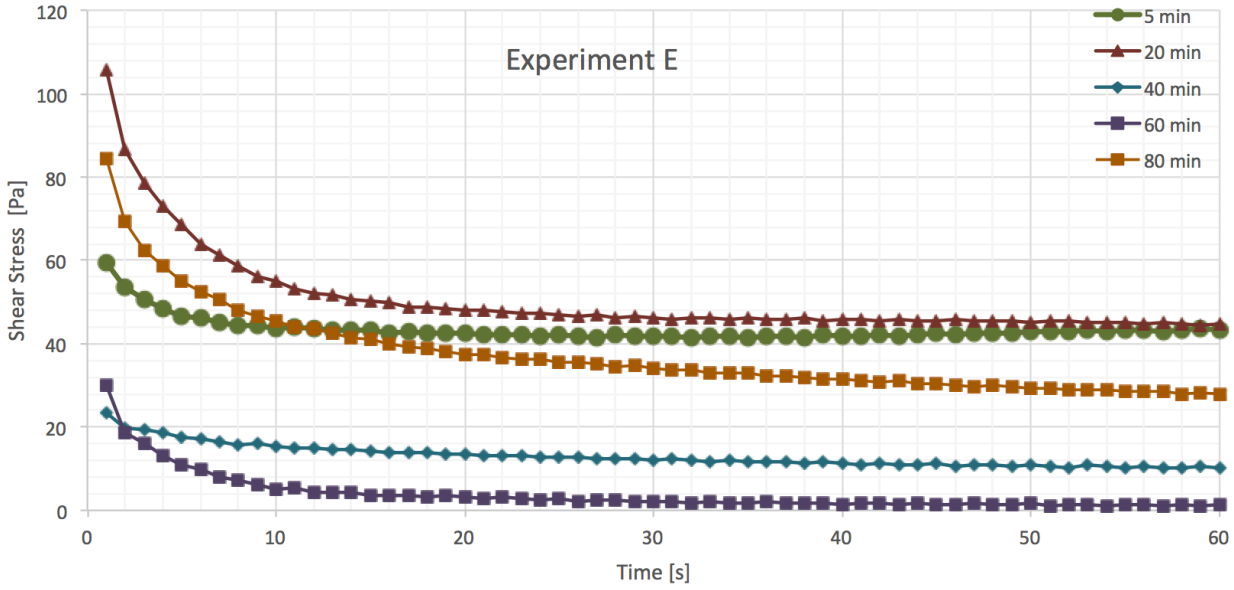

Fig. 5.19. Shear stress for Experiment E.

It is noticeable that all curves in Figure 5.19 show a steady state convergence, this convergence can also be observed by the average values of the last four results, as well as the standard deviation shown in Table 5.14. To reach the steady state convergence is important to guarantee that the transitional phase at the beginning passes and the samples achieve a reference state, so that the next measurements at various shear rates can be assumed to be done at the destructed state of the material. It is also noticeable that the shear rate curve for the time stamp 60 minutes is the lowest, followed by the one of 40 min, which seems surprising, since a lower shear stress was expected for the 5 mins time stamp curve.

Tab. 5.14. Shear stress steady state for Experiment E.

time stamp	shear stress last four values average	std dev
5	43.34	0.23
20	44.65	0.24
40	10.26	0.20
60	1.25	0.18
80	28.18	0.25

Applying the Bingham model to the obtained results for Experiment E we obtain the flow curves presented in Figure 5.20. These curves represent the ratio between the shear stress measured in the rheometer at each time stamp by the shear rate imposed in a set of curves, and by the shear stress computed using the Bingham model. Table 5.15 presents the numerical values for the Bingham model computation.

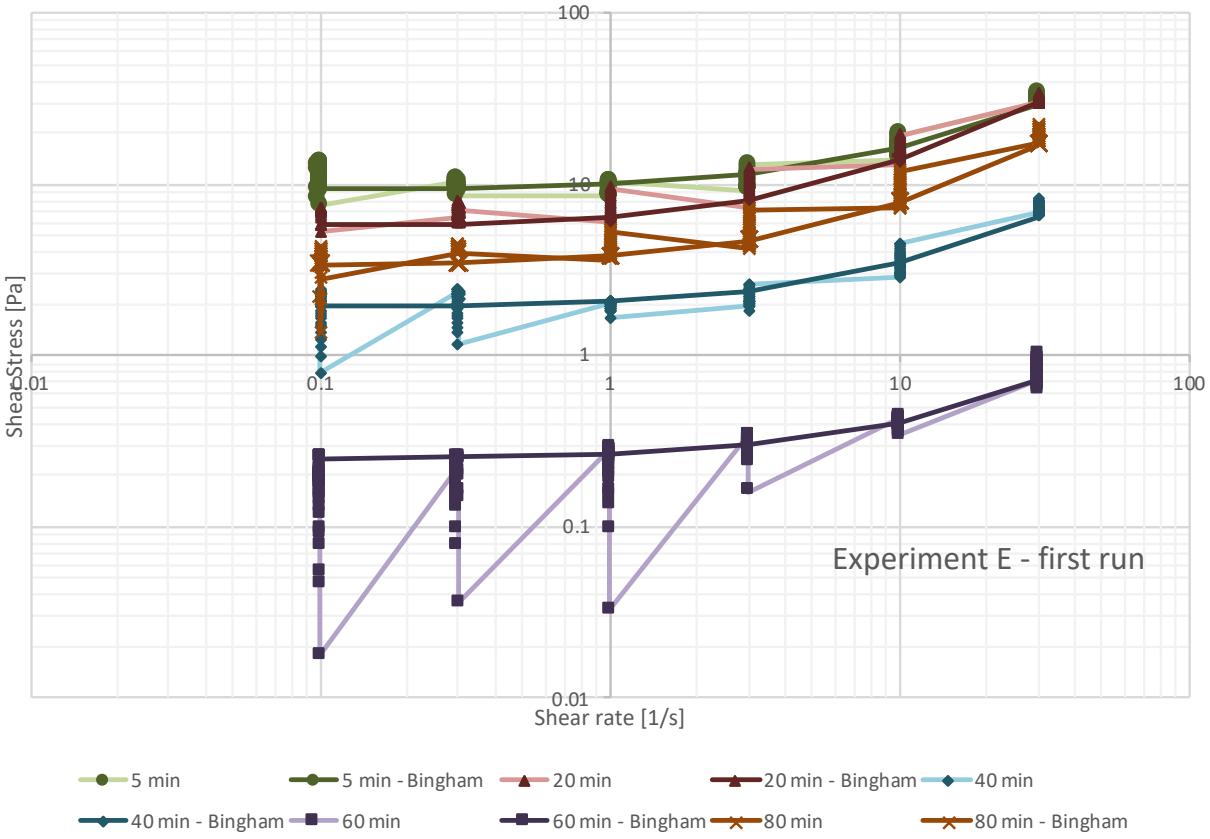

Fig. 5.20. Flow curves (shear rate and shear stress ratio) for Experiment E.

Analyzing the results from Table 5.15 and Figure 5.20, we notice an odd and detached behavior of the paste at 60 mins time stamp. The 60 mins time stamp curves show a much lower shear stress for low shear rates, but the other time stamps also show some less impacting but similar

behavior, as can be noticed clearly for 40 time stamp. This may be caused by the segregation of the mixture, resulting in a non-uniform mix caused by the way the preservation was made (P3).

Tab. 5.15. Numerical values of Bingham model for Experiment E.

time stamp	dynamic yield stress (τ_0)	plastic viscosity (μ)
5	9.331	0.673
20	5.678	0.800
40	1.926	0.153
60	0.250	0.016
80	3.332	0.456

Carrying on the gathering of numerical results for Experiment E, Figure 5.21 shows the viscosity versus the shear rate. We can see a thixotropy behavior as the apparent viscosity of the cement paste shows a progressive decrease in time while the change of level of shear rate is imposed. Table 5.16 presents the numeric values plotted in Figure 5.21. Again, we can notice the odd and detached behavior of the 60 min time stamp, and a less important, but similar behavior for the 40 min time stamp.

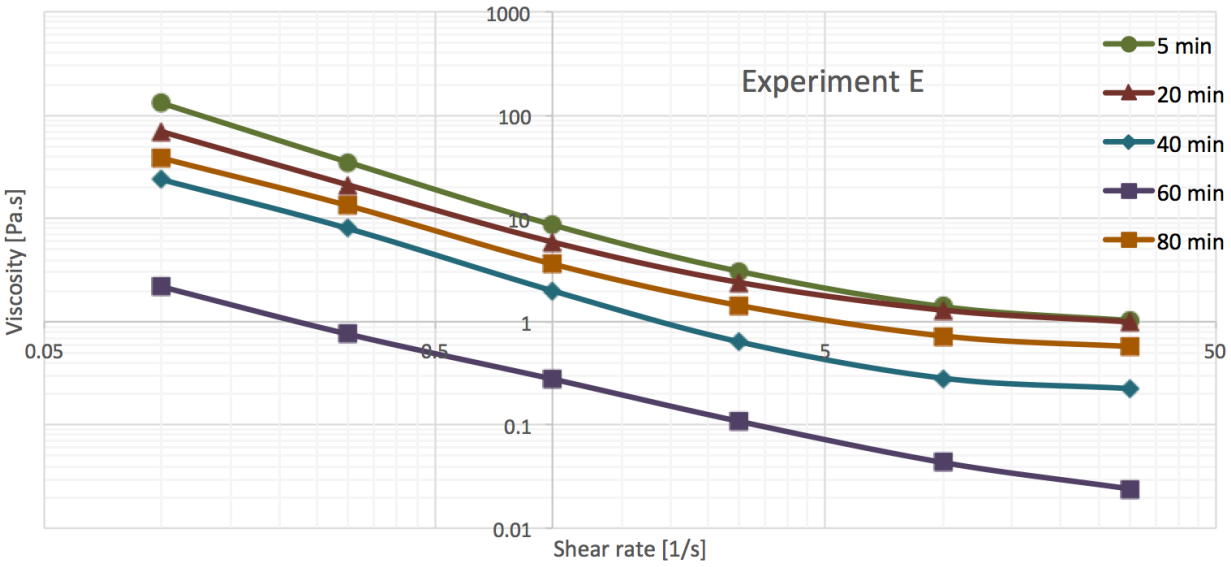

Fig. 5.21. Viscosity over shear rate for Experiment E.

Tab. 5.16. Viscosity over shear rate values for Experiment E.

Shear rate	5 min	20 min	40 min	60 min	80 min
30	1.019	0.996	0.225	0.024	0.571
10	1.401	1.295	0.284	0.042	0.721
3	3.081	2.406	0.640	0.114	1.395

Shear rate	5 min	20 min	40 min	60 min	80 min
1	8.684	5.922	1.997	0.279	3.625
0.3	35.080	21.130	7.990	0.758	13.310
0.1	130.900	69.300	23.790	2.176	38.430

Figure 5.22 presents the shear rate applied for almost eleven minutes (555 seconds) and the resulting viscosity at each time stamp for Experiment E. As expected, the apparent viscosity increases as the shear rate drops for all time stamps, but at the 60 mins time stamp the viscosity shows an odd behavior. Table 5.17 presents the numerical values shown in Figure 5.22.

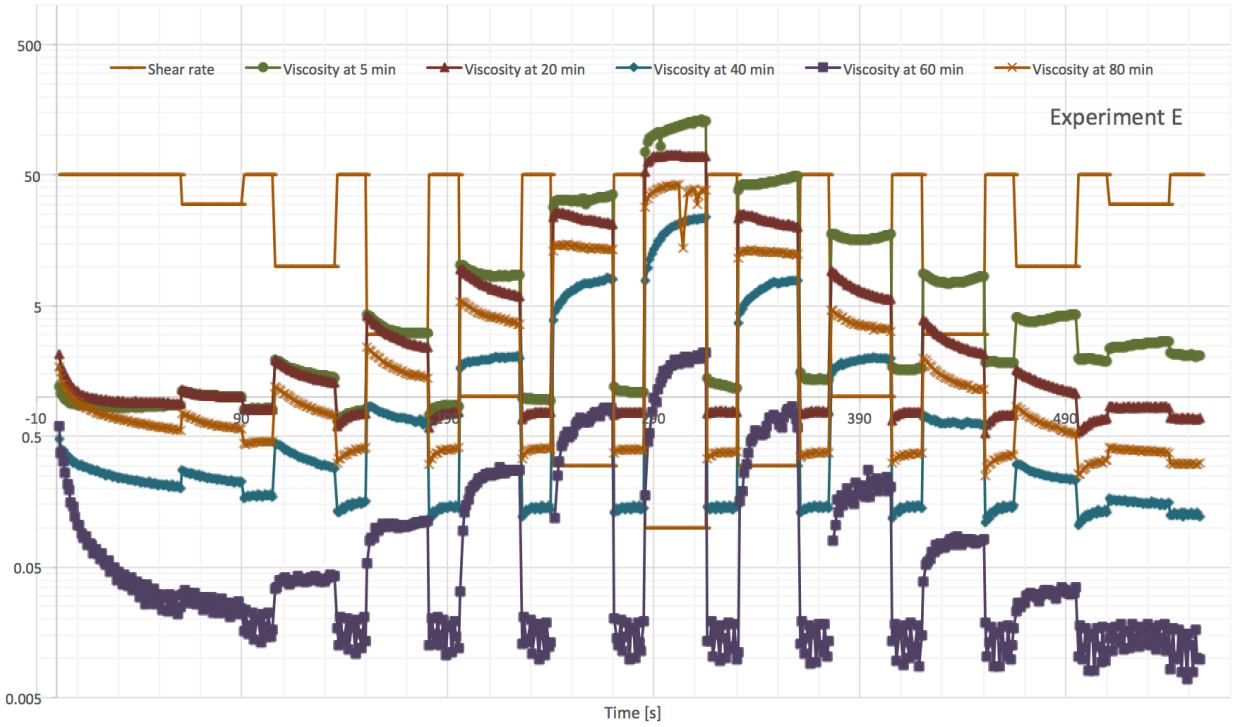

Fig. 5.22. Shear rate and viscosity over time for Experiment E.

Tab. 5.17. Shear rate and apparent viscosity over time values for Experiment E.

time	shear rate	apparent viscosity 5 min	apparent viscosity 20 min	apparent viscosity 40 min	apparent viscosity 60 min	apparent viscosity 80 min
60	50.0	0.87	0.89	0.20	0.02	0.56
90	30.0	1.02	1.00	0.23	0.02	0.57
105	50.0	0.81	0.81	0.17	0.02	0.46
135	10.0	1.40	1.30	0.28	0.04	0.72
150	50.0	0.80	0.75	0.16	0.01	0.41

time	shear rate	apparent viscosity 5 min	apparent viscosity 20 min	apparent viscosity 40 min	apparent viscosity 60 min	apparent viscosity 80 min
180	3.0	3.08	2.41	0.64	0.11	1.40
195	50.0	0.85	0.77	0.14	0.01	0.41
225	1.0	8.68	5.92	2.00	0.28	3.63
240	50.0	0.94	0.77	0.14	0.01	0.40
270	0.3	35.08	21.13	7.99	0.76	13.31
285	50.0	1.09	0.77	0.14	0.02	0.39
315	0.1	130.90	69.30	23.79	2.18	38.43
330	50.0	1.17	0.77	0.15	0.01	0.38
360	0.3	49.48	20.05	7.86	0.58	12.35
375	50.0	1.37	0.78	0.14	0.01	0.38
405	1.0	17.57	5.60	1.95	0.20	3.20
420	50.0	1.65	0.77	0.14	0.01	0.37
450	3.0	8.48	2.14	0.61	0.08	1.15
465	50.0	1.84	0.73	0.15	0.02	0.36
495	10.0	4.32	1.07	0.23	0.03	0.52
510	50.0	1.88	0.69	0.13	0.01	0.33
540	30.0	2.67	0.83	0.15	0.02	0.37
555	50.0	2.06	0.69	0.12	0.01	0.31

Analyzing Table 5.17 again we can notice the importance of the alternation between the constant high shear rate of 50 s-1 to constant lower values at each step of the shear rate. The application of the high shear rate is made for a time sufficiently long to ensure that the steps of lower shear rates start from a steady state of the material and with these values we can see that the sample tends to reach more or less the same viscosity value at shear rate of 50 s-1, guaranteeing that the sample is not changing in time due to the good preservation inside the rheometer.

In the sequence S3 our shear rate goes from a shear rate step test that goes from an initial high value to a final low value, characterizing an overall built up of the structure, and after the inverse procedure, going from this last low value to the initial high value, characterizing an overall structure breakdown. Comparing the initial and final values of the viscosity in time, a thixotropy behavior related to colloidal interactions would occur if the build up is reversible, which can be seen at the 20 min, 40 min and 80 min time stamps. At the 5 min time stamp, however, the results showed an increase of viscosity as time advances, probably due to the early hydration.

Observing these viscosity results in Figure 5.22 and Table 5.17, we once again acknowledge an improvement, but we also notice undesirable low values of viscosity, specifically for the 60 mins time stamp (where also it is noticeable that the viscosity values did not arrive to a clear steady state), which made us to suspect problems of segregation of the mixture. Possibly at 60 mins time stamp the mixture was not uniform and a more watery part was measured in the rheometer. These results let us believe that Experiment E, despite being better than the previous ones, still present problems to be tackled with the changes resulting in Experiment F.

For Experiment E, the paste footprint was analyzed with density analysis only at the 20 mins time stamp. Therefore, it was executed an analysis of the density and degased density, and an analysis of quantity of water at all time stamps (5 to 80 mins). Figure 5.23 depicts the results of quantity of water analysis and Table 5.18 shows all the numerical values.

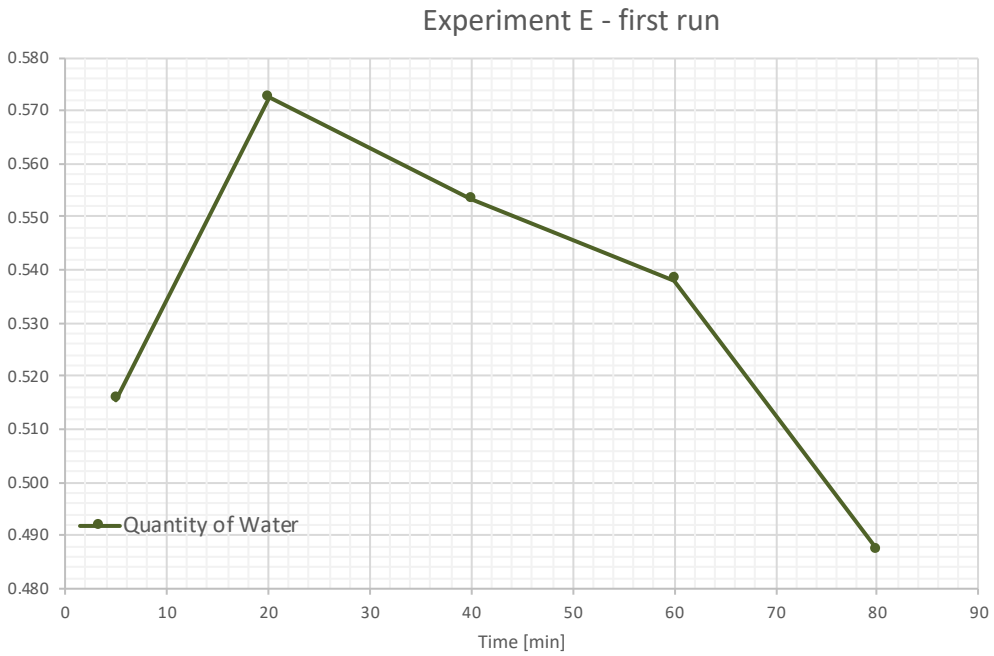

Fig. 5.23. Quantity of water paste footprint results for Experiment E.

Tab. 5.18. Paste footprint values for Experiment E.

measure	5 min	20 min	40 min	60 min	80 min
Quantity of water %	52%	57%	55%	54%	48%
Density of Degased Sample [Mg/m3]		1.834			
Density Sample [Mg/m3]		1.779			

Observing all numerical results for Experiment E we noticed an overall improvement, including, but not limited to, the expected higher density of the degased sample over the original sample. That being said, the percentage of water is not truly correspondent with the ratio w/c equal to 0.5 that was used, indicating the non-uniform mix caused by the preservation method P3. This segregation of the mixture makes the paste footprint not reliable, as we cannot assure that the

same sample condition measured by the rheometer at a given time stamp corresponds to the one that has the paste footprint analyzed at this same time stamp.

Finally, the mixture segregation was still found in the larger syringe and the proportion of the viscosity obtained at the end compared to the shear rate was still inadequate. Motivated by that, we decided to keep the shear strain sequence S3, but to try a new preservation method that keeps the prepared paste in a batch covered by wetted paper (P4), instead of using a large syringe (P3), thus leading us to Experiment F.

5.6. Experiment F

This experiment consists in the preservation method P4, shear strain sequence S3, time stamps of 5, 20, 40, 60, and 80 minutes, rheometer hood closed, and cement paste footprint F2, with density analysis at time stamp 20, and quantity of water at all time stamps. As Experiments A and B, Experiment F was performed twice. Figure 5.24 shows the shear stress curves obtained for the first 60 seconds after the shear strain sequence was started for both runs.

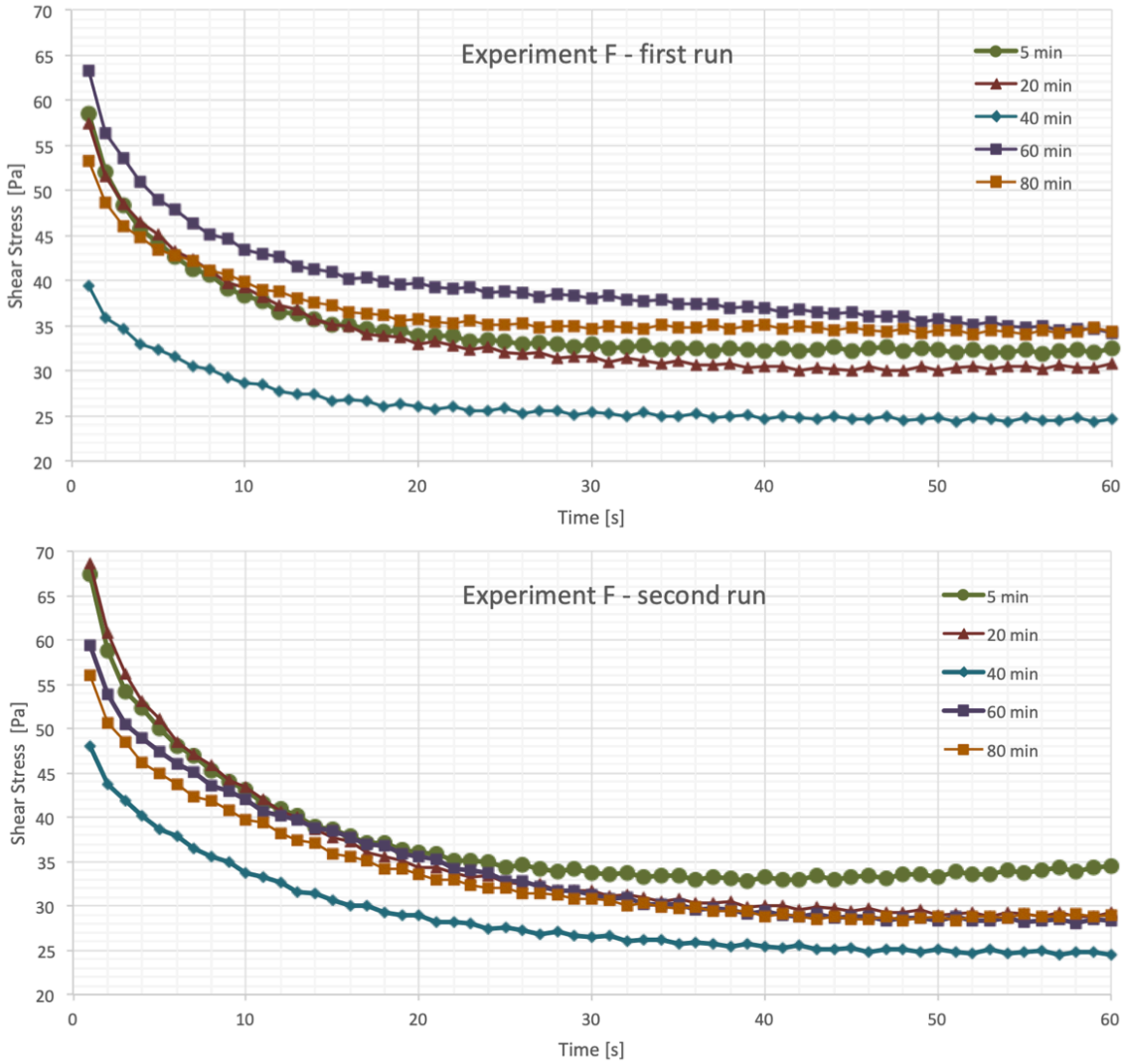

Fig. 5.24. Shear stress for both runs of Experiment F.

Tab. 5.19. Shear stress steady state for both runs of Experiment F.

run	time stamp	shear stress last four values average	std dev	run	time stamp	shear stress last four values average	std dev
1st	5	32.25	0.20	2nd	5	34.27	0.23
	20	30.55	0.19		20	29.04	0.20
	40	24.57	0.18		40	24.64	0.19
	60	34.47	0.20		60	20.54	0.09
	80	34.41	0.22		80	21.85	0.10

It is noticeable that all curves in Figure 5.24 show a steady state convergence, this convergence can also be observed by the average values of the last four results, as well as the standard deviation shown in Table 5.19. To reach the steady state convergence is important to guarantee that the transitional phase at the beginning passes and the samples achieve a reference state, so that the next measurements at various shear rates can be assumed to be done at the destructed state of the material.

It is also noticeable that the shear rate curve for the 40 mins time stamp is the lowest one, which seems surprising, since a lower shear stress was expected for the 5 minutes time stamp curve. This is verifiable for both runs of Experiment F, but it did not happen in any of the previous experiment runs. The results show values within a small range of variation comparing all the time stamps, which make us confirm an improvement of the method of preservation of the cement paste, controlling the hydration of the cement paste, so reducing the workability loss.

Applying the Bingham model to the obtained results for experiment F we obtain the flow curves presented in Figure 5.25. These curves represent the ratio between the shear stress measured in the rheometer at each time stamp by the shear stress computed using the Bingham model. With the sequence alternating high and low strains (S3) we are able to monitor what is happening at each shear rate step. In such way, it is noticeable the welcomed coincidence on the obtained values fitting the Bingham model. As expected, while the shear rate decreases, also does the shear stress. Also, the lowest values of shear stress are reached at the same shear rate for all time stamps. Table 5.20 presents the numerical values for the Bingham model.

Tab. 5.20. Numerical values of Bingham model for both runs of Experiment F.

time stamp	1st run dynamic yield stress (τ_0)	2nd run dynamic yield stress (τ_0)	1st run plastic viscosity (μ)	2nd run plastic viscosity (μ)
5	4.826	5.173	0.616	0.698
20	4.056	3.627	0.580	0.521
40	4.005	3.439	0.456	0.439
60	5.757	4.431	0.641	0.526
80	7.006	5.149	0.679	0.549

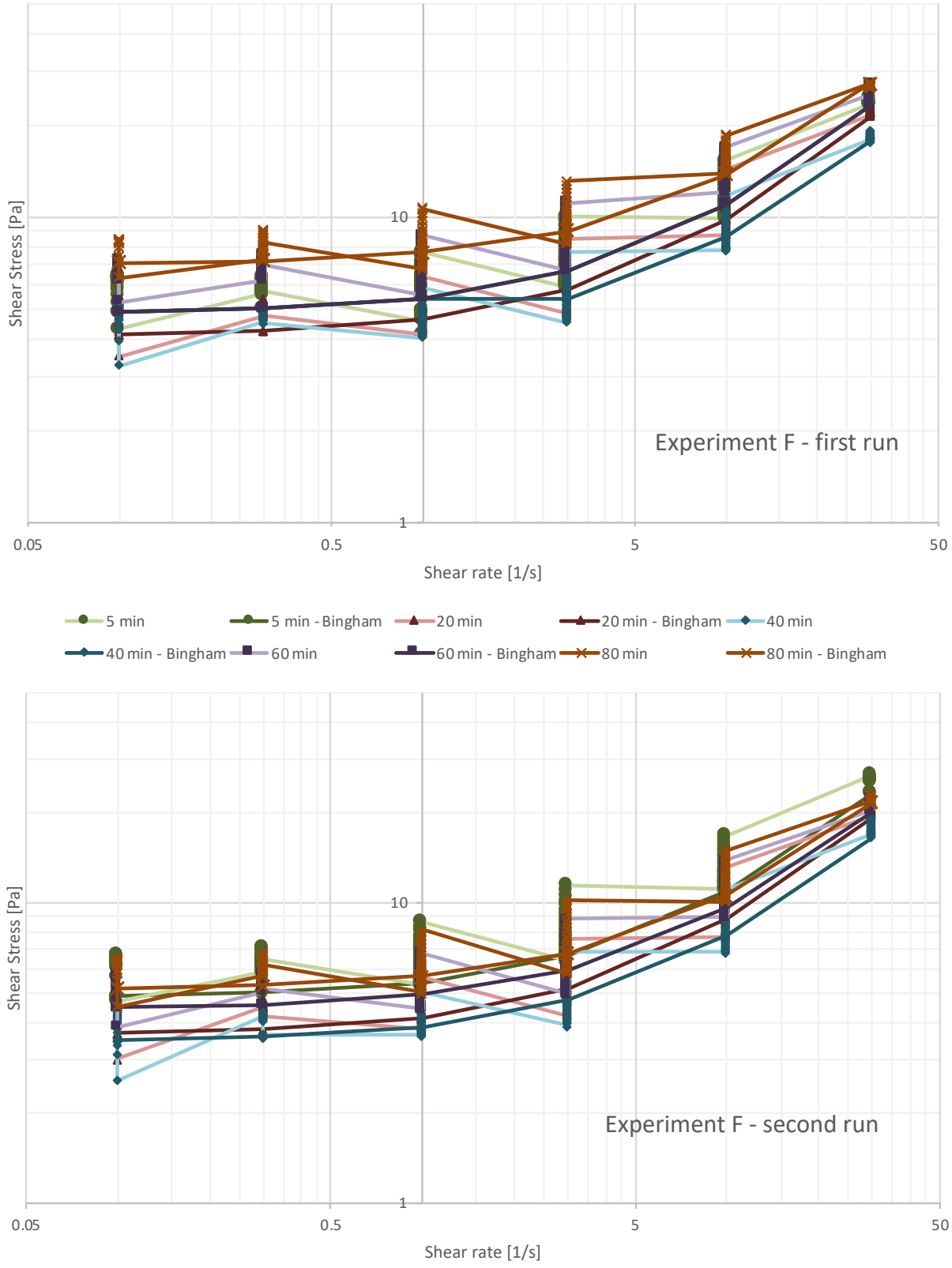

Fig. 5.25. Flow curves (shear rate and shear stress ratio) for both runs of Experiment F.

Observing these results, both in Table 5.20 and Figure 5.25 we noticed a difference from all previous experiments. Again we noticed a desirable small range of variation comparing all the time stamps, confirming the good preservation brought by P4. However, for both runs of Experiment F it is also possible to observe the adequacy between the measured values at the rheometer and the expected results computed in the Bingham model.

Carrying on, Figure 5.26 shows the viscosity versus the shear rate and Table 5.21 presents the numeric values plotted in Figure 5.26 for both runs of Experiment F. We can see a thixotropy behavior as the apparent viscosity of the cement paste shows a progressive decrease in time while the change of level of shear rate is imposed. Those results also show the adequacy of the obtained values and the small range between the time stamps, meaning that the preservation P4 is controlling the hydration of the cement paste.

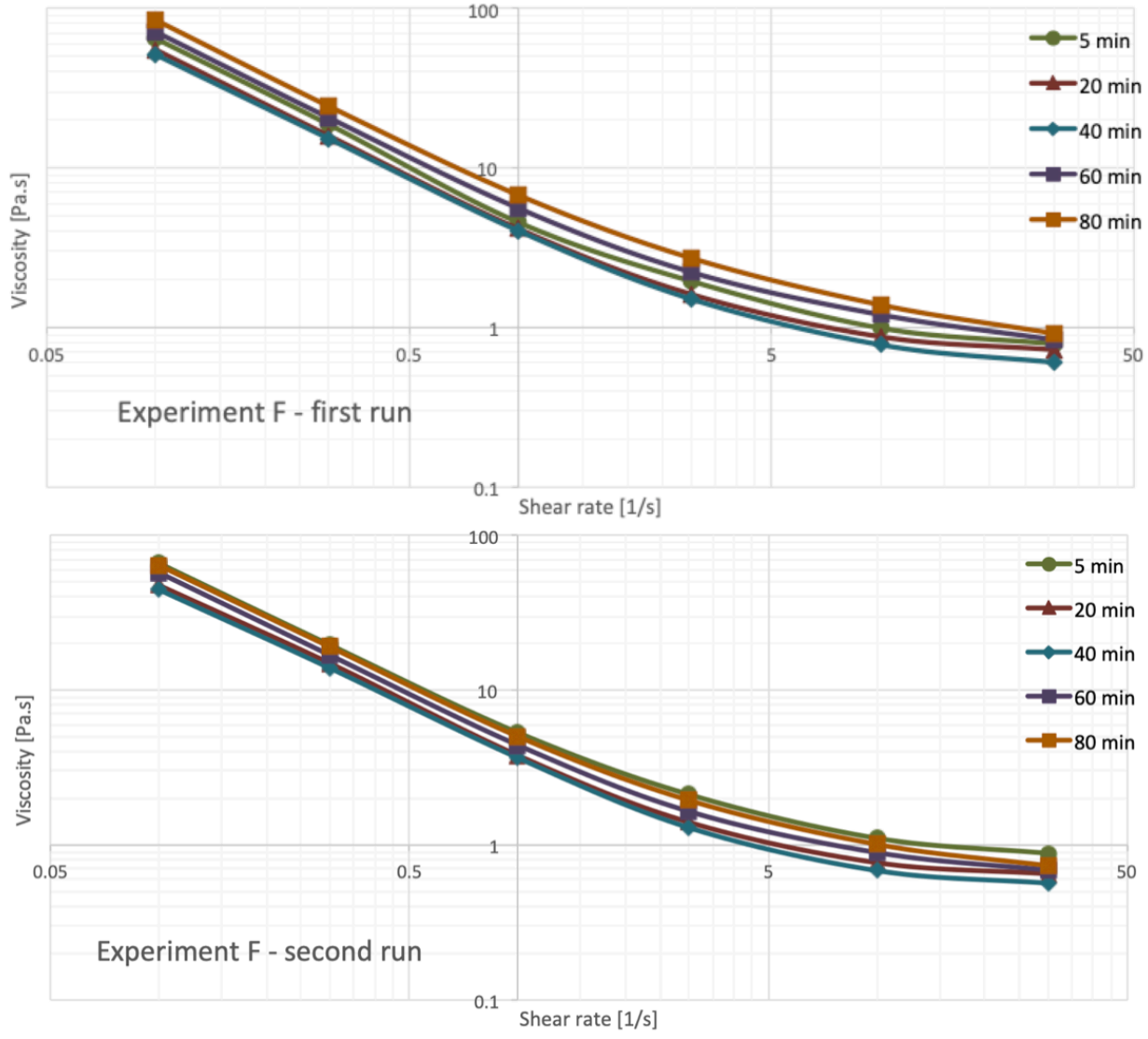

Fig. 5.26. Viscosity over shear rate for both runs of Experiment F.

Tab. 5.21. Viscosity over shear rate values for both runs of Experiment F.

Shear rate	1st run 5 m.	2nd run 5 m.	1st run 20 m.	2nd run 20 m.	1st run 40 m.	2nd run 40 m.	1st run 60 m.	2nd run 60 m.	1st run 80 m.	2nd run 80 m.
30	0.790	0.885	0.726	0.653	0.602	0.567	0.840	0.684	0.919	0.732
10	0.993	1.108	0.876	0.770	0.779	0.685	1.203	0.895	1.386	1.012
3	1.952	2.121	1.615	1.405	1.508	1.296	2.222	1.650	2.722	1.946
1	4.561	5.330	4.154	3.801	4.037	3.666	5.590	4.426	6.752	5.033
0.3	18.700	19.620	15.900	14.910	15.240	13.890	20.620	16.840	24.330	19.040
0.1	64.560	66.250	54.910	47.730	51.160	44.710	71.110	57.620	84.260	64.190

Figure 5.27 presents the shear rate applied for almost eleven minutes (555 seconds) and the resulting viscosity at each time stamp for Experiment F. As expected, the viscosity increases as the shear rate drops as also noticeable in the numerical values of Table 5.22.

Tab. 5.22. Shear rate and apparent viscosity over time values for both runs of Experiment F.

run	time	shear rate	apparent viscosity 5 min	apparent viscosity 20 min	apparent viscosity 40 min	apparent viscosity 60 min	apparent viscosity 80 min
1st	60	50.0	0.65	0.61	0.49	0.68	0.69
1st	90	30.0	0.79	0.73	0.60	0.84	0.92
1st	105	50.0	0.67	0.60	0.48	0.66	0.73
1st	135	10.0	0.99	0.88	0.78	1.20	1.39
1st	150	50.0	0.66	0.53	0.47	0.63	0.75
1st	180	3.0	1.95	1.62	1.51	2.22	2.72
1st	195	50.0	0.67	0.53	0.48	0.62	0.77
1st	225	1.0	4.56	4.15	4.04	5.59	6.75
1st	240	50.0	0.69	0.53	0.48	0.62	0.78
1st	270	0.3	18.70	15.90	15.24	20.62	24.33
1st	285	50.0	0.71	0.53	0.48	0.64	0.81
1st	315	0.1	64.56	54.91	51.16	71.11	84.26
1st	330	50.0	0.72	0.54	0.47	0.65	0.83
1st	360	0.3	18.47	15.48	14.71	20.34	24.31
1st	375	50.0	0.74	0.55	0.48	0.65	0.84
1st	405	1.0	4.91	3.92	3.75	5.40	6.76
1st	420	50.0	0.76	0.55	0.48	0.66	0.85

run	time	shear rate	apparent viscosity 5 min	apparent viscosity 20 min	apparent viscosity 40 min	apparent viscosity 60 min	apparent viscosity 80 min
1st	450	3.0	1.91	1.48	1.38	2.13	2.76
1st	465	50.0	0.76	0.53	0.49	0.67	0.88
1st	495	10.0	1.07	0.71	0.75	1.12	1.65
1st	510	50.0	0.77	0.50	0.49	0.62	0.89
1st	540	30.0	0.95	0.60	0.62	0.78	1.23
1st	555	50.0	0.78	0.50	0.48	0.60	0.91
2nd	60	50.0	0.69	0.58	0.49	0.57	0.58
2nd	90	30.0	0.88	0.65	0.57	0.68	0.73
2nd	105	50.0	0.75	0.55	0.45	0.57	0.60
2nd	135	10.0	1.11	0.77	0.68	0.90	1.01
2nd	150	50.0	0.78	0.46	0.42	0.53	0.61
2nd	180	3.0	2.12	1.41	1.30	1.65	1.95
2nd	195	50.0	0.80	0.46	0.41	0.54	0.63
2nd	225	1.0	5.33	3.80	3.67	4.43	5.03
2nd	240	50.0	0.82	0.47	0.40	0.54	0.65
2nd	270	0.3	19.62	14.91	13.89	16.84	19.04
2nd	285	50.0	0.84	0.47	0.41	0.54	0.66
2nd	315	0.1	66.25	47.73	44.71	57.62	64.19
2nd	330	50.0	0.86	0.48	0.40	0.56	0.67
2nd	360	0.3	19.65	14.41	13.12	16.51	18.47
2nd	375	50.0	0.88	0.49	0.39	0.56	0.68
2nd	405	1.0	5.30	3.74	3.27	4.25	4.96
2nd	420	50.0	0.89	0.49	0.39	0.56	0.69
2nd	450	3.0	2.21	1.39	1.14	1.58	1.91
2nd	465	50.0	0.90	0.47	0.38	0.55	0.70
2nd	495	10.0	1.36	0.61	0.51	0.81	1.13
2nd	510	50.0	0.90	0.43	0.33	0.55	0.70
2nd	540	30.0	1.14	0.52	0.38	0.68	0.92
2nd	555	50.0	0.93	0.45	0.29	0.55	0.71

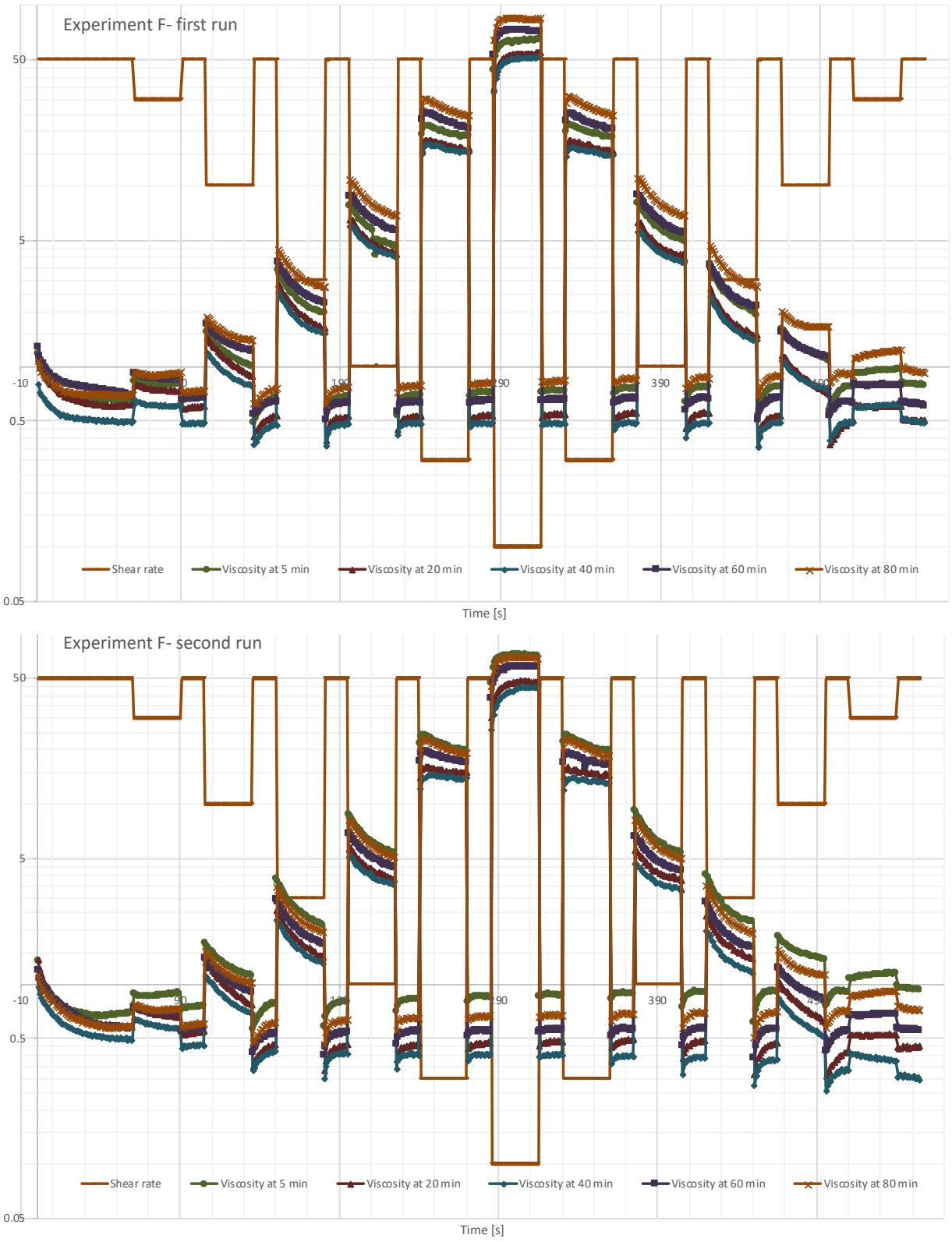

Fig. 5.27. Shear rate and viscosity over time for both runs of Experiment F.

The results presented in Figure 5.27 and detailed in Table 5.22 are another indication of the adequacy of Experiment F runs. The curves not only show the expected behavior with the viscosity increasing as the shear rate drops and vice versa, but the odd behavior previously detected in 60 mins time stamp of Experiment E was not presented in any of the time stamps of both runs for Experiment F. We consider this as a clear indication of the success of the Experiment F as the right protocol for taking rheometer measures of cement paste.

Once again we observe the benefits of the adopted shear sequence S3 that assures the application of the high shear rate for long enough to ensure that all steps of lower shear rates start from a steady state of the material. Besides, the values of apparent viscosity results at each step of high shear rate allow us to verify how the sample is changing in time. As we can see on Table 5.22, the results kept at a small range of variation in both runs, which is positive, indicating a good preservation of the sample inside the rheometer due to the efficient hood position H2.

In the sequence S3 our shear rate goes from a shear rate step test that goes from an initial high value to a final low value, characterizing an overall built up of the structure, and after the inverse procedure, going from this last low value to the initial high value, characterizing an overall structure breakdown. Comparing the initial and final values of the viscosity in time, a thixotropy behavior related to colloidal interactions would occur if the build up is reversible, which can be seen at the 20 min, 40 min and 60 min time stamps. At the 5 min time stamp, however, the results showed an increase of viscosity as time advances, probably due to the early hydration. At the 80 min time stamp we can also notice an increase of viscosity, which agrees with the literature that after one hour, the reversible and irreversible effects would co-contribute to the structural build-up of the cement paste. In fact, the irreversible effects, or permanent changes, are related to the ridification of the C-S-H bridges.

Similar to Experiment E, we have noticed on the results an overall thixotropic behavior as the build up is reversible. However, some small permanent changes could be seen at the end and are defined as workability loss combined with thixotropy, that is a result of a combination of non reversible structural build up and the thixotropy of the cement paste.

For Experiment F, the paste footprint was analyzed with density analysis only at the 20 mins time stamp. Therefore, it was executed an analysis of the density and degased density, and an analysis of water quantity at all time stamps (5 to 80 mins). Figure 5.28 depicts the results of such quantity of water analysis and Table 5.23 presents the numerical values observed for all footprint analysis.

Tab. 5.23. Paste footprint values for both runs of Experiment F.

measure	1st run 5 m.	2nd run 5 m.	1st run 20 m.	2nd run 20 m.	1st run 40 m.	2nd run 40 m.	1st run 60 m.	2nd run 60 m.	1st run 80 m.	2nd run 80 m.
Quantity of water %	50%	50%	50%	50%	51%	51%	50%	50%	50%	51%
Density of Degased Sample [Mg/m3]			1.886	1.812						
Density Sample [Mg/m3]			1.796	1.784						

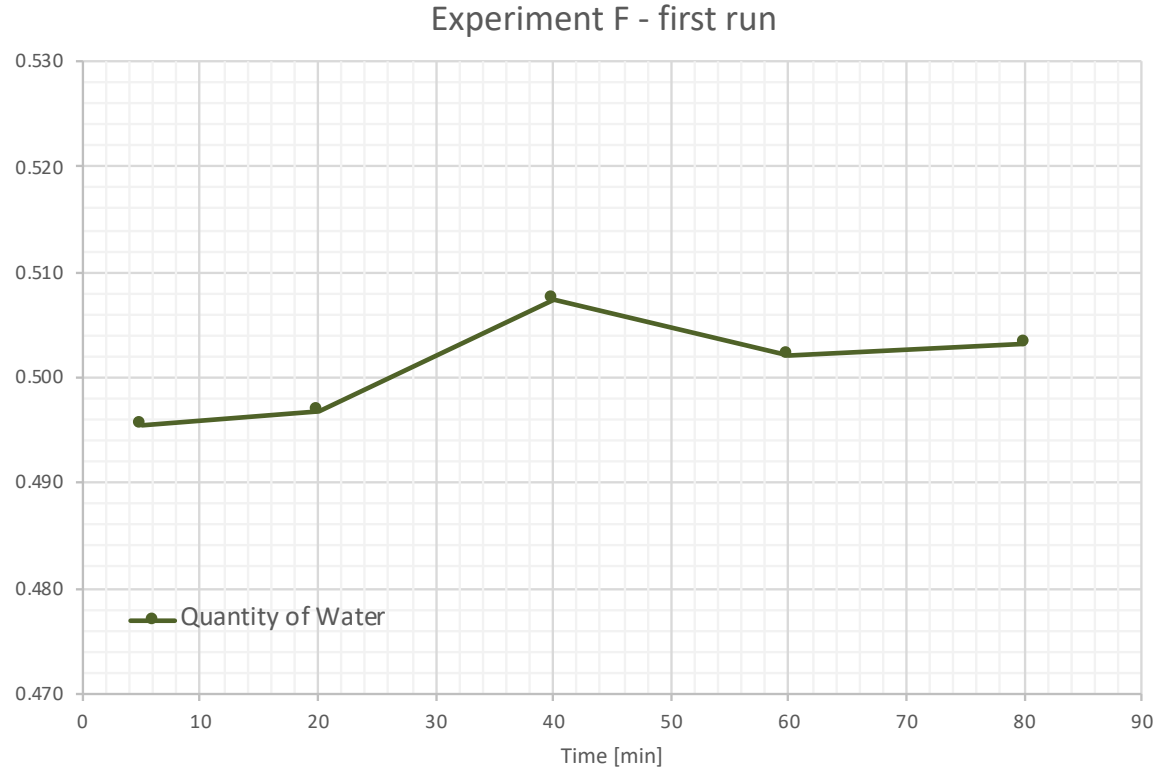

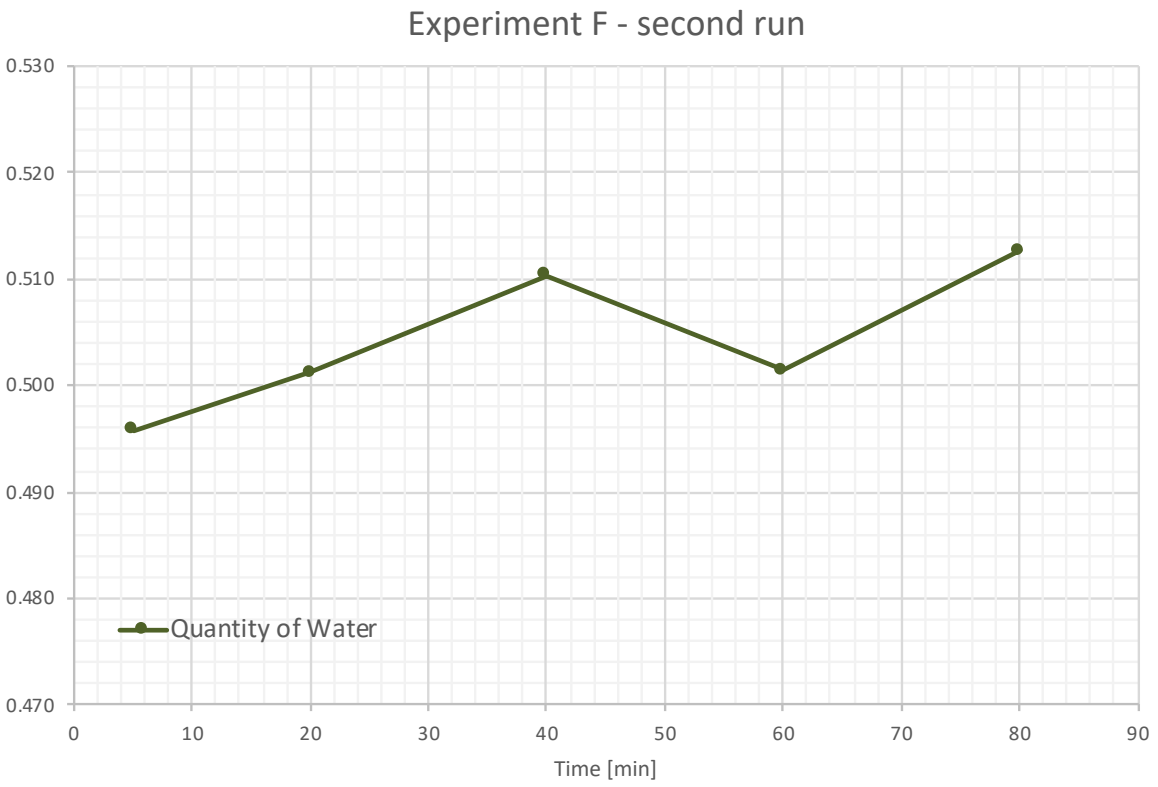

Fig. 5.28. Quantity of water paste footprint results for both runs of Experiment F.

The values of the paste footprint once again seem consistent with our expectations, as we have a degased density higher than the density of the sample and the percentage of water is correspondent with the ratio w/c equal to 0.5 that was used, confirming a uniform mix, well preserved by P4, and so, a reliable measurement, as the same condition of the sample was used to measure the footprint and to the rheometer measurement at each time stamp. They are an additional indication of Experiment F success. In fact, we believe that all numerical results obtained for Experiment F indicates the procedure conducted as the appropriated methodology to perform rheology measures.

5.7. Comparison Between Preservation Methods

For all shear sequences (S1, S2 and S3) there is a common initial high constant shear rate of 50 s-1 for 60s which allows the cement paste to reach the so important steady state convergence. This convergence is important to guarantee the transitional phase at the beginning passes and that the samples achieve a reference state. This is necessary for the next measurements that are assumed to be done at the destructed state of the material.

Due to this similar initial sequence for all experiments, we are able to compare the influence of the preservation method to reach the steady state at each time stamp. The values got from one preservation to another change due to its capability/incapability of preserve the cement paste sample from hydrate and segregation.

The segregation of the mixture results in a non-uniform mix caused by the way the preservation was made, leading to inconsistent results. The early hydration causes the cement particles to be bonded more strongly together and/or increase the number of inter particle bonds. It provokes an increasing of yield stress, that is the dominant parameter of the workability of the cement-based materials, characterizing the setting of the cement paste.

The macroscopic flow is achieved as soon as the stress applied to the system overcomes what can be supported by the network of particles in interaction, the yield stress. The cement paste above the yield stress shows shear thinning, an indication that the micro-structure is progressively breaking down under shear.

Furthermore, Struble and Lei (1995) stated that the setting time measured using the yield stress decreased when the w/c ratio was reduced, and, consequently, a paste with a lower w/c ratio has a shorter initial setting time. Therefore, the initial high constant shear rate of 50 s-1 for 60s used in this thesis' experiments is enough to reach steady state convergence for cement pastes with w/c ratio less or equal to 0.5.

To illustrate that, Table 5.24 presents the summary of the comparison developed in this subsection by showing the numerical value of the average of the shear stress as indicator of steady state for each experiment and time stamp.

Tab. 5.24. Shear stress steady state for Experiments A to F.

shear stress last four values average						
time stamp	Experiment A	Experiment B	Experiment C	Experiment D	Experiment E	Experiment F
5	45.50	59.20	34.60	39.30	43.34	33.26
20	22.49	157.86	38.23	24.35	44.65	29.79
35	68.93	94.19	-	-	-	-
40	-	-	43.67	38.23	10.26	24.60
50	103.77	19.12	-	-	-	-
60	-	-	74.20	30.55	1.25	27.50
80	-	-	-	33.89	28.18	28.13

5.7.1. Experiments A and B

Experiments A and B are characterized by different preservation methods: respectively, P2 and P1, the same shear sequence S1, the same open position of air circulation H1, and the same time stamps measurements at 5, 20, 35 and 50 min.

Figure 5.29 show the shear stress curves for 5, 20, 35 and 50 times stamps. Observing these results we notice that only for the 5 minutes time stamp both models present similar values, but for the other time stamps there is a great discrepancy. We believe the reason is that the 5 minutes time stamp is less impacted by the preservation method, since the tests are performed just after placing the cement paste into the rheometer.

For 20, 35, and 50 mins time stamps the influence of the preservation method becomes stronger as we notice the difference between P1 (Experiment B) and P2 (Experiment A) increasing as the time stamp increases, thus, influencing by a huge variability of shear stresses values. Such conclusion was the basic reason to abandon preservation method P2.

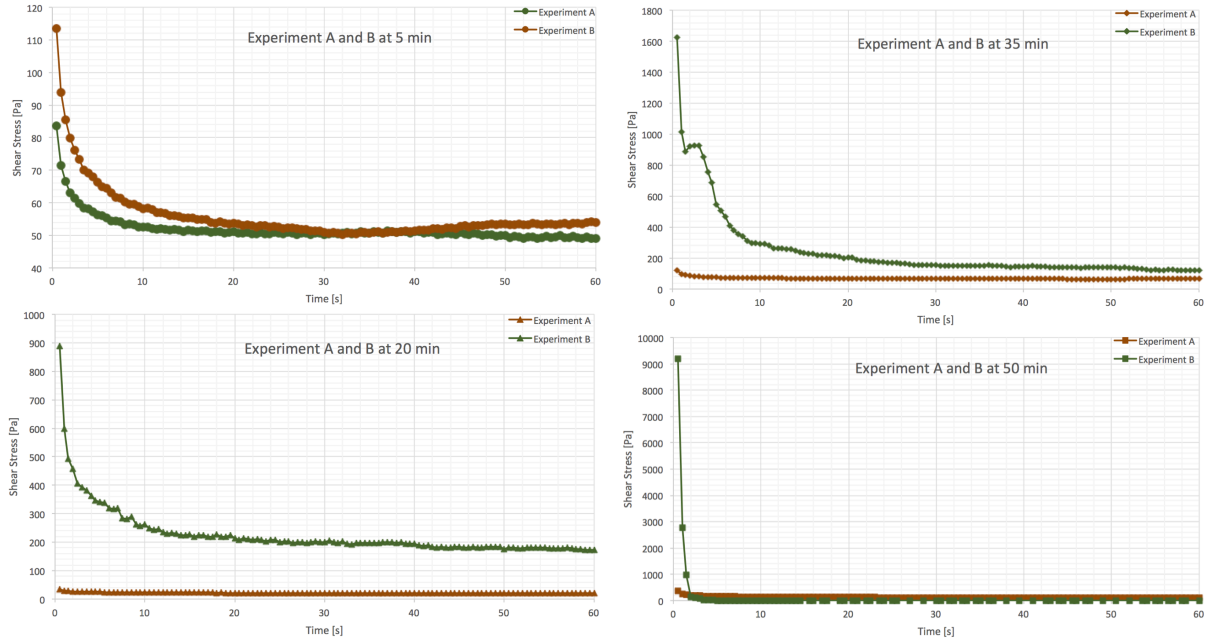

Fig. 5.29. Shear stress for Experiments A and B at 5, 20, 35, and 50 mins time stamps.

5.7.2. Experiments C and D

Experiments C and D are characterized by different preservation methods (respectively, P2 and P3), the same shear sequence S2, different hood position, open position of air circulation H1 (Experiment C) and closed position of air circulation (Experiment D), and measured at time stamps 5, 20, 40, and 60 min, plus 80 min for Experiment D only.

Figure 5.30 depicts the shear stress values for 5, 20, 40, 60 mins time stamps for Experiments C and D, and Figure 5.31 depicts the shear stress values for 80 mins time stamps for Experiment D. As stated before, the preservation P2, did not allow a measurement at 80 min, due to the cement paste hardening, that prevent us to carry on the measures to larger time stamps. This fact is illustrated by an impressive 142 value for viscosity reached for the 60 min time stamp. Preservation P3 instead allowed the measurement of the 80 mins time stamp, but did not prevented well enough the segregation of the mixture during the experiment, resulting in a non-uniform mix, and, and consequently unreliable results.

Observing this comparison we can notice once again that at 5 mins time stamp there is a pronounced coincidence between preservation methods, now P2 (Experiment C) and P3 (Experiment D). This is one more time expected since at 5 mins time stamp the preservation method is less impacting. However, for larger time stamps we can see a stronger influence of the preservation method, noticing the difference between P2 and P3 summed with the effect of the open and close position of the air circulation (H1 and H2). The values now are less discrepant than those for the comparison between Experiments A and B, but still there is an

unwelcome variability between the results for Experiments C and D, thus threatening the reliability of the obtained results.

The clear advantage of P3 is to provide an adequate preservation for the 80 mins time stamp (Figure 5.31), since the cement paste remains with a sufficient viscosity, thus, enhancing the capacity of measurement and consequently more reliable results. Despite that, we keep pursuing similar shear stress values for all time stamps, which was not found between Experiments C and D.

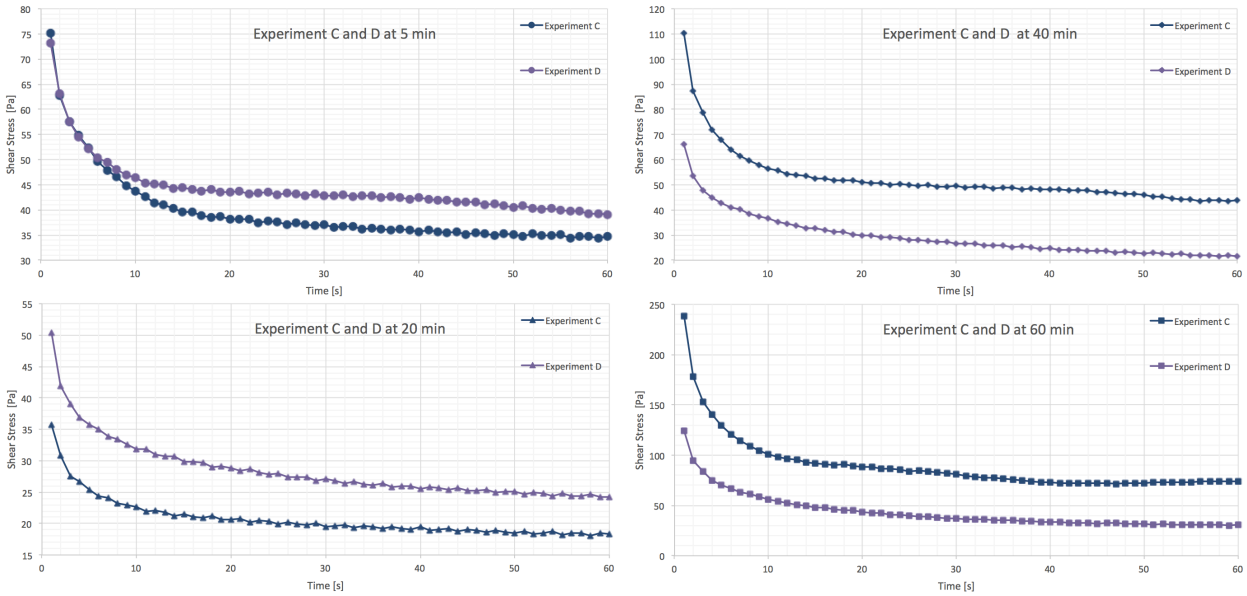

Fig. 5.30. Shear stress for Experiments C and D at 5, 20, 40, and 60 mins time stamps.

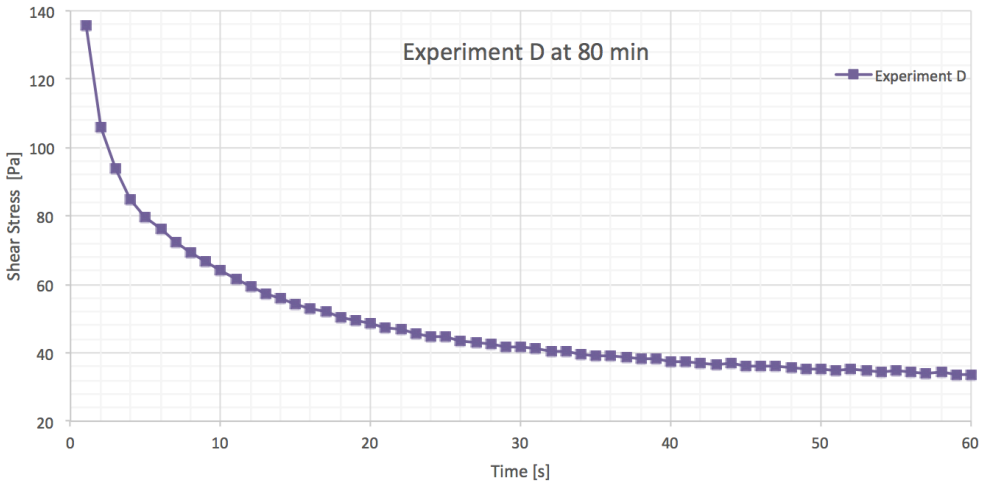

Fig. 5.31. Shear stress for Experiment D at 80 mins time stamp.

5.7.3. Experiments E and F

Experiments E and F are characterized by different preservation methods, respectively P3 and P4, the same shear sequence S3, the same closed position of air circulation H2, and measurements at the same time stamps (5, 20, 40, 60 and 80 min).

Figure 5.32 presents the shear stress for all time stamps from 5 to 60 mins for Experiments E and F, while Figure 5.33 presents the same for 80 mins time stamp. We can notice from these results the better coupling of the observed values between the two experiments. Unlike the previous comparisons, now the values above 5 minutes stamp deliver similar results that also provide more confidence for the measurements. In fact, for 60 minutes time stamp we found the largest difference between shear stress, and these values are considerably smaller than those found in the previous comparisons.

As stated before, for preservation method P3 it was noticed a segregation of the mixture, provoking a non-uniform mixture and so, an odd and detached behavior of the paste at 60 min time stamp. Therefore, we assume that, for Experiment E, possibly at 60 time stamp the mixture was not uniform and a more watery part was measured in the rheometer. This preservation method P3 problem was solved by the employment of the preservation method P4 for Experiment F.

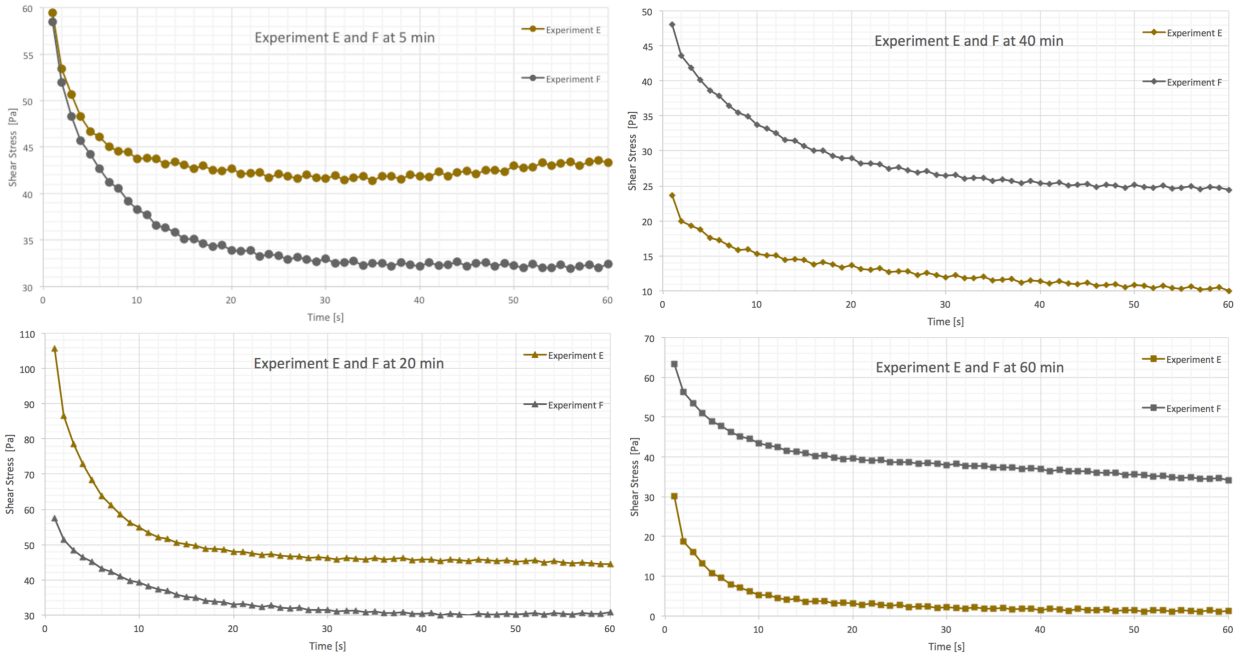

Fig. 5.32. Shear stress for Experiments E and F at 5, 20, 40, and 60 mins time stamp.

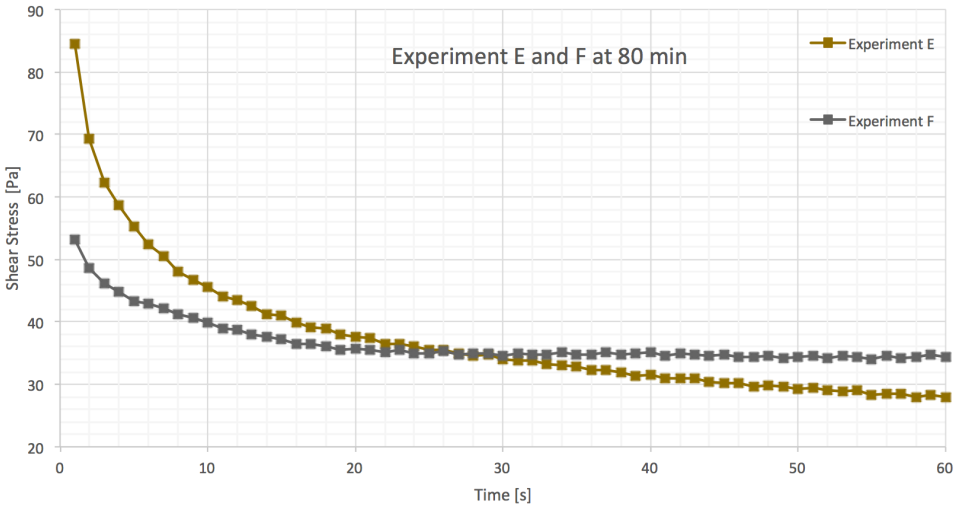

Fig. 5.33. Shear stress for Experiments E and F at 80 mins time stamps.

6. Proposed Standard Protocol

After the series of conducted experiments, the final proposed standard protocol is defined based on Experiment F that according to the analysis presented in Chapter 5 is the more successful experiment. This chapter formally describes the proposed protocol defining the key points to establish reproducible measurement steps by reducing the variability of cement paste materials.

6.1. Raw material

The cement is sieved at size < 63 µm with an automatic sieve. This automatic sieve is ruled by the UNI EN 933-1, where it indicates the quantity of material that can be placed for sieve each time.

6.2. Preparation of samples

The procedure was defined assuming the use of an automatic mixing with Heidolph RZR 2041 LAISS, match with blade BR 11 Straight Blade Impeller (shaft Ø 8 mm, blade size 50 × 12 mm) for the mixing procedure. Figure 6.1 describes the recommended sample preparation process.

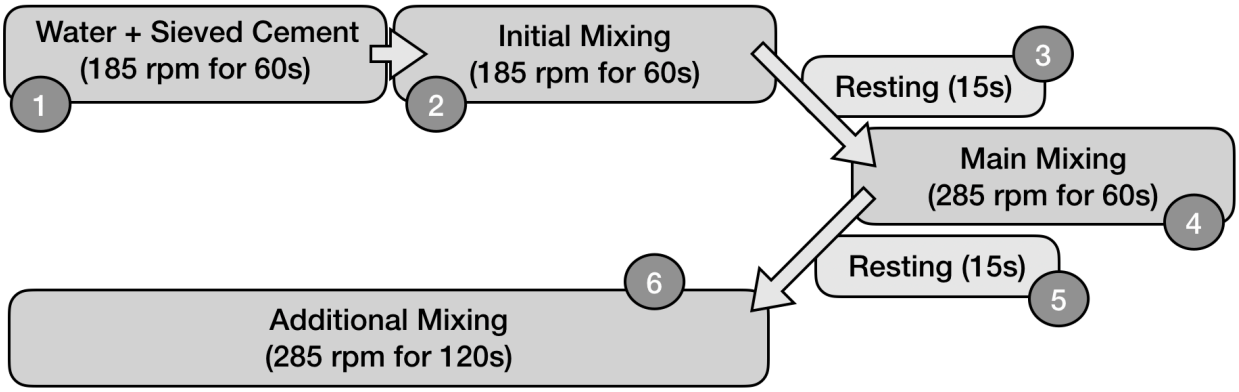

Fig. 6.1. Procedure for sample preparation.

6.3. Preservation technique

Once prepared, the cement paste is stored in a batch isolated with wetted paper in order to preserve the cement properties prior to its application into the rheometer and to the analysis of the paste footprint. This preservation technique has been proved adequate to hold cement paste at least for 80 minutes, which was the longer wait time in our experiments, but likely longer waits could be envisaged.

It is important to ensure homogeneity of the material analyses so, at each step, before the sample is placed on the rheometer, a hand-mixing with a small spoon is performed for 30s to guarantee homogeneity of the mixture, the sample is putted with the spoon inside a big syringe (by its barrel) with the spoon and, finally, placed on the rheometer plates.

6.4. Time stamps

The time stamps for rheometer tests recommended goes from 5 to 80 minutes with intervals of 15 to 20 minutes. For our more successful experiment, the time intervals were at 5, 20, 40, 60 and 80 minutes. However, other time stamps within this interval from 5 to 80 minutes are likely to be also adequate.

6.5. Test and measuring equipment

The rotational rheometer works placing the cement mixture between two cross-hatched stainless-steel parallel plates with a rough dented surface, specifically, a pair of PP25 P2 plates, according to Ferraz et al. (2020) this rough geometry guarantees shear without slipping during the tests. Furthermore, to prevent evaporation of water from the sample during the rheometer operation, according to the Ley-Hernandez & Feys (2020) it is enough to have a temperature-controlled hood placed on the top of the measuring system. For the conducted experiments, the machine is set to a constant temperature of 20 ^{o}C and we had kept the hood in the closed position for the air circulation. Therefore, this is the recommended position in our proposed protocol.

6.6. Measurement protocols

The most important definition within the measurement protocol is the definition of the shear sequence to be imposed on the sample. For the proposed protocol the recommended shear sequence defines strain rates alternating the highest value (50 s^{-1}) with intervals with lower values decreasing the slower rates until the middle of the experiment, and then increasing the slower values symmetrically. Specifically, with lower value intervals: 30, 10, 3, 1, 0.3, 0.1, 0.3, 1, 3, 10, 30 s^{-1} for a total a little above 9 minutes (555 seconds). Such shear sequence, called S3 in the previous chapters, is depicted in Figure 6.2 and its shear rate numerical values are stated in Table 6.1.

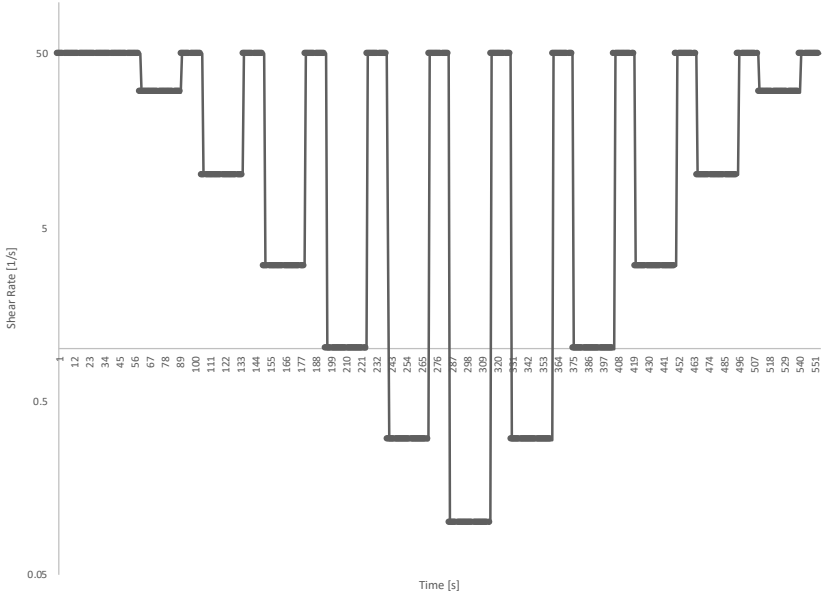

Fig. 6.2. Proposed shear sequence (S3) strain rates variation.

Tab. 6.1. Proposed shear sequence (S3) timeline and values - 555 seconds.

time (s)	duration (s)	measure points	shear strain
0	60	120	50 s^{-1}
60	30	15	30 s^{-1}
90	15	15	50 s^{-1}
105	30	15	10 s^{-1}
135	15	15	50 s^{-1}
150	30	15	3 s^{-1}
180	15	15	50 s^{-1}
195	30	15	1 s^{-1}
225	15	15	50 s^{-1}
240	30	15	0.3 s^{-1}
270	15	15	50 s^{-1}
285	30	15	0.1 s^{-1}
315	15	15	50 s^{-1}
330	30	15	0.3 s^{-1}
360	15	15	50 s^{-1}
375	30	15	1 s^{-1}
405	15	15	50 s^{-1}
420	30	15	3 s^{-1}
450	15	15	50 s^{-1}
465	30	15	10 s^{-1}
495	15	15	50 s^{-1}
510	30	15	30 s^{-1}
540	15	15	50 s^{-1}

6.7. Footprint measurement

The proposed measurement of the density of the mixture follows the procedure UNI EN 1097-7: 2000, which takes approximately 15 minutes to be undertaken. In fact, it is recommended to conduct two density measures: one of the sample as it is; and another one after submitting the sample to a depressurizer engine, giving us the density without air voids (degased sample). Finally, the paste footprint includes the measurement of the quantity of water present in the sample and this should be made heating a small 5g sample into an oven up to 110º celsius until it dries. It is also recommended to perform the cement paste footprint analysis as: the densities only at one time stamp and the water quantity measures at all time stamps. For example, in our successful experiment we conduct the cement paste footprint as doing the densities analysis only at the 20 minutes time stamp and the water quantity measure at all time stamps.

7. Conclusion

The rheological measurements on cement pastes are influenced by intrinsic factors such as the raw materials, water/cement ratio, presence of admixtures, air void content, and also by external conditions such as mixing procedure, humidity, temperature, air circulation, stress history, chemical reactions associated with the drying and curing phase of such filler pastes and wall slip effects. This variability interferes in an appropriate rheological measurement of cement paste in laboratory. In fact, the use of rheometers becomes challenging because of a lack of proper testing protocol, so it is primordial to reduce the variability in test results, and for this goal a primary importance has to be given to the definition of a standard protocol that take into account all these factors.

In this thesis we have fulfilled our objective to define a standard protocol for our lab to test cement paste materials, to experiment the standard protocol, and to compare results obtained, while analyzing the footprint of the paste to evaluate and validate the results gotten from the rheological measures. After executing six different experiments described in detail in Chapters 3, 4, and 5 we came to propose of a standard protocol to perform rheologic measurements as detailed in Chapter 6.

The proposed standard protocol defines the key points to provide a reproducible measurement to reduce the variability of cement paste materials. These key points set standards for the sample preparation and preservation, the geometry of the rheometer and its hood configuration, the shear rate sequence imposed in the rheometer, the time stamps for each test, and finally how to obtain the footprint of the analyzed cement paste.

The sample preparation was defined adapting both, the ASTM C305 standard and the extension of the ASTM C305 given by Han & Ferron (2016). The preservation was tested as a better way to use a single-batch approach, conserving in a batch covered with wetted paper and with additional hand-mixing each time a sample was going to be placed in the rheometer, and also to perform the paste footprint analysis adapted from the UNI EN 1097-7:2000 procedure.

The geometry of the rheometer was two cross-hatched stainless-steel parallel plates with a rough dented surface, where the rough geometry guarantees shear without slipping during the tests. The rheometer's hood was defined as better closed, to avoid air circulation, which would contribute to the hardening of the paste. The time stamps were defined in a way considering the preparation of the rheometer sample, the time of the shear test, and the footprint test, being defined in 15 to 20 minutes intervals within a 5 to 80 time frame.

The obtained results offer an interesting and precise method to be applied to rheological measurement of samples. However, it is natural to foresee future works to perform a larger set of experiments to different cement pastes. Specifically, it would be interesting to apply the proposed standard protocol to:

- Cement pastes with different water/cement ratios;
- Cement pastes containing additives such as air entrainment agents;
- Cement pastes containing silica fume or limestone.

Such additional experiments would allow a greater confidence in the proposed protocol, as well as discover the rheological effect caused by different ratios of air voids, or even the effect of superplasticizers elements.

Another interesting future work would be the adaptation of the proposed protocol to different rheometer geometries as the Vane-in-cup. Such future work would likely benefit from several discoveries of this thesis as the sample preparation and preservation, but other protocol aspect of such as the shear sequence may be considerably different for different rheometer geometries.

Finally, it is important to stress that the main contribution of this thesis is the proposition of a protocol in order to facilitate the analysis of rheological cement paste properties using small quantities in a rheometer. In such way, the proposition of standard protocol is already an advancement towards a better understand of cement paste rheological properties, and consequently a faster analysis to contribute to the discovery of improved cement paste-based materials and, thus, improved concrete structures.

8. References

Agostinho, L.B. et al (2020). **The Use of Parallel-Plate Rotational Rheometry to Determine the Superplasticizer to be Used in Cement Pastes Admixtures**. RILEM Bookseries.

ASTM C305-14 (2014). **Standard Practice for Mechanical Mixing of Hydraulic Cement Pastes and Mortars of Plastic Consistency**. ASTM International.

Banfill, P.F.G. (1991). **Rheology of Fresh Cement and Concrete**. Heriot-Watt University.

Carotenuto, C. et al (2015). **Predicting the Apparent Wall Slip When Using Roughened Geometries: A Porous Medium Approach.** Journal of Rheology - The Society of Rheology.

Chen, T. (2015). **Preventing Wall Slip in Rheology Experiments.** TA Instruments.

Ferraris, C. and Gaidis, J. (1992). **Connection between the Rheology of Concrete and Rheology of Cement Paste**. ACI Materials Journal.

Ferraris, C. (1999). **Measurement of the Rheological Properties of High Performance Concrete: State of the Art Report**. Journal of Research of the National Institute of Standards and Technology.

Ferraz, D.F et al (2020). **Effect of Mixing Procedure on the Rheological Properties and Hydration Kinetics of Portland Cement Paste**. RILEM Bookseries.

Feys, D. et al (2017). **Measuring Rheological Properties of Cement Pastes: Most Common Techniques, Procedures and Challenges**. RILEM Technical Letters.

Han, D. and Ferron, R. (2016). **Influence of High Mixing Intensity on Rheology, Hydration, and Microstructure of Fresh State Cement Paste**. Cement and Concrete Research - Elsevier Ltd.

Himmel, T. and Wagner, M.H. (2013). **Experimental Determination of Interfacial Slip Between Polyethylene and Thermoplastic Elastomers.** Journal of Rheology - The Society of Rheology.

Ivanova, I. and Mechtcherine, V. (2020). **Evaluation of Structural Build-Up Rate of Cementitious Materials by Means of Constant Shear Rate Test: Parameter Study**. RILEM Bookseries.

Keentok, M. and Xue, S. (1999). **Edge Fracture in Cone-plate and Parallel Plate Flows.** Rheological Acta 38 - Springer-Verlag.

Koehler, E.P. and Fowler, D.W. (2003). **Summary of Concrete Workability Test Methods**. ICAR 105-1.

Ley-Hernández, A.M. and Feys, D. (2020). **Challenges in Rheological Characterization of Cement Pastes Using a Parallel-Plates Geometry**. RILEM Bookseries.

Edited by Mechtcherine V. et al (2020). **Rheology and Processing of Construction Materials RheoCon2 & SCC9**. RILEM Bookseries.

Mukhopadhyay, A.K. and Jang, S. (2009). **Using Cement Paste Rheology to Predict Concrete Mix Design Problems: Technical Report**. Texas Transportation Institute.

Ovarlez, G. (2012). **Introduction to the Rheometry of Complex Suspensions**. Woodhead Publishing Limited.

Rixon, R. and Mailvaganam, N. (2012). **Chemical Admixtures for Concrete**. E & FN Spon.

Edited by Roussel, N. (2012). **Understanding the Rheology of Concrete**. Woodhead Publishing Limited.

Roussel, N. et al (2012). **The Origins of Thixotropy of Fresh Cement Pastes.** Cement and Concrete Research - Elsevier Ltd.

Sant, G., Ferraris, C. and Weiss J. (2008). **Rheological Properties of Cement Pastes: A Discussion of Structure Formation and Mechanical Property Development**. Cement and Concrete Research - Elsevier Ltd.

Sheinn, A.A.M et al (2002). **Rheological Model for Self-Compacting Concrete Paste Rheology**. CI-Premier PTE LTD.

Struble, L.J. and Lei, W. (1995). **Rheological Changes Associated with Setting of Cement Paste.** Advanced Cement Based Materials - Elsevier Science Inc.

Struble, L. and Jiang, Q. (2018). **Effects of Air Entrainment on Rheology**. ACI Materials Journal.

UNI EN 1097-7 (2008). **Tests for Mechanical and Physical Properties of Aggregates - Part 7: Determination of the Particle Density of Filler - Pyknometer Method**. UNI Standard.

UNI EN 933-1 (2012). **Tests for Geometrical Properties of Aggregates - Part 1: Determination of Particle Size Distribution - Sieving Method**. CEN Standard.

Vance, K., Sant, G. and Neithalath, N. (2015). **The Rheology of Cementitious Suspensions: A closer Look at Experimental Parameters and Property Determination Using Common Rheological Models**. Cement and Concrete Research - Elsevier Ltd.

Wallevik, J.E. (2020). **Measuring Thixotropic Properties in a Truck Mixer - Analysis by Numerical Simulation Using the PFI Material Model.** RILEM Bookseries.

Williams, D.A. et al (1999). **The Influence of Mixing on the Rheology of Fresh Cement Paste**. Cement and Concrete Research - Pergamon.

Yuan, Q. et al (2017). **On the Measurement of Evolution of Structural Build-up of Cement Paste with Time by Static Yield Stress Test vs. Small Amplitude Oscillatory Shear Test.** Cement and Concrete Research - Elsevier Ltd.

A. Annex - Numerical Results for Experiment A

This first annex presents the numerical results of Experiment A as described in Chapter 4. This experiment consists in the preservation method P2, shear strain sequence S1, time stamps of 5, 20, 35, and 50 minutes, rheometer hood open, and no cement paste footprint analysis. Experiment A was performed twice, therefore the results are presented for both runs. Figure A.1 shows the shear stress curves obtained for the first 60 seconds after the shear strain sequence was started. Table A.1 presents the last four results to each curve, plus the average and the standard deviation.

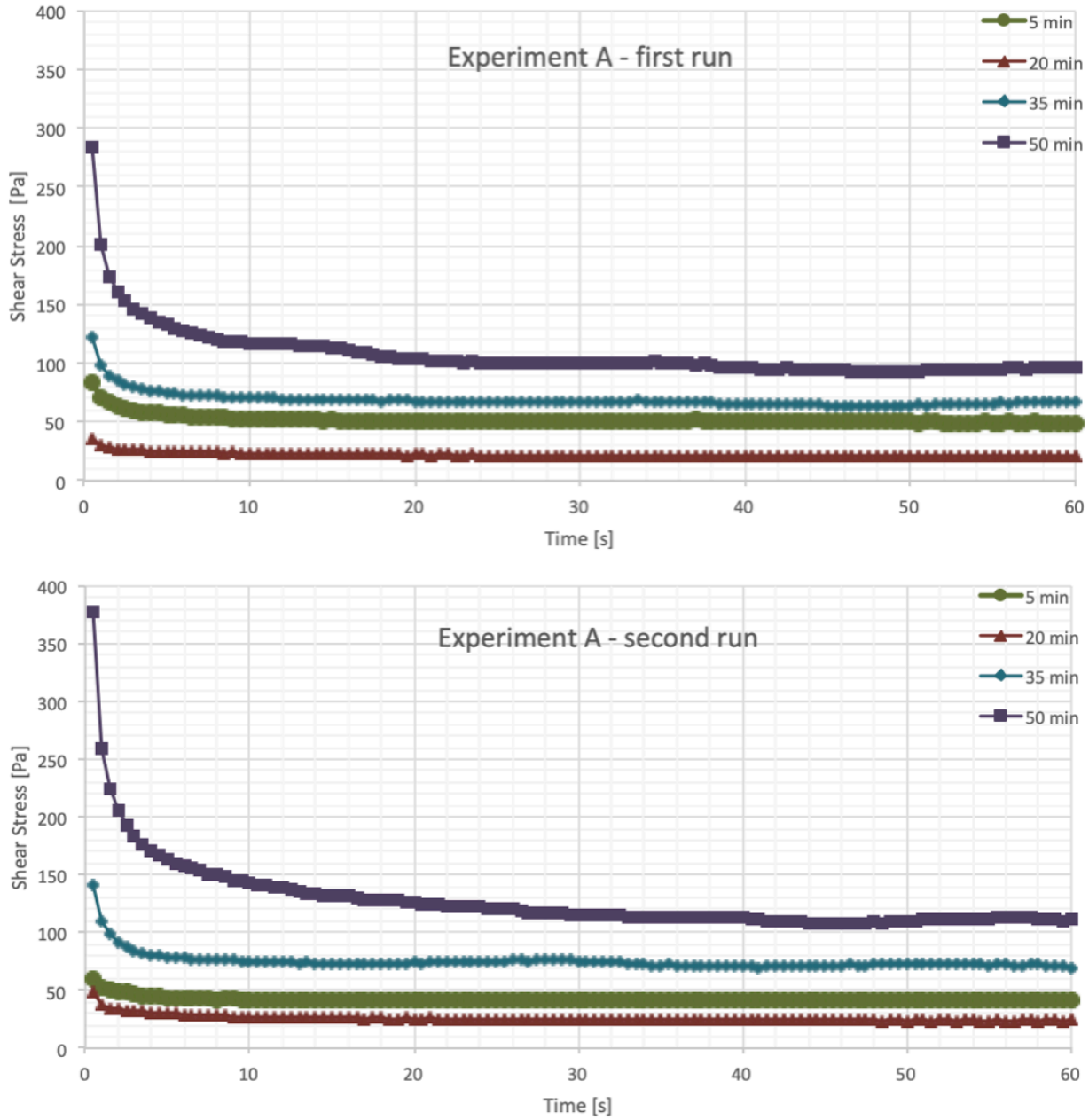

Fig. A.1. Shear stress for both runs of Experiment A.

Tab. A1. Shear stress steady state for both runs of Experiment A.

run	time stamp	shear stress last four values				average	std dev
1st	5	49.11	49.41	49.16	48.93	49.15	0.20
	20	20.85	21.00	21.30	20.89	21.01	0.20
	35	66.71	66.53	66.90	67.08	66.81	0.24
	50	96.10	95.68	96.78	96.50	96.27	0.48
2nd	5	42.02	42.15	41.62	41.57	41.84	0.29
	20	24.16	23.98	23.67	24.07	23.97	0.21
	35	71.36	71.59	71.13	70.10	71.05	0.66
	50	111.80	111.40	111.60	111.30	111.53	0.22

Applying the Bingham model to the obtained results for experiment A we obtain the flow curves presented in Figure A.2. These curves represent the ratio between the shear stress measured in the rheometer at each time stamp by the shear rate measured in a set of curves, and by the shear rate computed using the Bingham model. Table A.2 presents the numerical values for the Bingham model computation.

Tab. A.2. Numerical values of Bingham model for both runs of Experiment A.

time stamp	1st run dynamic yield stress (τ_0)	2nd run dynamic yield stress (τ_0)	1st run plastic viscosity (μ)	2nd run plastic viscosity (μ)
5	18.599	13.013	0.562	0.536
20	3.323	3.544	0.363	0.414
35	18.386	35.894	0.894	0.512
50	46.928	89.659	0.686	0.000

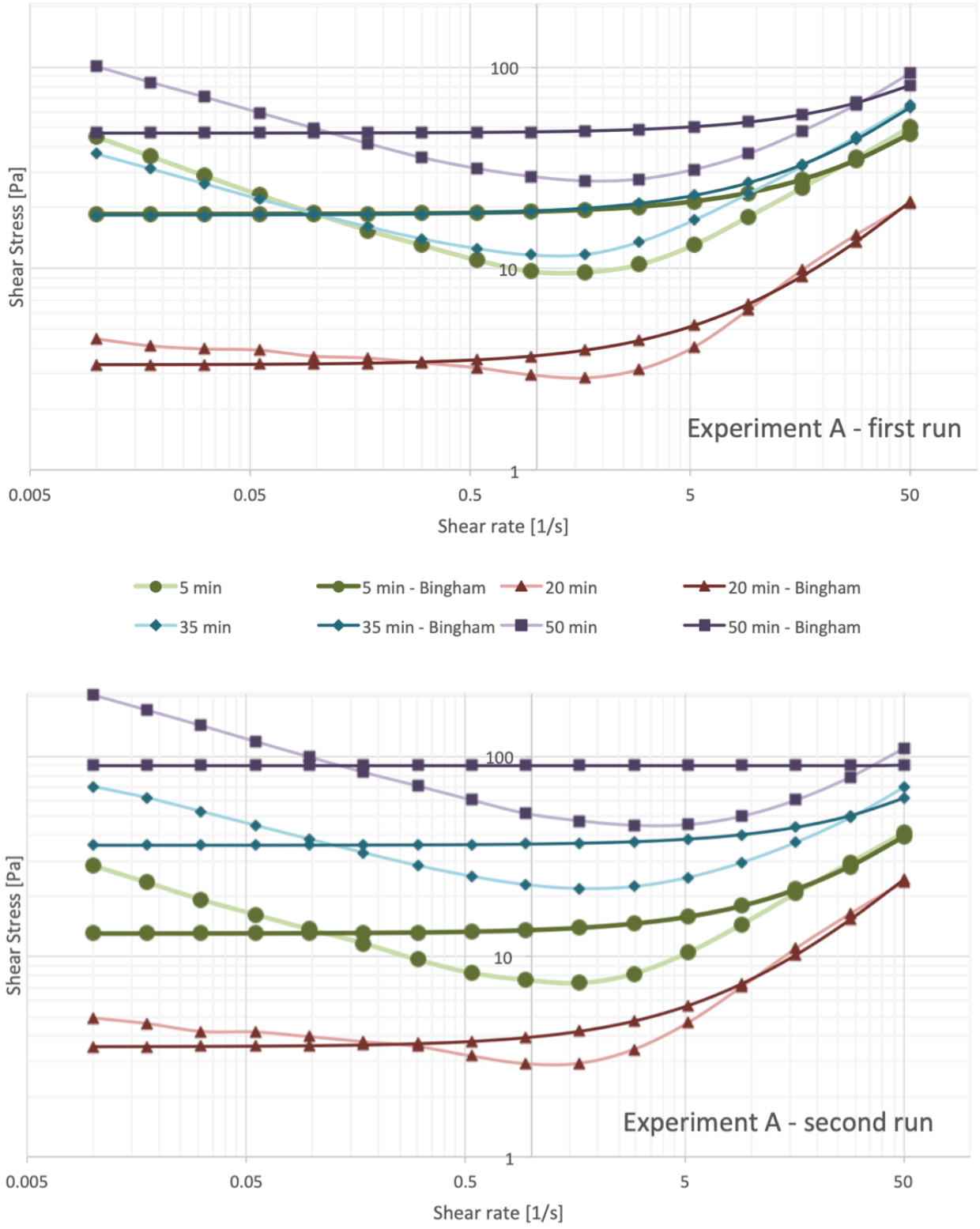

Fig. A.2. Flow curves (shear rate and shear stress ratio) for both runs of Experiment A.

Figure A.3 presents numerical results for the viscosity versus the shear rate for both runs of Experiment A. Table A.3 presents the numerical values for these curves.

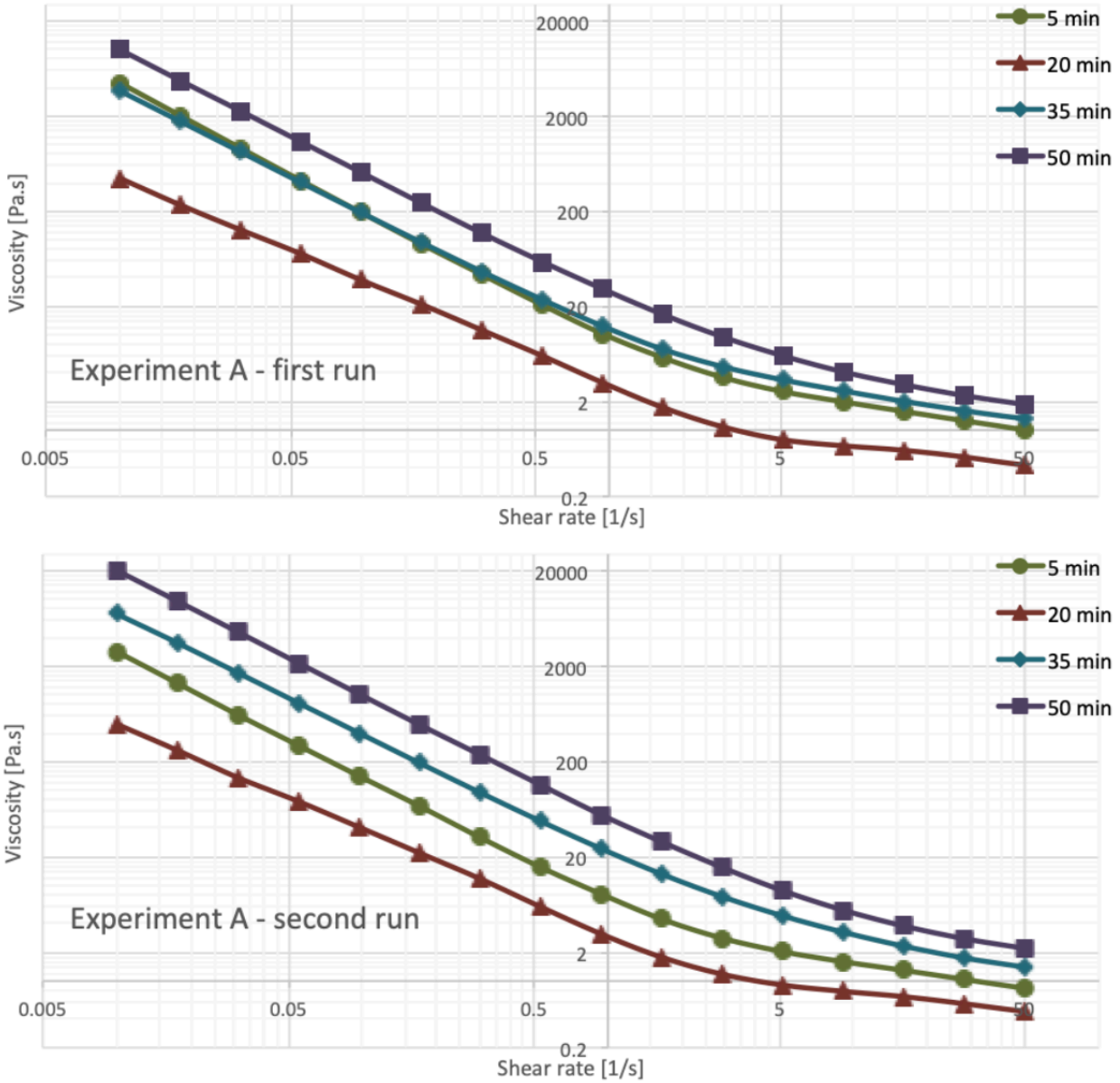

Fig. A.3. Viscosity over shear rate for both runs of Experiment A.

Tab. A.3. Viscosity over shear rate values for both runs of Experiment A.

Shear rate	1st run 5 min	2nd run 5 min	1st run 20 min	2nd run 20 min	1st run 35 min	2nd run 35 min	1st run 50 min	2nd run 50 min
28.340	1.2	1.0	0.5	0.6	1.6	1.7	2.3	2.8
9.103	2.0	1.6	0.7	0.8	2.6	3.2	4.1	5.5
2.924	3.6	2.8	1.1	1.2	4.6	7.6	9.5	15.5
0.939	10.3	8.1	3.2	3.1	12.4	24.3	30.5	55.2

Shear rate	1st run 5 min	2nd run 5 min	1st run 20 min	2nd run 20 min	1st run 35 min	2nd run 35 min	1st run 50 min	2nd run 50 min
0.302	43.2	32.0	11.3	11.8	46.4	94.5	117.6	235.5
0.097	194.0	141.1	37.8	41.0	193.7	398.3	512.9	1,022.0
0.031	925.0	618.0	127.9	135.7	843.8	1,704.0	2,273.0	4,564.0
0.010	4,498.0	2,847.0	446.9	493.4	3,701.0	7,062.0	10,060.0	20,200.0

In Figure A.4, it is presented the shear rate applied for six minutes (360 seconds) and the resulting viscosity at each time stamp for both runs of Experiment A. Table 5.4 presents the numerical values shown in Figure 5.4.

Tab. A.4. Shear rate and apparent viscosity over time values for both runs of Experiment A.

run	time	shear rate	shear stress 5 min	apparent viscosity 5 min	shear stress 20 min	apparent viscosity 20 min	shear stress 35 min	apparent viscosity 35 min	shear stress 50 min	apparent viscosity 50 min
1st	60	50.00	48.93	0.98	20.89	0.42	67.08	1.34	96.50	1.93
	75	50.00	50.11	1.00	20.97	0.42	64.53	1.29	92.56	1.85
	105	16.06	25.12	1.56	9.81	0.61	32.10	2.00	48.05	2.99
	150	2.92	10.43	3.57	3.15	1.08	13.50	4.62	27.72	9.48
	195	0.53	11.01	20.69	3.21	6.04	12.55	23.57	31.36	58.92
	225	0.13	15.44	90.29	3.59	20.98	16.09	94.13	41.68	243.80
	270	0.03	28.78	925.00	3.98	127.90	26.26	843.80	70.77	2,273.00
	300	0.01	44.98	4,498.00	4.47	446.90	37.01	3,701.00	100.60	10,060.00
	360	0.01	95.13	9,510.00	6.60	659.10	71.52	7,158.00	195.00	19,500.00
2nd	60	50.00	41.57	0.83	24.07	0.48	70.10	1.40	111.30	2.23
	75	50.00	41.37	0.83	23.67	0.47	69.59	1.39	109.70	2.19
	105	16.06	20.71	1.29	10.98	0.68	37.11	2.31	60.35	3.76
	150	2.92	8.197	2.80	3.44	1.18	22.34	7.64	45.20	15.46
	195	0.53	8.281	15.56	3.18	5.98	25.16	47.27	60.40	113.50
	225	0.13	11.63	68.03	3.76	21.97	33.00	193.00	83.15	486.50
	270	0.03	19.23	618.00	4.23	135.70	53.03	1,704.00	142.10	4,564.00
	300	0.01	28.44	2,847.00	4.93	493.40	70.63	7,062.00	202.00	20,200.00
	360	0.01	60.09	6,006.00	7.57	766.20	133.70	13,370.00	396.10	39,530.00

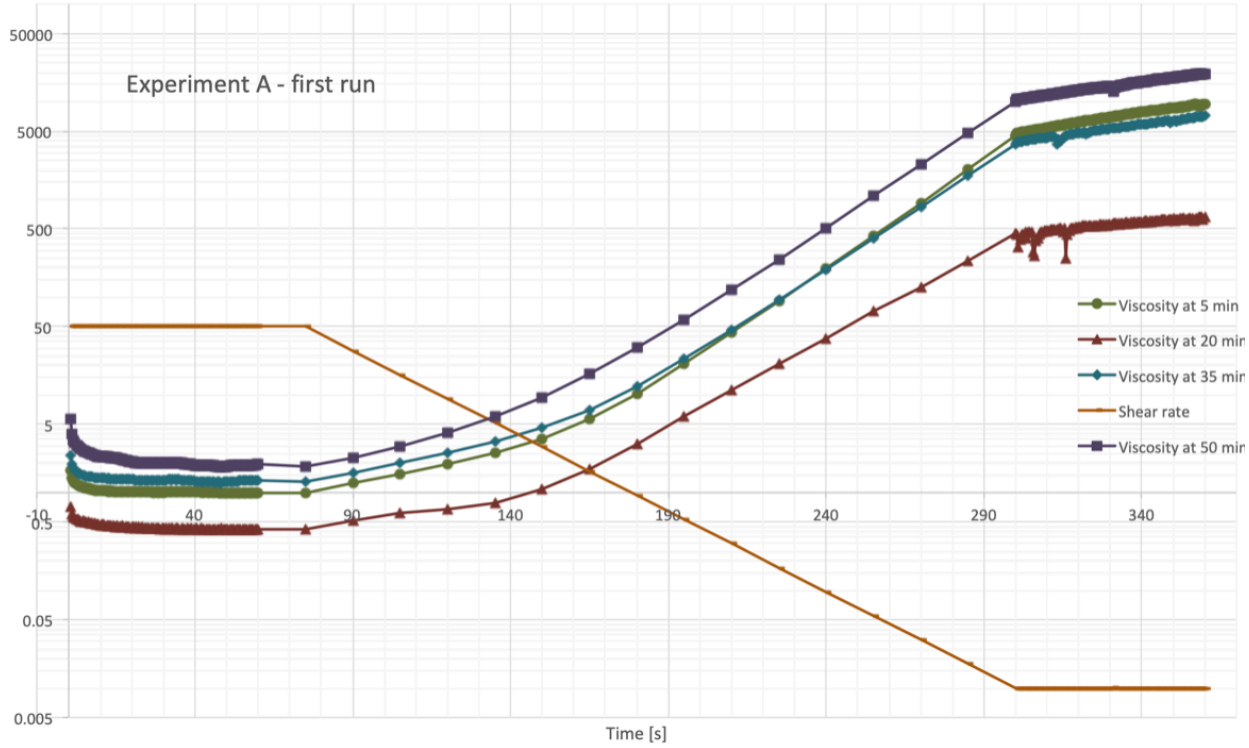

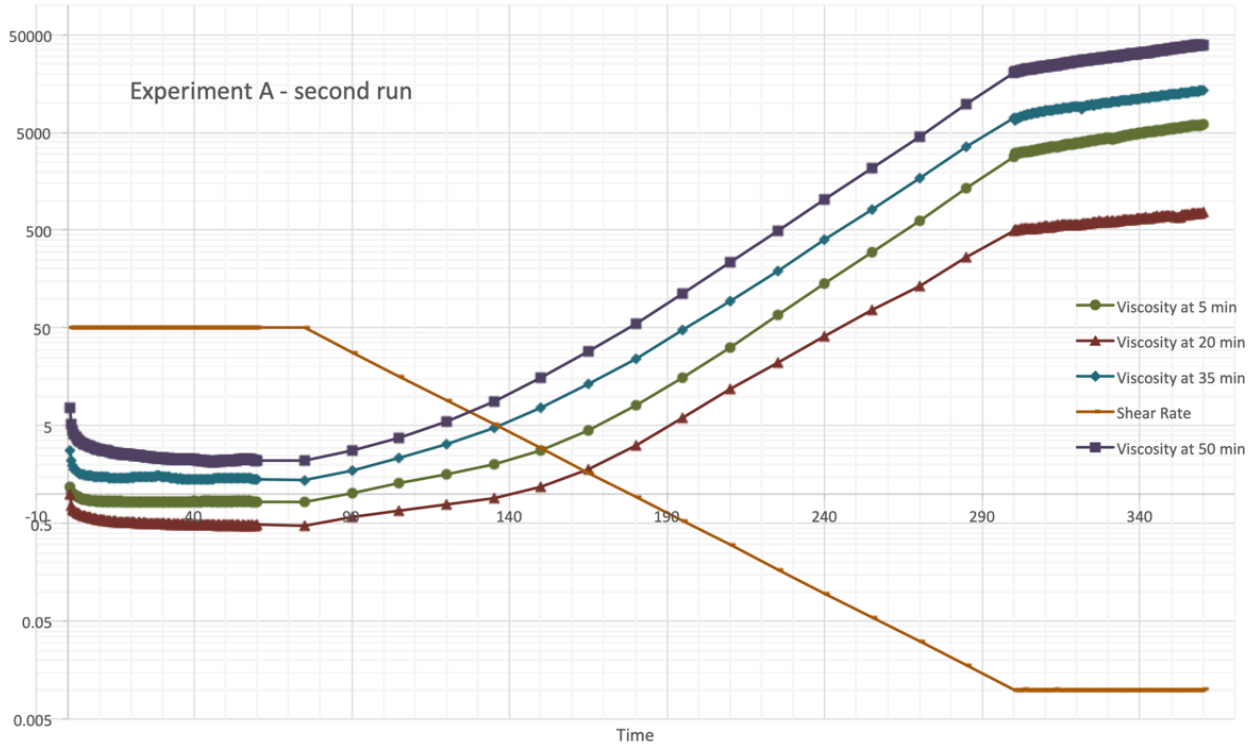

Fig. A.4. Shear rate and viscosity over time for both runs of Experiment A.

B. Annex - Numerical Results for Experiment B

This second annex presents the numerical results of Experiment B as described in Chapter 4. This experiment consists in the preservation method P1, shear strain sequence S1, time stamps of 5, 20, 35, and 50 minutes, rheometer hood open, and no cement paste footprint analysis. Experiment B was performed twice, therefore the results are always presented for both runs. Figure B.1 shows the shear stress curves obtained for the first 60 seconds after the shear strain sequence was started. Table B.1 presents the last four results to each curve, plus the average and the standard deviation.

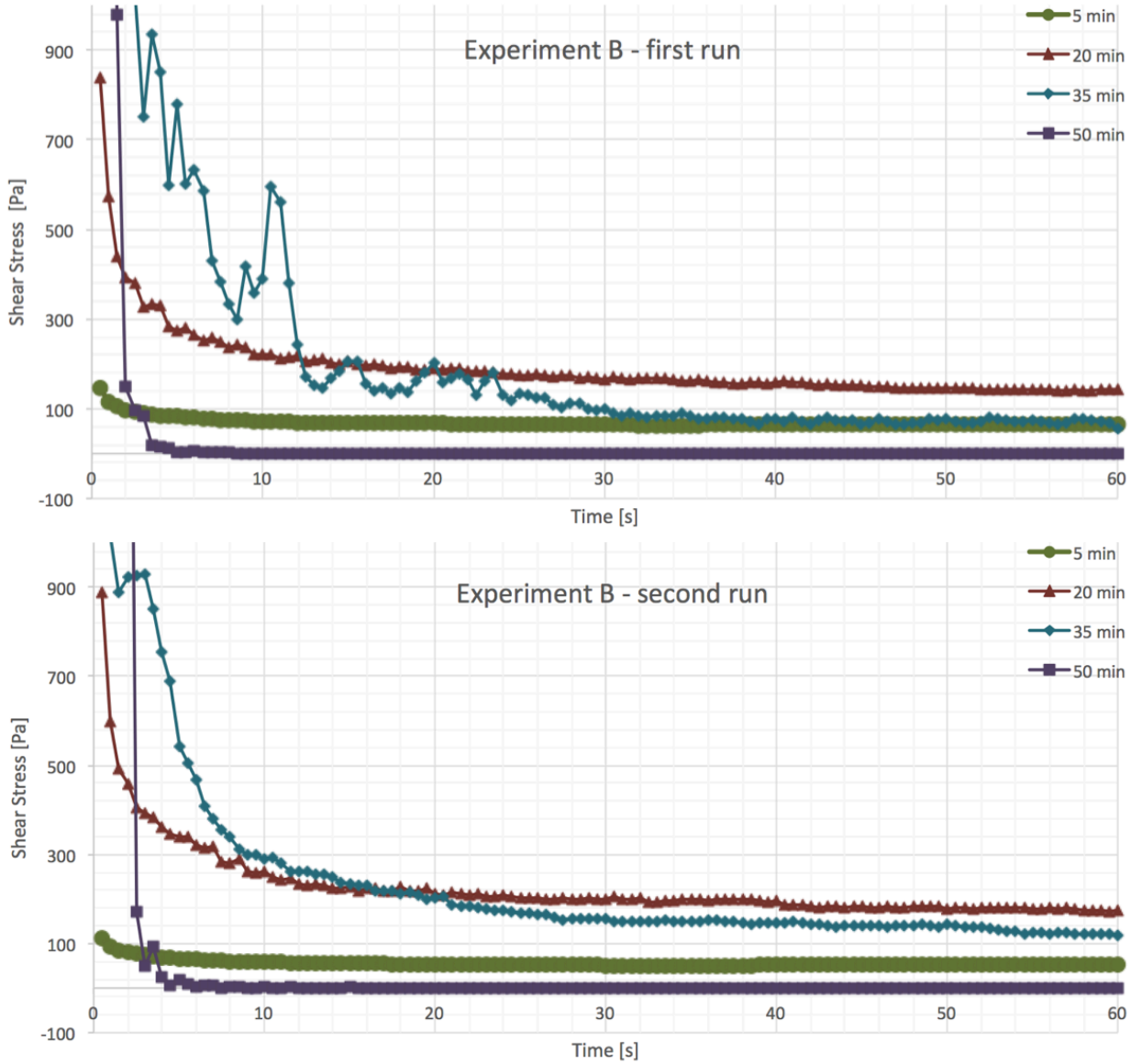

Fig. B.1. Shear stress for both runs of Experiment B.

Tab. B.1. Shear stress steady state for both runs of Experiment B.

run	time stamp	shear stress last four values				average	std dev
1st	5	64.55	64.38	64.70	64.53	64.54	0.13
	20	140.7	142.4	142.3	142.2	141.90	0.80
	35	73.16	71.24	67.29	55.72	66.85	7.81
	50	38.23	38.23	38.23	38.23	38.23	0.00
2nd	5	53.55	53.89	54.08	53.89	53.85	0.22
	20	175.8	173.7	172.6	173.2	173.83	1.39
	35	121.4	122.8	122.2	119.7	121.53	1.35
	50	0.02	0.26	-0.19	-0.06	0.01	0.19

Applying the Bingham model to the obtained results for experiment B we obtain the flow curves presented in Figure B.2. Analogously to Experiment A results, these curves represent the ratio between the shear stress measured in the rheometer at each time stamp by the shear rate measured in a set of curves, and by the shear rate computed using the Bingham model. Table B.2 presents the numerical values for the Bingham model computation.

Tab. B.2. Numerical values of Bingham model for both runs of Experiment B.

time stamp	1st run dynamic yeld stress (τ_0)	2nd run dynamic yeld stress (τ_0)	1st run plastic viscosity (μ)	2nd run plastic viscosity (μ)
5	48.153	28.203	0.128	0.479
20	132.817	160.031	0.000	0.000
35	68.189	134.886	0.000	0.000
50	0.005	0.095	0.000	0.000

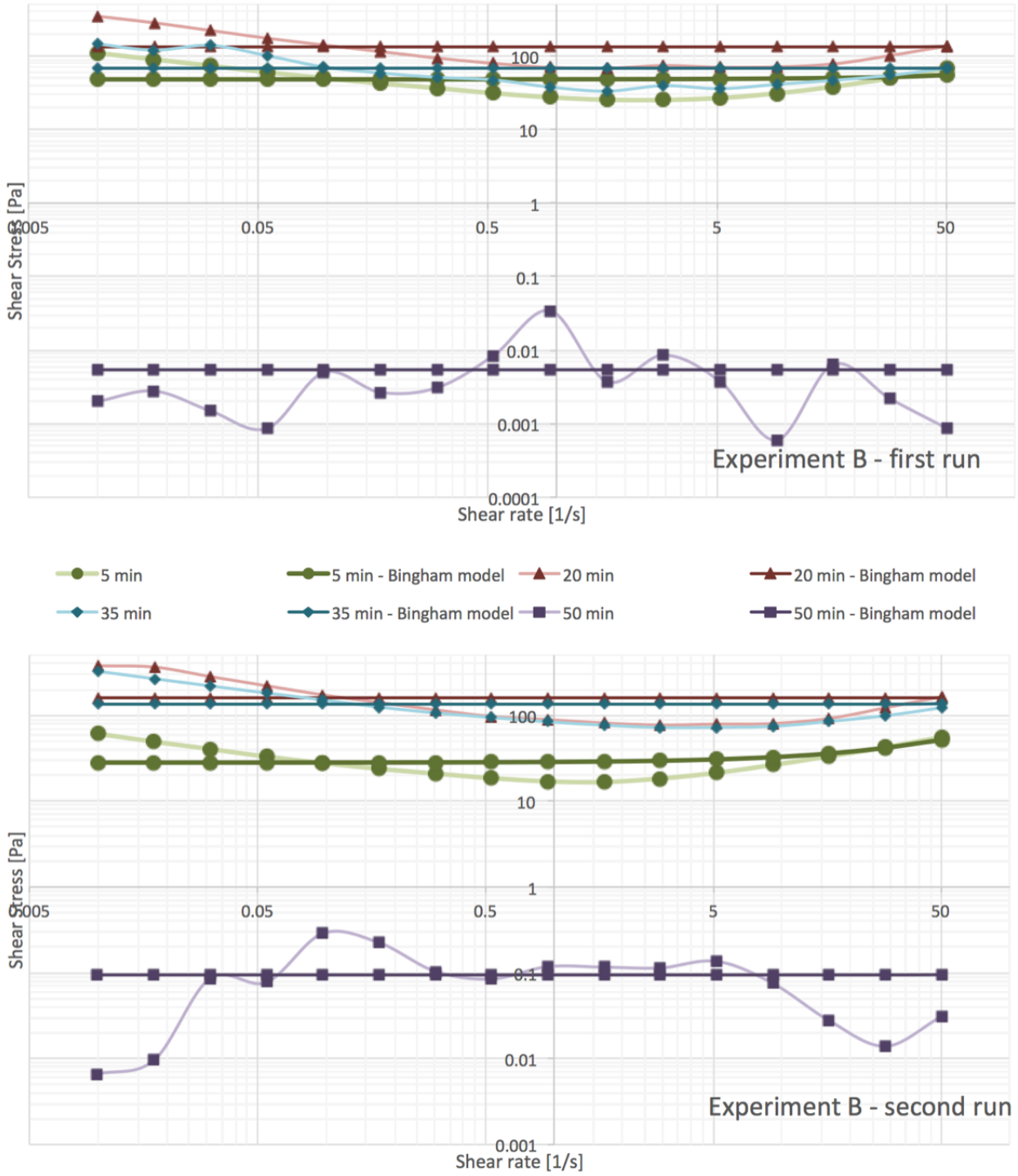

Fig. B.2. Flow curves (shear rate and shear stress ratio) for both runs of Experiment B.

The remainder results obtained from Experiment B are the numerical results for the viscosity versus the shear rate as show in Figure B.3. This figure presents the results of the viscosity in function with the shear rate for both runs of Experiment B. Table B.3 presents the numeric values plotted in Figure B.3.

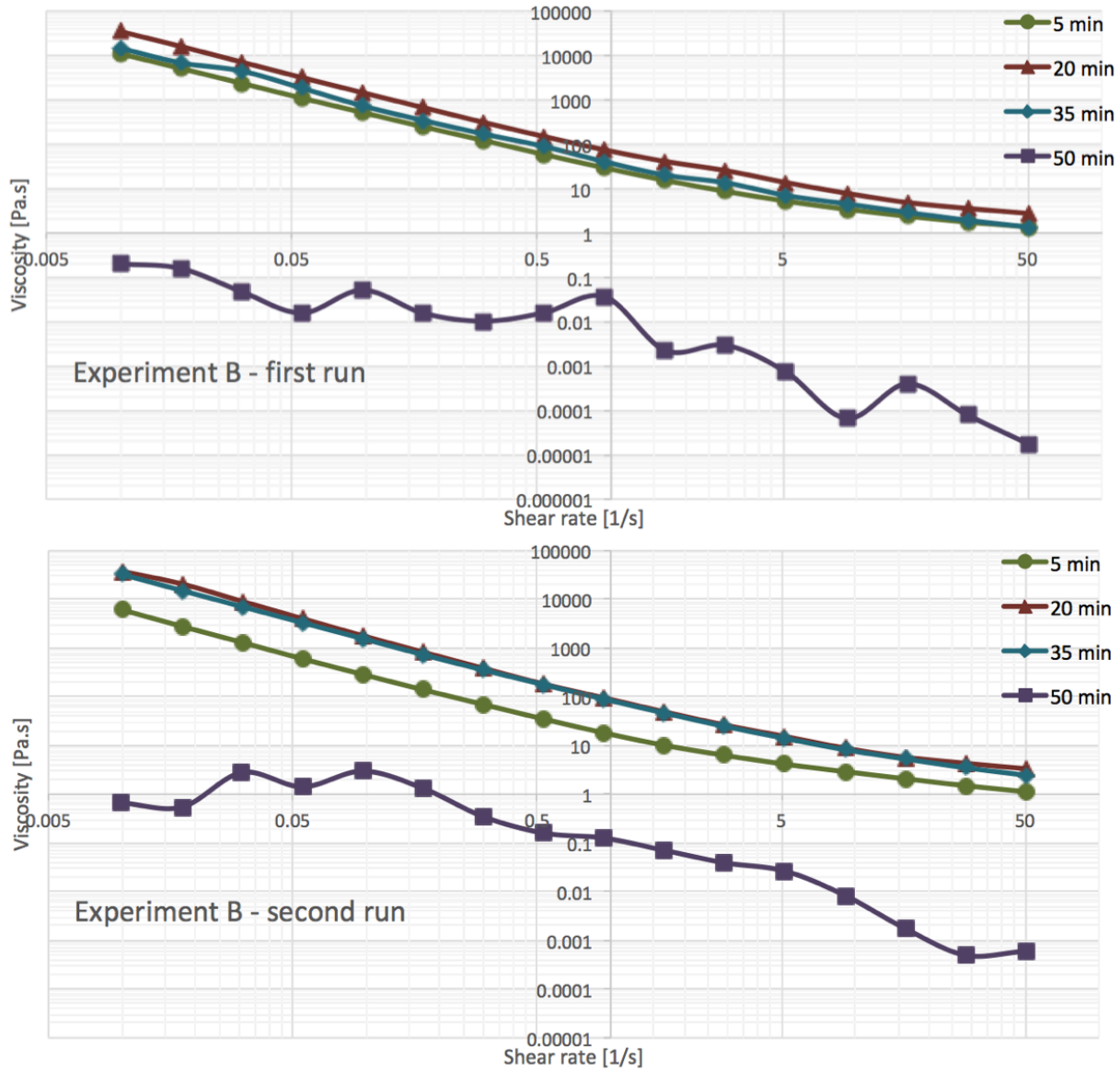

Fig. B.3. Viscosity over shear rate for both runs of Experiment B.

Tab. B.3. Viscosity over shear rate values for both runs of Experiment B.

Shear rate	1st run 5 min	2nd run 5 min	1st run 20 min	2nd run 20 min	1st run 35 min	2nd run 35 min	1st run 50 min	2nd run 50 min
28.340	1.8	1.5	3.6	4.3	1.9	3.5	0.0	0.0
9.103	3.4	2.9	7.8	8.8	4.5	8.2	0.0	0.0
2.924	8.6	6.3	25.4	26.4	13.5	24.7	0.0	0.0
0.939	29.2	18.1	74.4	94.9	40.3	89.5	0.0	0.1
0.302	121.4	69.5	311.0	384.5	170.2	354.3	0.0	0.3
0.097	518.2	286.6	1454.0	1787.0	732.3	1561.0	0.1	3.0

Shear rate	1st run 5 min	2nd run 5 min	1st run 20 min	2nd run 20 min	1st run 35 min	2nd run 35 min	1st run 50 min	2nd run 50 min
0.031	2367.0	1300.0	7132.0	9079.0	4470.0	7067.0	0.1	2.8
0.010	10940.0	6099.0	34740.0	37790.0	14570.0	32600.0	0.2	0.7

In Figure B.4, it is presented the shear rate applied for six minutes (360 seconds) and the resulting viscosity at each time stamp for both runs of Experiment B. Table B.4 presents the numerical values shown in Figure B.4.

Tab. B.4. Shear rate and apparent viscosity over time values for both runs of Experiment B.

run	time	shear rate	shear stress 5 min	apparent viscosity 5 min	shear stress 20 min	apparent viscosity 20 min	shear stress 35 min	apparent viscosity 35 min	shear stress 50 min	apparent viscosity 50 min
1st	60	38.23	64.53	1.29	142.20	2.85	55.72	1.11	0.25	0.01
	75	38.23	67.89	1.36	137.70	2.75	67.77	1.36	0.00	0.00
	105	12.28	38.21	2.38	77.96	4.854	46.66	2.91	0.01	0.00
	150	2.24	25.23	8.63	74.22	25.39	39.46	13.50	0.01	0.00
	195	0.41	31.17	58.56	79.30	149.00	47.27	88.81	0.01	0.02
	225	0.13	42.32	247.60	114.80	671.40	58.73	343.50	0.00	0.02
	270	0.02	73.69	2,367.00	222.00	7,132.00	139.20	4,470.00	0.00	0.05
	300	0.01	109.40	10,940.00	347.40	34,740.00	145.70	14,570.00	0.00	0.20
	360	0.01	221.40	22,160.00	760.90	76,170.00	453.00	45,300.00	-0.00	-0.28
2nd	60	38.23	53.89	1.08	173.20	3.46	119.70	2.39	-0.06	-0.00
	75	38.23	56.17	1.12	165.70	3.32	122.10	2.44	0.03	0.00
	105	12.28	33.27	2.07	91.75	5.71	84.83	5.28	0.03	0.00
	150	2.24	18.36	6.28	77.07	26.36	72.18	24.69	0.11	0.04
	195	0.41	18.56	34.88	97.08	182.40	94.31	177.20	0.08	0.16
	225	0.13	23.82	139.30	141.20	826.20	124.90	730.40	0.22	1.31
	270	0.02	40.45	1,300.00	282.70	9,079.00	220.00	7,067.00	0.09	2.78
	300	0.01	60.99	6,099.00	377.90	37,790.00	326.10	32,600.00	0.01	0.67
	360	0.01	131.70	13,170.00	885.80	88,630.00	675.00	67,650.00	0.05	4.90

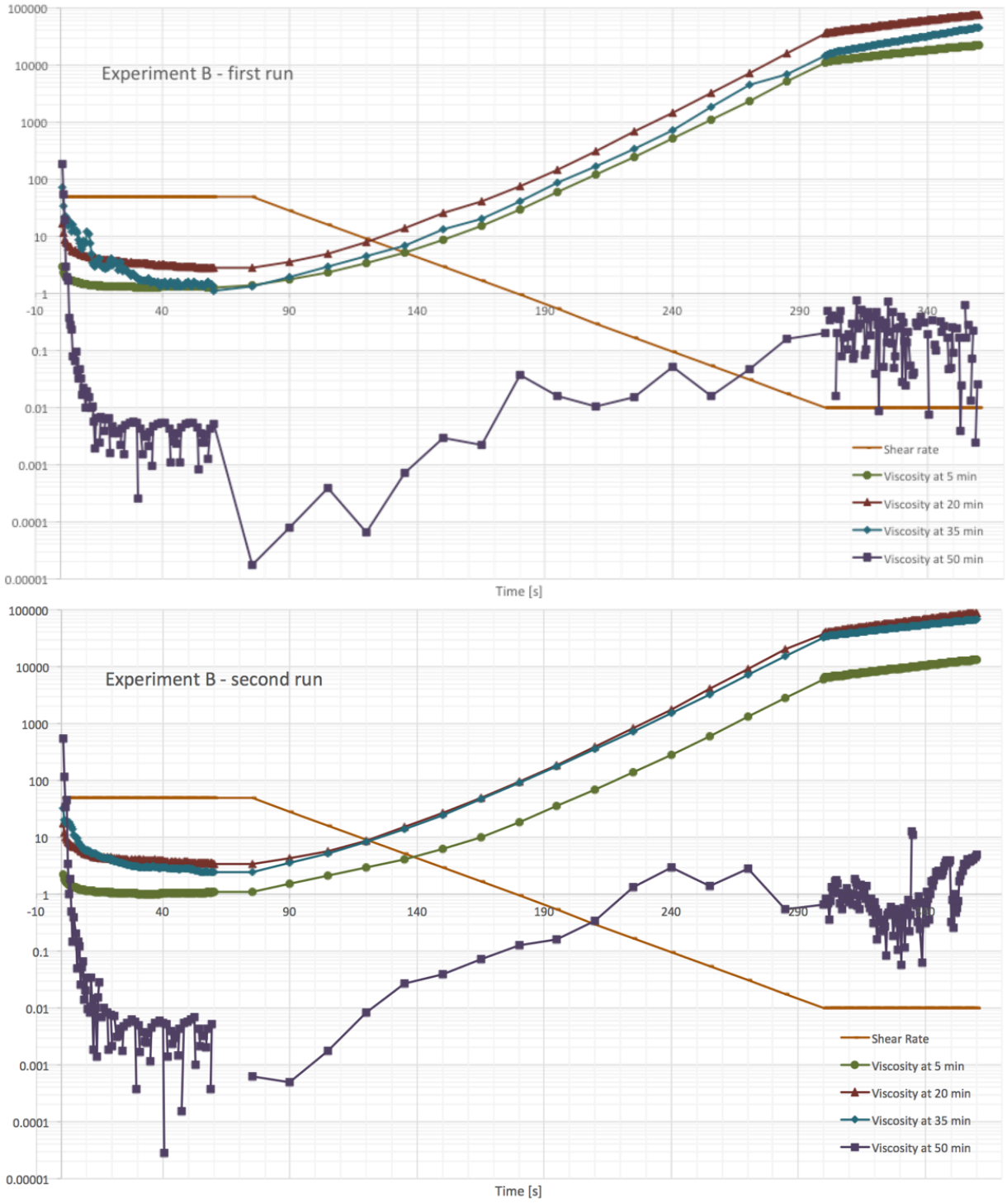

Fig. B.4. Shear rate and viscosity over time for both runs of Experiment B.

C. Annex - Numerical Results for Experiment C

This third annex presents the numerical results of Experiment C as described in Chapter 4. This experiment consists in the preservation method P2, shear strain sequence S2, time stamps of 5, 20, 40, and 60 minutes, rheometer hood open, and no cement paste footprint analysis. Unlike experiments A and B, Experiment C was performed only once. Figure C.1 shows the shear stress curves obtained for the first 60 seconds after the shear strain sequence was started. Table C.1 presents the last four results to each curve, plus the average and the standard deviation.

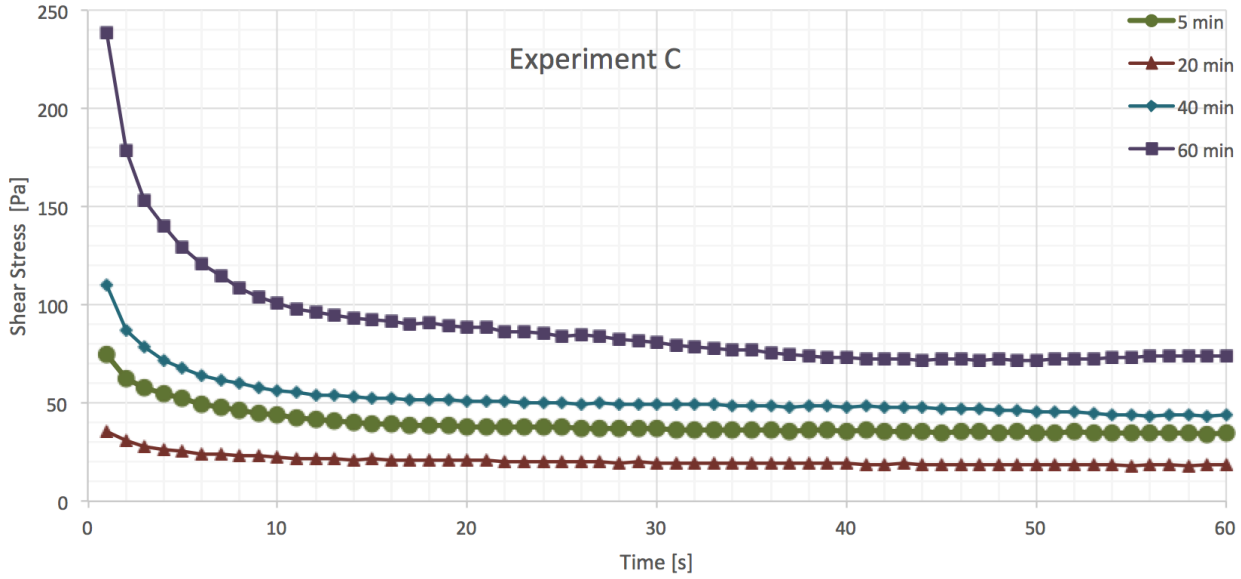

Fig. C.1. Shear stress for Experiment C.

Tab. C.1. Shear stress steady state for Experiment C.

time stamp	shear stress last four values				average	std dev
5	34.73	34.70	34.29	34.68	34.60	0.21
20	38.23	38.23	38.23	38.23	38.23	0.00
40	43.71	43.75	43.38	43.84	43.67	0.20
60	74.31	73.75	74.36	74.38	74.20	0.30

Applying the Bingham model to the obtained results for experiment C we obtain the flow curves presented in Figure C.2. These curves represent the ratio between the shear stress measured in the rheometer at each time stamp by the shear rate measured in a set of curves, and by the shear rate computed using the Bingham model. Table C.2 presents the numerical values for the Bingham model computation.

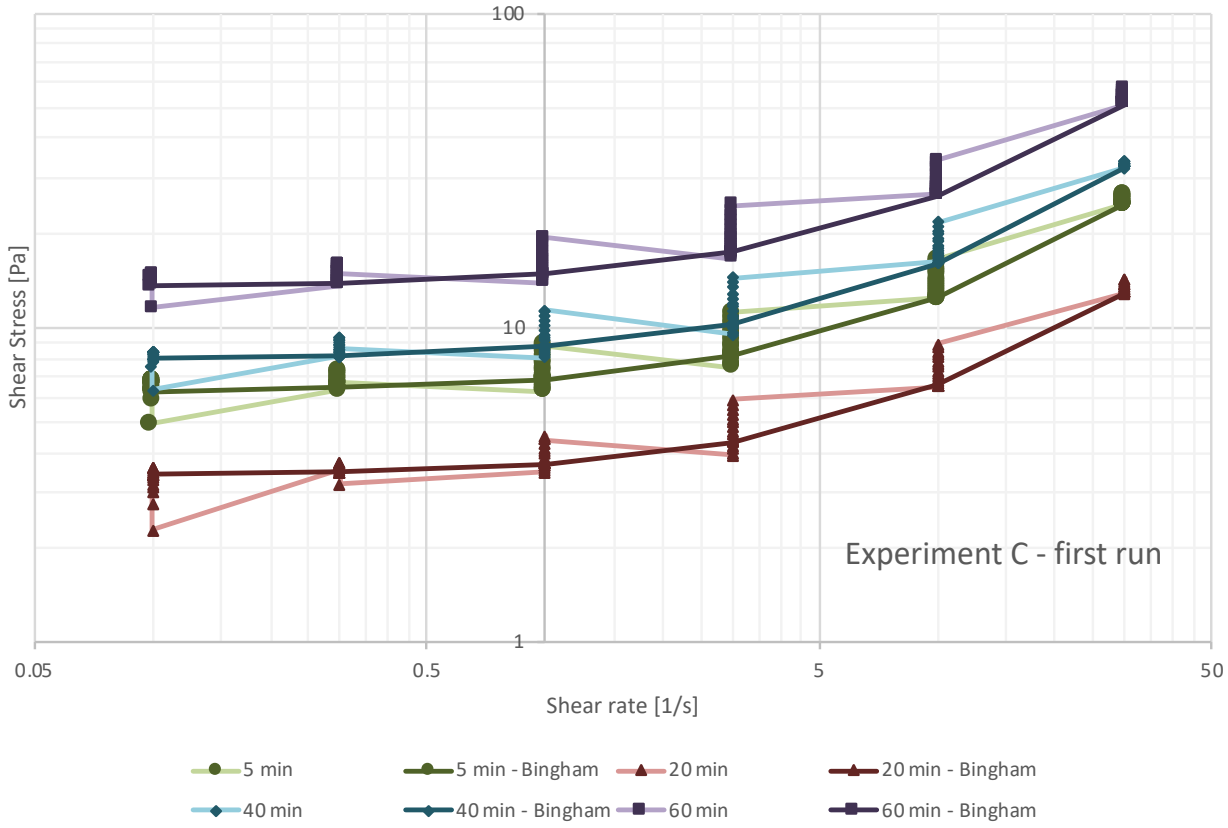

Fig. C.2. Flow curves (shear rate and shear stress ratio) for Experiment C.

Tab. C.2. Numerical values of Bingham model for Experiment C.

time stamp	dynamic yield stress (τ_0)	plastic viscosity (μ)
5	6.234	0.614
20	3.368	0.320
40	7.859	0.822
60	13.579	1.267

Carrying on the gathering of numerical results for Experiment C, Figure C.3 shows the viscosity versus the shear rate. Table C.3 presents the numeric values plotted in Figure C.3.

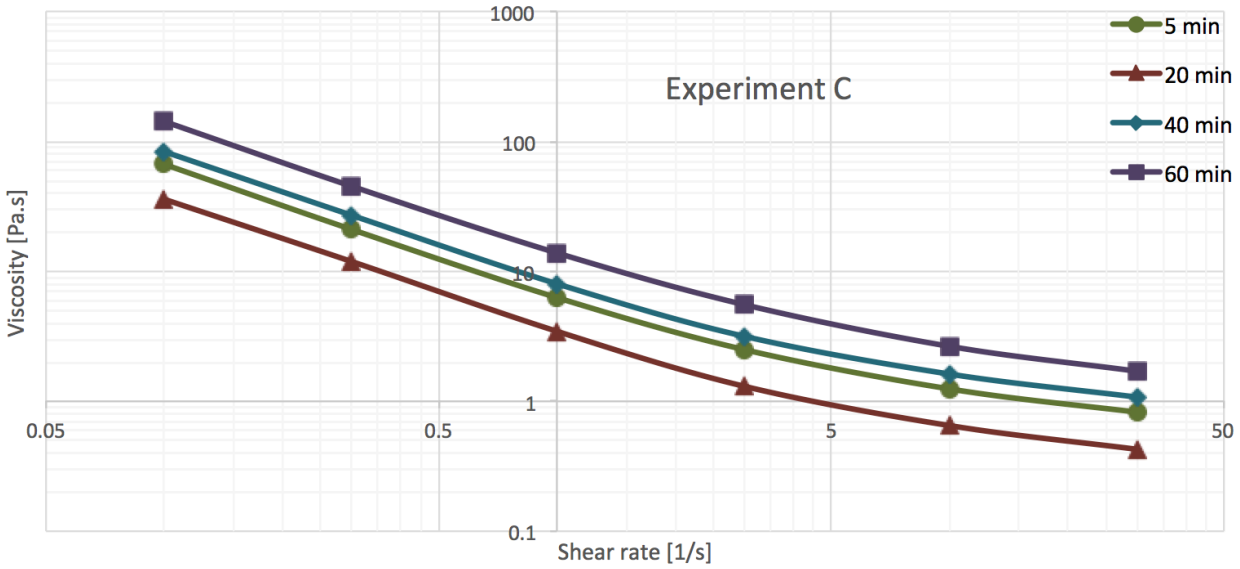

Fig. C.3. Viscosity over shear rate for Experiment C.

Tab. C.3. Viscosity over shear rate values for Experiment C.

Shear rate	5 min	20 min	40 min	60 min
30.0	0.8	0.4	1.1	1.7
10.0	1.2	0.7	1.6	2.7
3.0	2.5	1.3	3.2	5.6
1.0	6.3	3.5	8.0	13.9
0.3	21.1	11.9	27.1	45.3
0.1	66.8	36.0	83.7	142.9

Figure C.4 presents the shear rate applied for almost four minutes (225 seconds) and the resulting viscosity at each time stamp for Experiment C. Table C.4 presents the numerical values shown in Figure C.4.

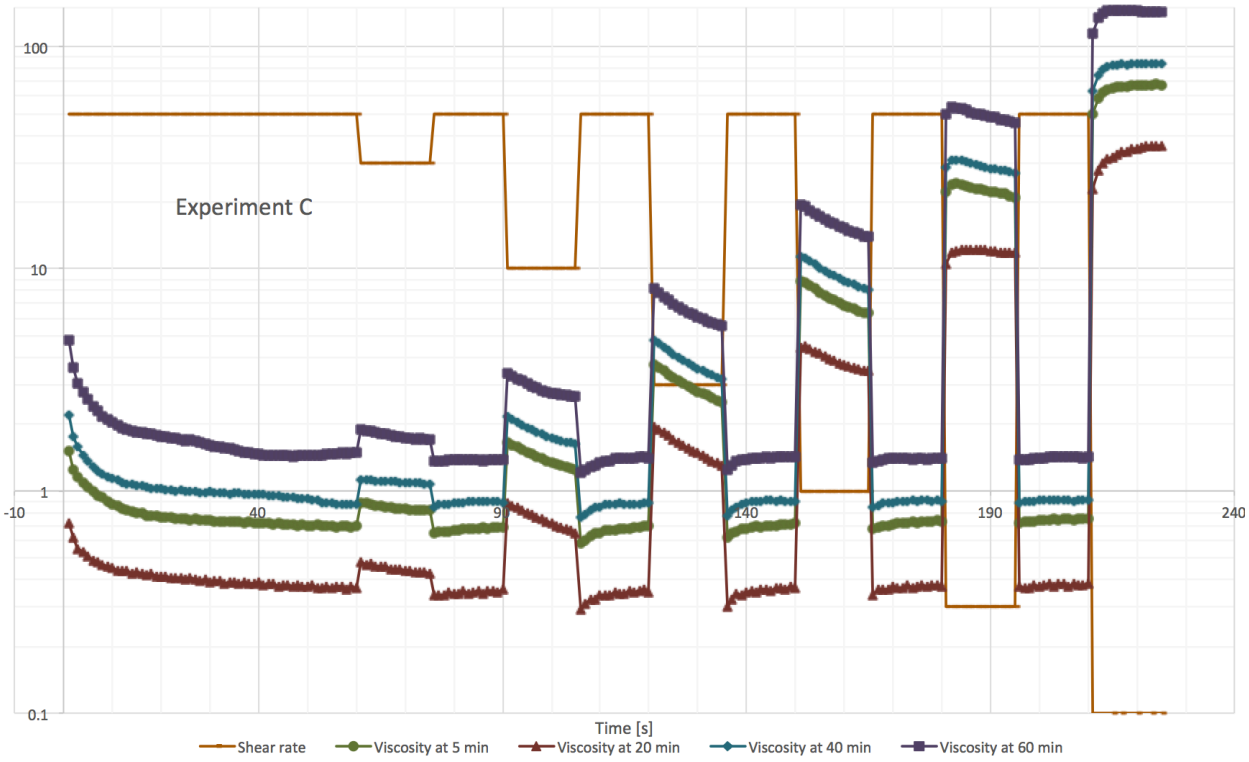

Fig. C.4. Shear rate and viscosity over time for Experiment C.

Tab. C.4. Shear rate and apparent viscosity over time values for Experiment C.

time	shear rate	shear stress 5 min	apparent viscosity 5 min	shear stress 20 min	apparent viscosity 20 min	shear stress 40 min	apparent viscosity 40 min	shear stress 60 min	apparent viscosity 60 min
60	50.0	34.68	0.69	18.27	0.37	43.84	0.88	74.38	1.49
75	30.0	24.59	0.82	12.82	0.43	32.35	1.08	51.19	1.71
90	50.0	34.08	0.68	17.99	0.36	44.51	0.89	69.33	1.39
105	10.0	12.46	1.25	6.51	0.65	16.22	1.62	26.52	2.65
120	50.0	34.92	0.70	17.62	0.35	44.18	0.88	70.68	1.41
135	3.0	7.51	2.50	3.92	1.31	9.50	3.17	16.66	5.55
150	50.0	35.88	0.72	18.25	0.37	45.07	0.90	70.72	1.42
165	1.0	6.29	6.29	3.46	3.46	8.04	8.04	13.89	13.89
180	50.0	36.59	0.73	18.55	0.37	45.11	0.90	69.79	1.40
195	0.3	6.33	21.07	3.58	11.93	8.12	27.09	13.61	45.34
210	50.0	37.42	0.75	19.23	0.38	45.20	0.90	71.41	1.43
225	0.1	6.69	66.84	3.60	35.97	8.37	83.70	14.28	142.90

D. Annex - Numerical Results for Experiment D

This fourth annex presents the numerical results of Experiment D as described in Chapter 4. This experiment consists in the preservation method P3, shear strain sequence S2, time stamps of 5, 20, 40, 60, and 80 minutes, rheometer hood closed, cement paste footprint F1, with density analysis starting at time stamp 20 and quantity of water for all time stamps. As Experiment C, Experiment D was performed only once. Figure D.1 shows the shear stress curves obtained for the first 60 seconds after the shear strain sequence was started. Table D.1 presents the last four results to each curve, plus the average and the standard deviation.

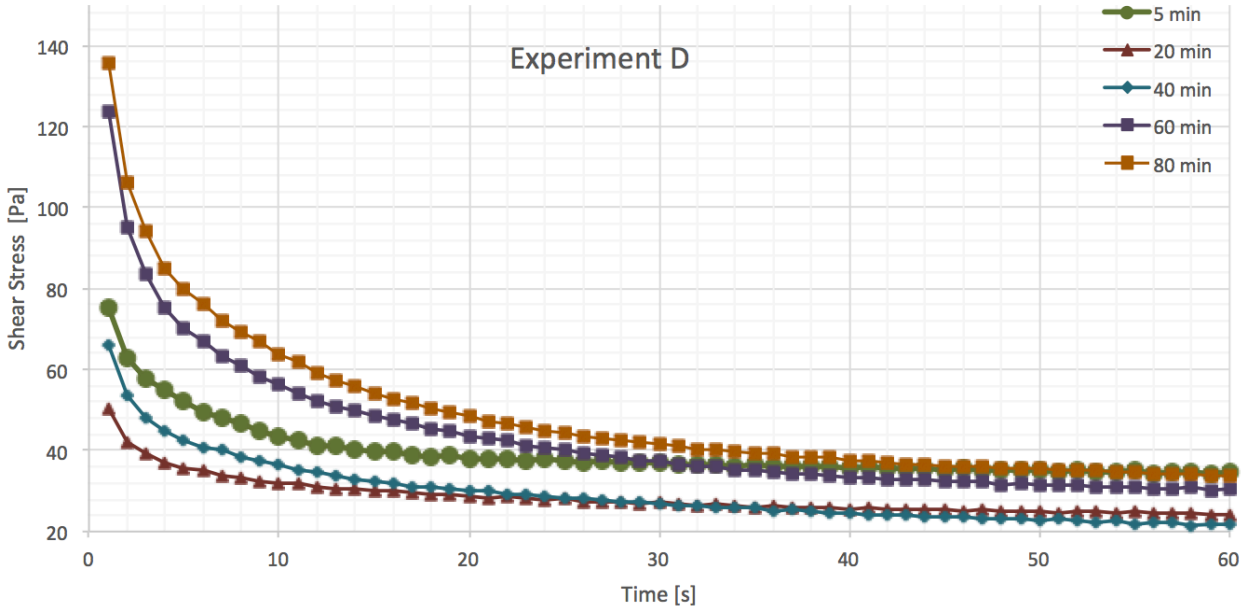

Fig. D.1. Shear stress for Experiment D.

Tab. D.1. Shear stress steady state for Experiment D.

time stamp	shear stress last four values				average	std dev
5	39.73	39.14	39.21	39.13	39.30	0.29
20	24.32	24.64	24.17	24.26	24.35	0.20
40	38.23	38.23	38.23	38.23	38.23	0.00
60	30.73	30.78	30.22	30.46	30.55	0.26
80	34.03	34.22	33.65	33.64	33.89	0.29

Applying the Bingham model to the obtained results for experiment D we obtain the flow curves presented in Figure D.2. These curves represent the ratio between the shear stress measured in the rheometer at each time stamp by the shear rate measured in a set of curves, and by the shear rate computed using the Bingham model. Table D.2 presents the numerical values for the Bingham model computation.

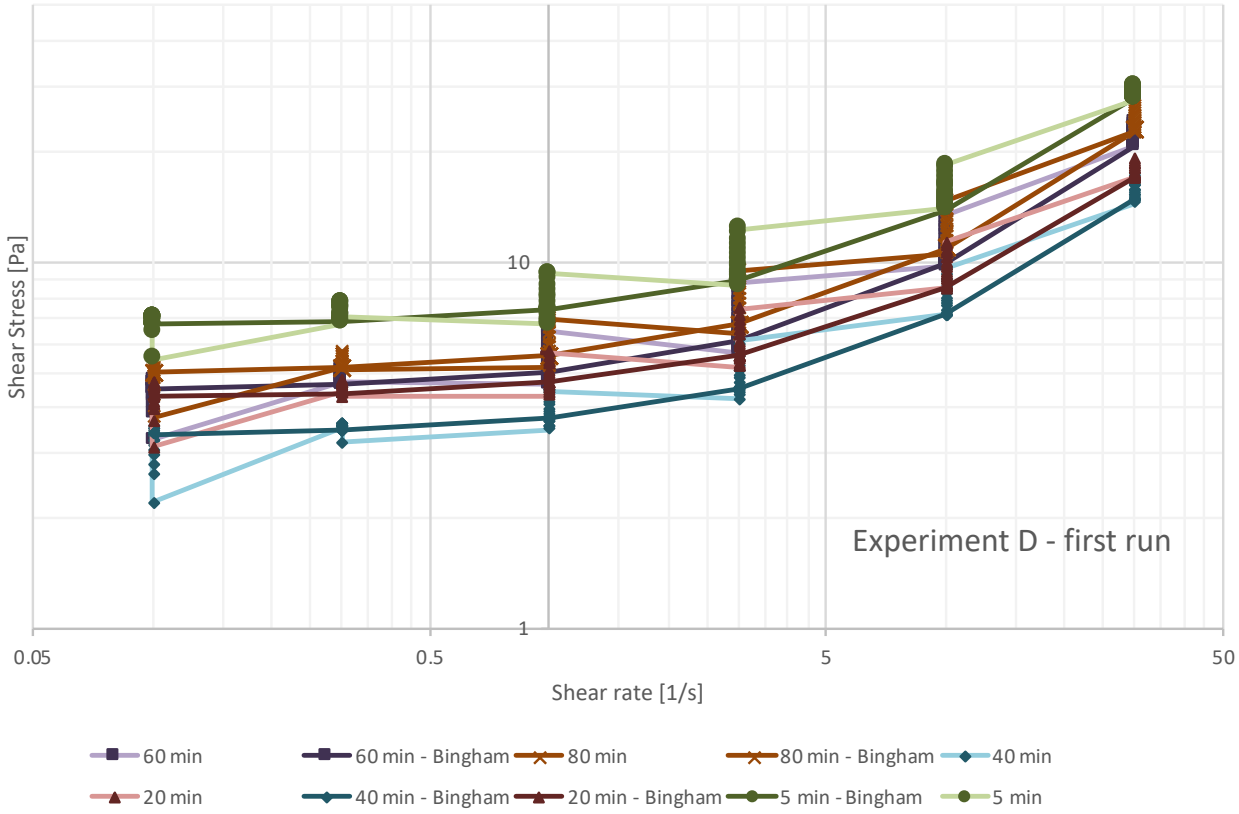

Fig. D.2. Flow curves (shear rate and shear stress ratio) for Experiment D.

Tab. D.2. Numerical values of Bingham model for Experiment D.

time stamp	dynamic yield stress (τ_0)	plastic viscosity (μ)
5	6.704	0.711
20	4.269	0.428
40	3.367	0.381
60	4.452	0.547
80	4.949	0.595

Carrying on the gathering of numerical results for Experiment D, Figure D.3 shows the viscosity versus the shear rate. Table D.3 presents the numeric values plotted in Figure D.3.

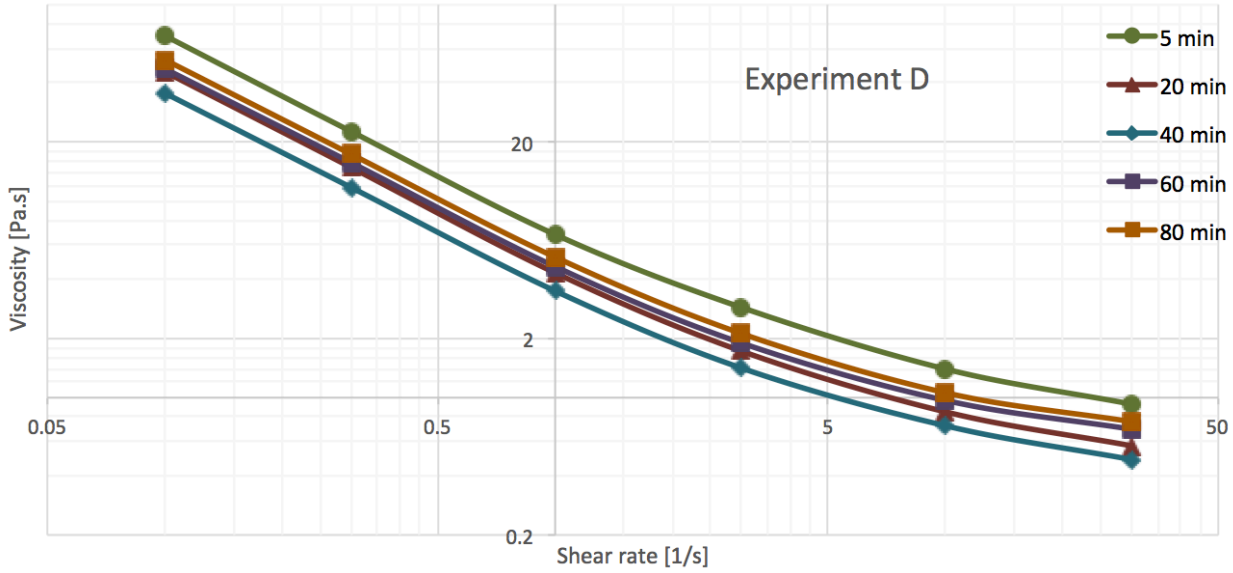

Fig. D.3. Viscosity over shear rate for Experiment D.

Tab. D.3. Viscosity over shear rate values for Experiment D.

Shear rate	5 min	20 min	40 min	60 min	80 min
30	0.9265	0.5686	0.4841	0.6907	0.7539
10	1.398	0.8463	0.7188	0.9679	1.059
3	2.877	1.725	1.414	1.897	2.119
1	6.76	4.315	3.49	4.643	5.187
0.3	22.63	14.85	11.74	15.71	17.33
0.1	69.49	45.53	35.44	47.18	52.43

In Figure D.4, it is presented the shear rate applied for almost four minutes (225 seconds) and the resulting viscosity at each time stamp for Experiment D. As expected, the viscosity increases as the shear rate drops for all time stamps. Table D.4 presents the numerical values shown in Figure D.4.

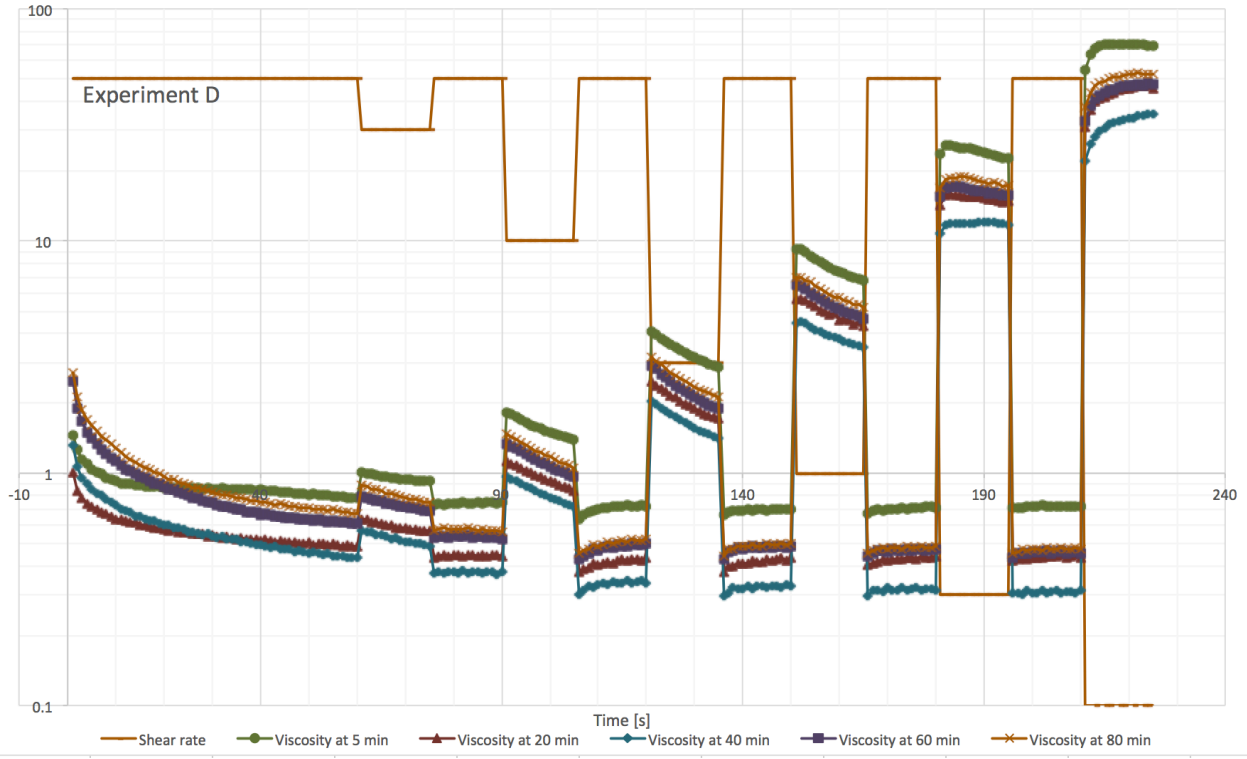

Fig. D.4. Shear rate and viscosity over time for Experiment D.

Tab. D.4. Shear rate and apparent viscosity over time values for Experiment D.

time	shear rate	shear stress 5 m.	app. visc. 5 m.	shear stress 20 m.	app. visc. 20 m.	shear stress 40 m.	app. visc. 40 m.	shear stress 60 m.	app. visc. 60 m.	shear stress 80 m.	app. visc. 80 m.
60	50.0	39.13	0.78	24.26	0.49	21.60	0.43	30.46	0.61	33.64	0.67
75	30.0	27.79	0.93	17.05	0.57	14.52	0.48	20.72	0.69	22.61	0.75
90	50.0	37.47	0.75	21.95	0.44	18.75	0.38	26.11	0.52	27.96	0.56
105	10.0	13.98	1.40	8.46	0.85	7.19	0.72	9.68	0.97	10.59	1.06
120	50.0	36.07	0.72	21.64	0.43	16.79	0.34	24.93	0.50	26.00	0.52
135	3.0	8.63	2.88	5.17	1.73	4.24	1.41	5.69	1.90	6.36	2.12
150	50.0	34.95	0.70	21.58	0.43	16.24	0.32	24.20	0.48	24.86	0.50
165	1.0	6.76	6.76	4.32	4.32	3.49	3.49	4.64	4.64	5.19	5.19
180	50.0	35.66	0.71	21.95	0.44	15.60	0.31	23.49	0.47	24.24	0.49
195	0.3	6.79	22.63	4.46	14.85	3.53	11.74	4.71	15.71	5.19	17.33
210	50.0	36.19	0.72	21.78	0.44	15.60	0.31	22.56	0.45	23.55	0.47
225	0.1	6.94	69.49	4.56	45.53	3.54	35.44	4.72	47.18	5.24	52.43

For Experiment D the paste footprint was analyzed from the 20 time stamp. Therefore, it was executed an analysis of density of the sample at time stamps 20, 40, 60, and 80. It was also measured the quantity of water in all time stamps (5 to 80). Finally, an analysis of the degased sample was performed one single time at the 20 time stamp. Figure D.5 depicts the results of such analysis and in Table D.5 the numerical values are informed.

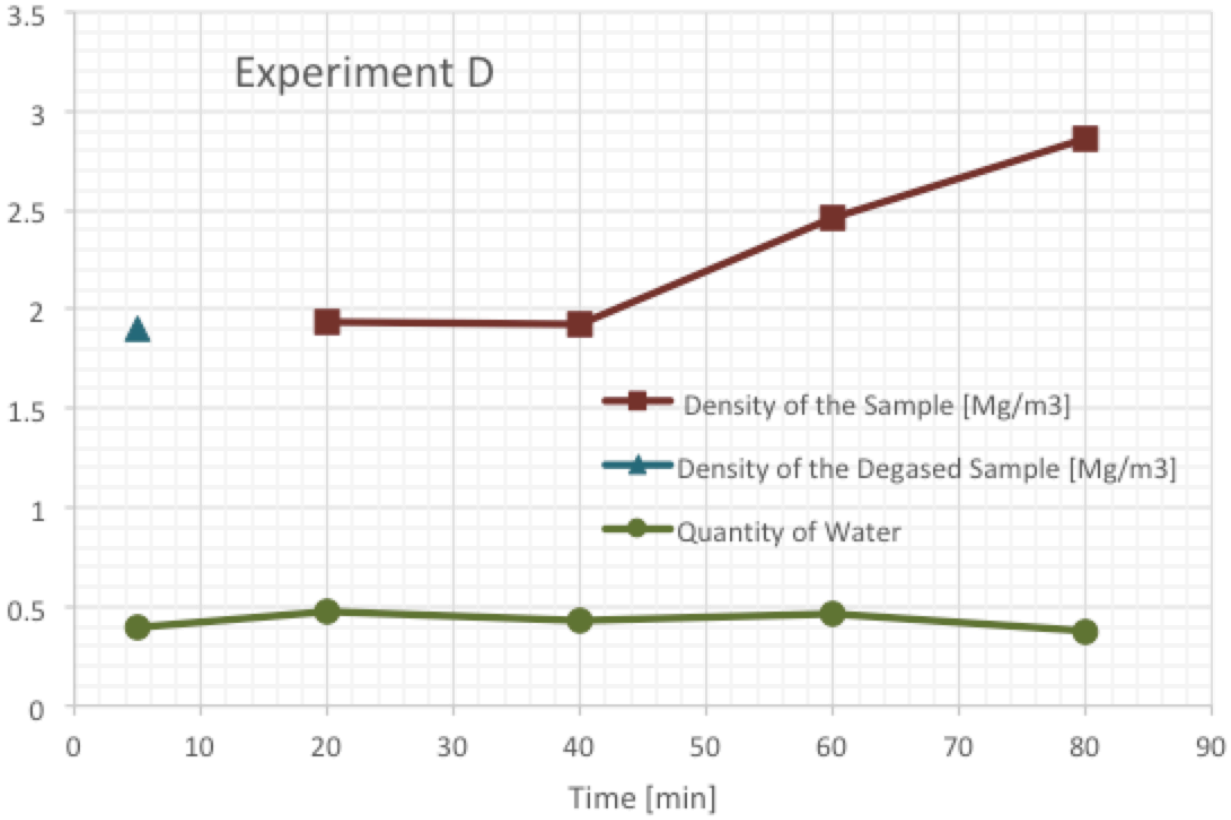

Fig. D.5. Paste footprint results for Experiment D.

Tab. D.5. Paste footprint values for Experiment D.

measure	5 min	20 min	40 min	60 min	80 min
Quantity of water %	40%	47%	43%	47%	38%
Density of Degased Sample [Mg/m3]		1.905			
Density Sample [Mg/m3]		1.938	1.920	2.459	2.863

E. Annex - Numerical Results for Experiment E

This fifth annex presents the numerical results of Experiment E as described in Chapter 4. This experiment consists in the preservation method P3, shear strain sequence S3, time stamps of 5, 20, 40, 60, and 80 minutes, rheometer hood closed, and cement paste footprint F2, with density analysis at time stamp 20 and quantity of water for all time stamps. As Experiments C and D, Experiment E was performed only once. Figure E.1 shows the shear stress curves obtained for the first 60 seconds after the shear strain sequence was started. Table E.1 presents the last four results to each curve, plus the average and the standard deviation.

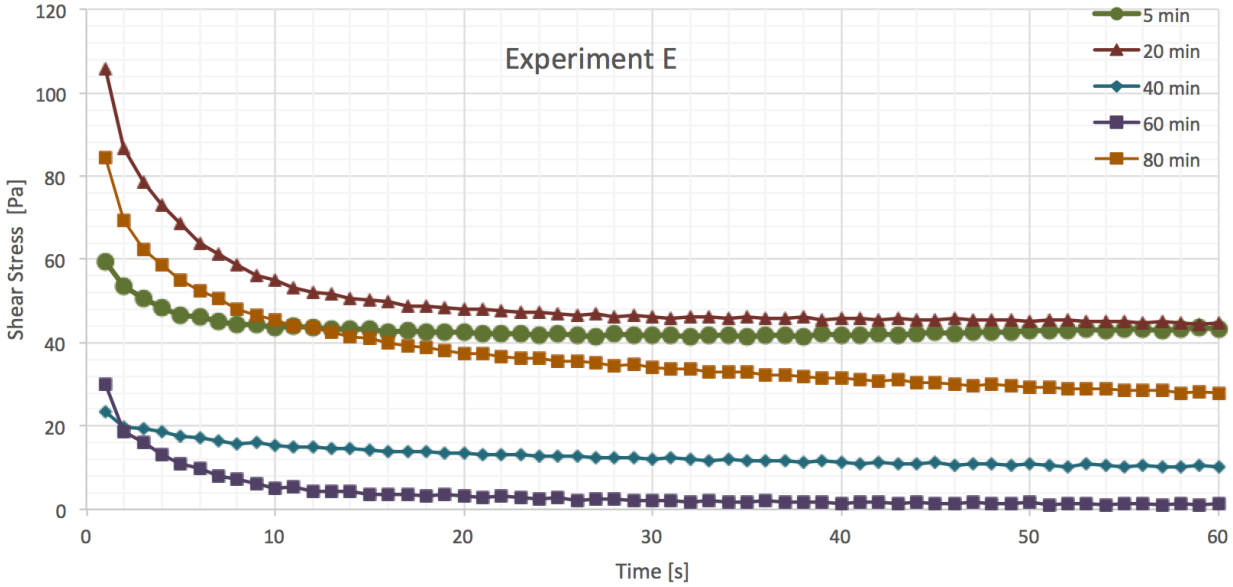

Fig. E.1. Shear stress for Experiment E.

Tab. E.1. Shear stress steady state for Experiment E.

time stamp	shear stress last four values				average	std dev
5	43.02	43.44	43.56	43.35	43.34	0.23
20	44.99	44.6	44.44	44.57	44.65	0.24
40	10.19	10.33	10.48	10.02	10.26	0.20
60	1.174	1.5	1.076	1.239	1.25	0.18
80	28.52	27.99	28.22	27.98	28.18	0.25

Applying the Bingham model to the obtained results for Experiment E we obtain the flow curves presented in Figure E.2. These curves represent the ratio between the shear stress measured in the rheometer at each time stamp by the shear rate measured in a set of curves, and by the shear rate computed using the Bingham model. Table E.2 presents the numerical values for the Bingham model computation.

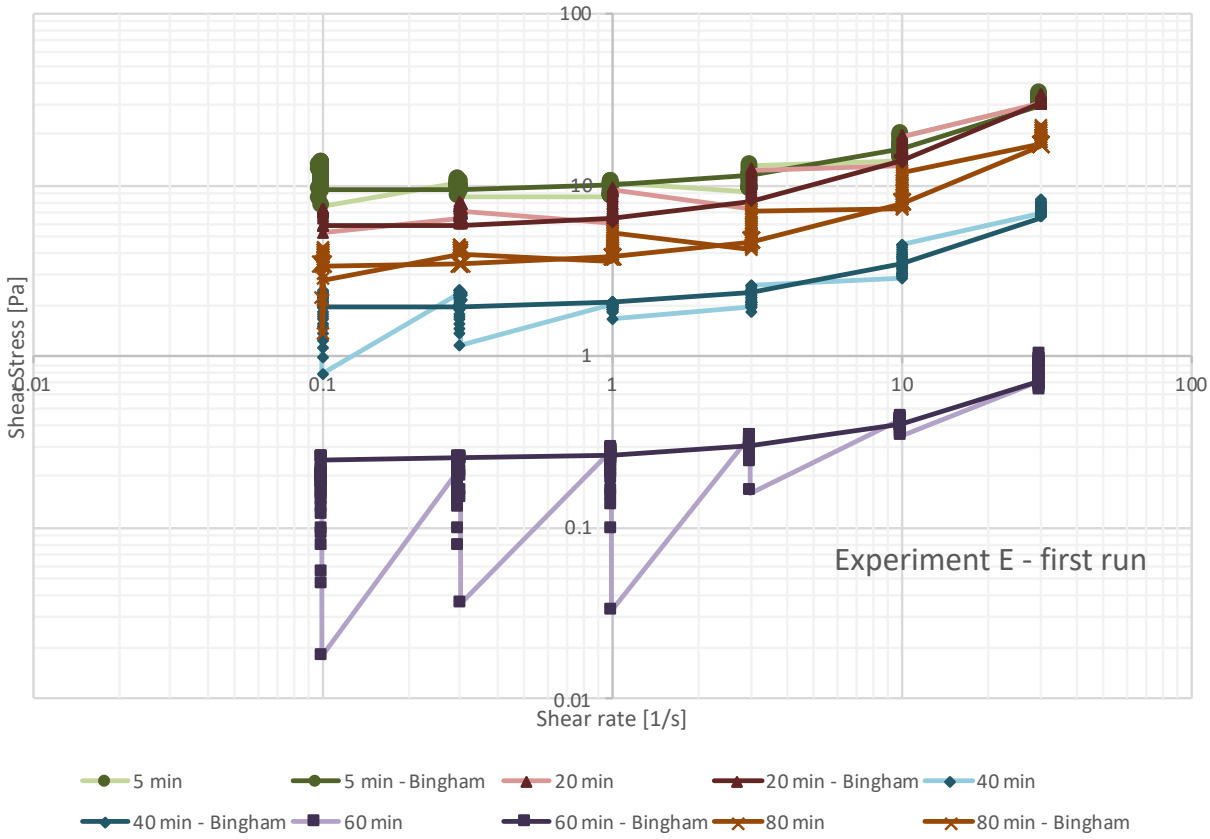

Fig. E.2. Flow curves (shear rate and shear stress ratio) for Experiment E.

Tab. E.2. Numerical values of Bingham model for Experiment E.

time stamp	dynamic yield stress (τ_0)	plastic viscosity (μ)
5	9.331	0.673
20	5.678	0.800
40	1.926	0.153
60	0.250	0.016
80	3.332	0.456

Carrying on the gathering of numerical results for Experiment E, Figure E.3 shows the viscosity versus the shear rate. Table E.3 presents the numeric values plotted in Figure E.3.

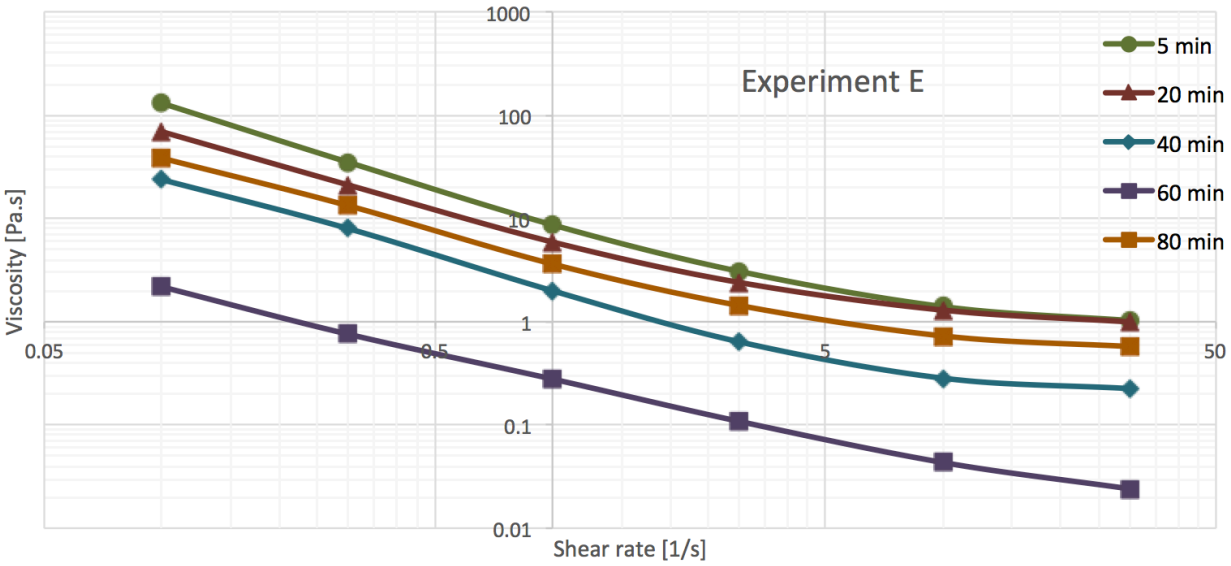

Fig. E.3. Viscosity over shear rate for Experiment E.

Tab. E.3. Viscosity over shear rate values for Experiment E.

Shear rate	5 min	20 min	40 min	60 min	80 min
30	1.019	0.996	0.225	0.024	0.571
10	1.401	1.295	0.284	0.042	0.721
3	3.081	2.406	0.640	0.114	1.395
1	8.684	5.922	1.997	0.279	3.625
0.3	35.080	21.130	7.990	0.758	13.310
0.1	130.900	69.300	23.790	2.176	38.430

In Figure E.4, it is presented the shear rate applied for almost eleven minutes (555 seconds) and the resulting viscosity at each time stamp for Experiment E. As expected, the viscosity increases as the shear rate drops for all time stamps. Table E.4 presents the numerical values shown in Figure E.4.

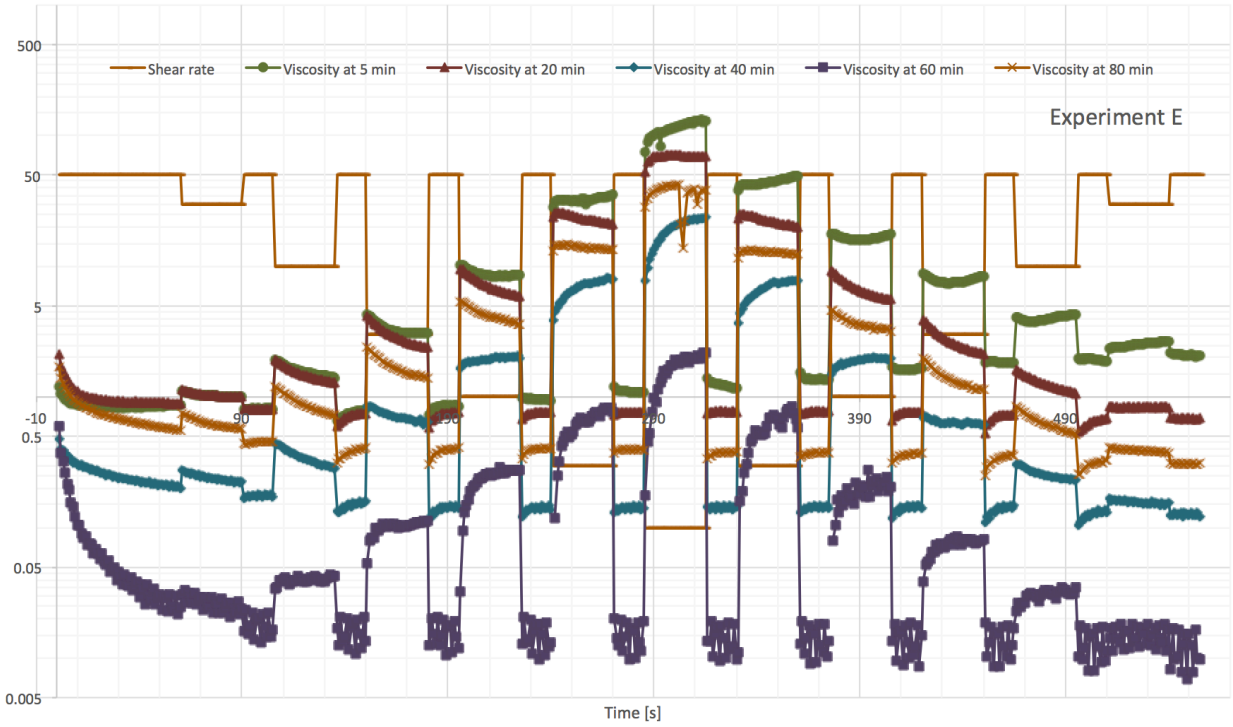

Fig. E.4. Shear rate and viscosity over time for Experiment E.

Tab. E.4. Shear rate and apparent viscosity over time values for Experiment E.

time	shear rate	shear stress 5 m.	app. visc. 5 m.	shear stress 20 m.	app. visc. 20 m.	shear stress 40 m.	app. visc. 40 m.	shear stress 60 m.	app. visc. 60 m.	shear stress 80 m.	app. visc. 80 m.
60	50.0	43.35	0.87	44.57	0.89	10.02	0.20	1.24	0.02	27.98	0.56
90	30.0	30.55	1.02	29.89	1.00	6.76	0.23	0.72	0.02	17.13	0.57
105	50.0	40.57	0.81	40.26	0.81	8.65	0.17	0.83	0.02	22.81	0.46
135	10.0	14.01	1.40	12.94	1.30	2.84	0.28	0.42	0.04	7.21	0.72
150	50.0	40.01	0.80	37.67	0.75	8.06	0.16	0.68	0.01	20.35	0.41
180	3.0	9.24	3.08	7.22	2.41	1.92	0.64	0.34	0.11	4.19	1.40
195	50.0	42.71	0.85	38.26	0.77	7.09	0.14	0.59	0.01	20.39	0.41
225	1.0	8.68	8.68	5.92	5.92	2.00	2.00	0.28	0.28	3.63	3.63
240	50.0	47.14	0.94	38.38	0.77	6.90	0.14	0.66	0.01	20.23	0.40
270	0.3	10.52	35.08	6.34	21.13	2.40	7.99	0.23	0.76	3.99	13.31
285	50.0	54.25	1.09	38.42	0.77	7.08	0.14	0.95	0.02	19.53	0.39
315	0.1	13.09	130.90	6.93	69.30	2.38	23.79	0.22	2.18	3.84	38.43
330	50.0	58.28	1.17	38.74	0.77	7.29	0.15	0.49	0.01	19.04	0.38

time	shear rate	shear stress 5 m.	app. visc. 5 m.	shear stress 20 m.	app. visc. 20 m.	shear stress 40 m.	app. visc. 40 m.	shear stress 60 m.	app. visc. 60 m.	shear stress 80 m.	app. visc. 80 m.
360	0.3	14.84	49.48	6.02	20.05	2.36	7.86	0.17	0.58	3.71	12.35
375	50.0	68.25	1.37	39.06	0.78	6.99	0.14	0.68	0.01	18.80	0.38
405	1.0	17.57	17.57	5.60	5.60	1.95	1.95	0.20	0.20	3.20	3.20
420	50.0	82.66	1.65	38.34	0.77	7.05	0.14	0.74	0.01	18.39	0.37
450	3.0	25.42	8.48	6.41	2.14	1.82	0.61	0.24	0.08	3.46	1.15
465	50.0	91.77	1.84	36.32	0.73	7.32	0.15	0.85	0.02	17.88	0.36
495	10.0	43.19	4.32	10.68	1.07	2.34	0.23	0.35	0.03	5.20	0.52
510	50.0	94.07	1.88	34.31	0.69	6.46	0.13	0.56	0.01	16.27	0.33
540	30.0	80.04	2.67	25.05	0.83	4.61	0.15	0.49	0.02	11.21	0.37
555	50.0	103.10	2.06	34.29	0.69	6.13	0.12	0.50	0.01	15.48	0.31

For Experiment E, the paste footprint was analyzed with density analysis only at the 20 mins time stamp. Therefore, it was executed an analysis of the density and degased density, and an analysis of water quantity at all time stamps (5 to 80 mins). Figure E.5 depicts the results of such analysis and Table E.5 shows the numerical values.

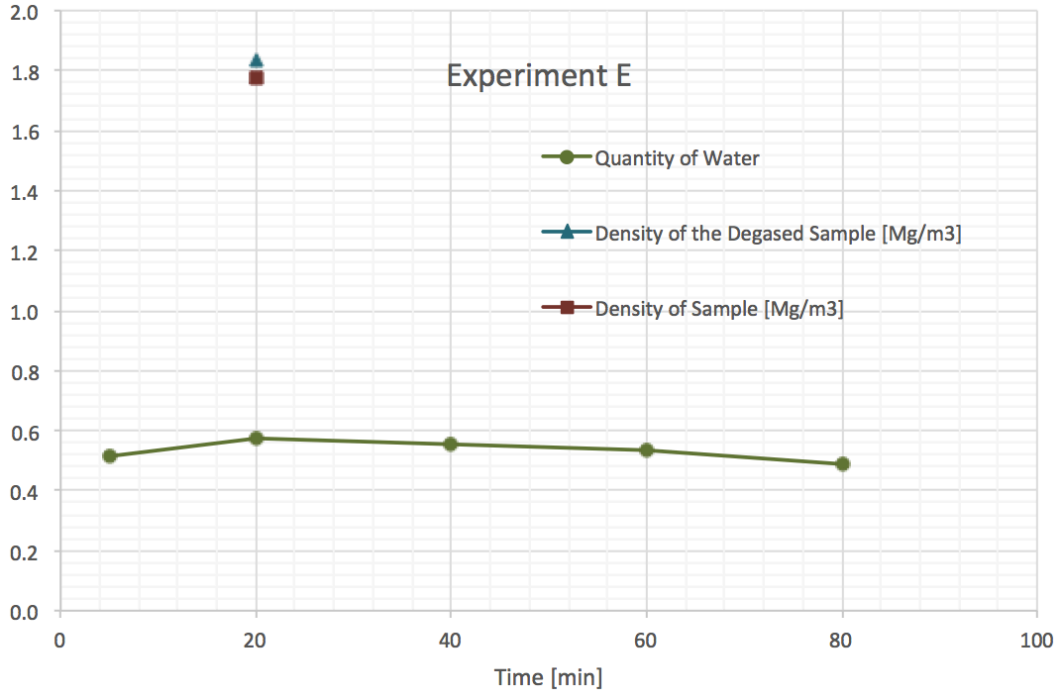

Fig. E.5. Paste footprint results for Experiment E.

Tab. E.5. Paste footprint values for Experiment E.

measure	5 min	20 min	40 min	60 min	80 min
Quantity of water %	52%	57%	55%	54%	48%
Density of Degased Sample [Mg/m3]		1.834			
Density Sample [Mg/m3]		1.779			

F. Annex - Numerical Results for Experiment F

This sixth annex presents the numerical results of Experiment F as described in Chapter 4. This experiment consists in the preservation method P4, shear strain sequence S3, time stamps of 5, 20, 40, 60, and 80 minutes, rheometer hood closed, and cement paste footprint F2, with density analysis at time stamp 20 and quantity of water for all time stamps.. As Experiments A and B, Experiment F was performed twice. Figure F.1 shows the shear stress curves obtained for the first 60 seconds after the shear strain sequence was started for both runs. Table F.1 presents the last four results to each curve, plus the average and the standard deviation.

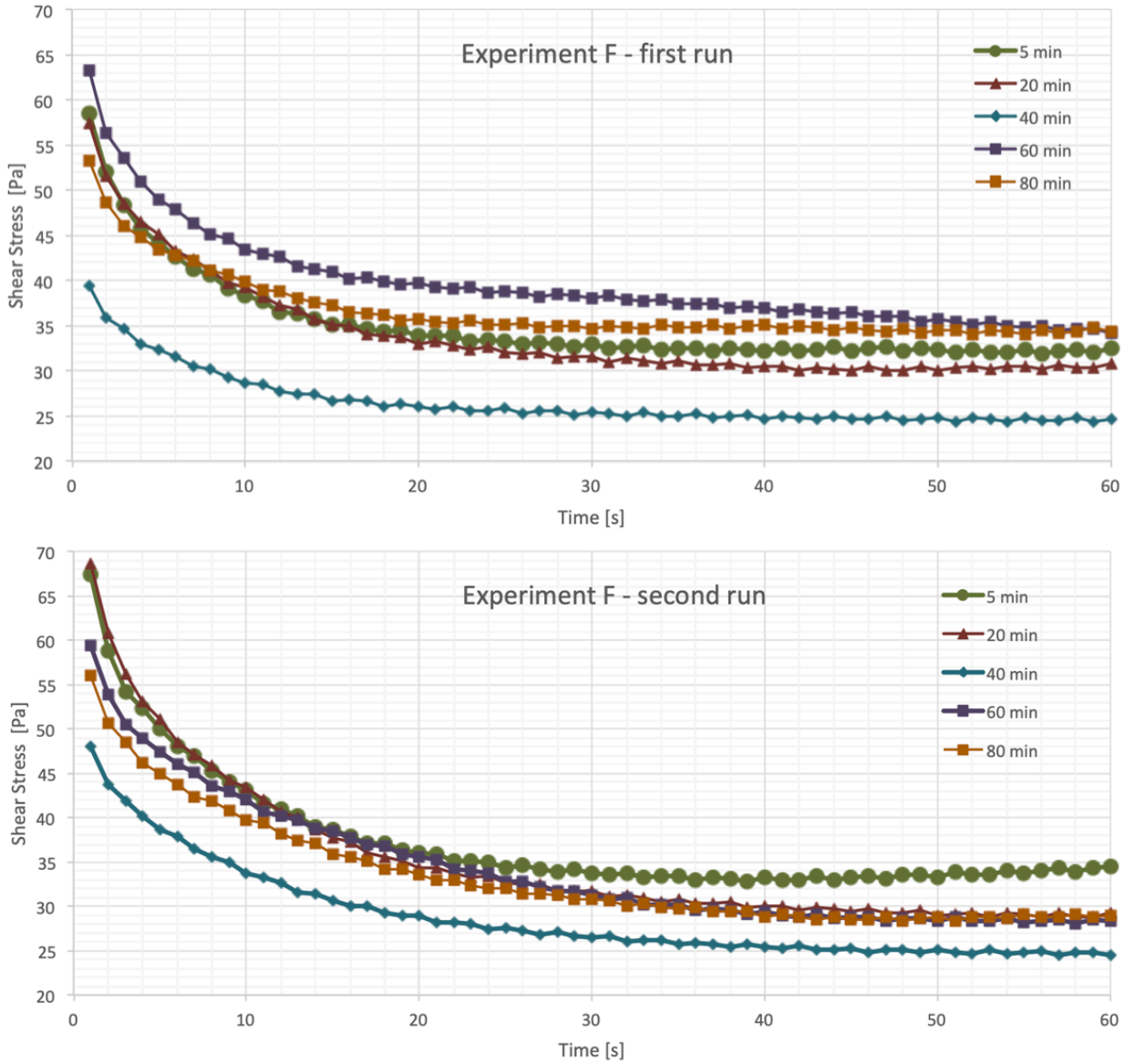

Fig. F.1. Shear stress for both runs of Experiment F.

Tab. F.1. Shear stress steady state for both runs of Experiment F.

run	time stamp	shear stress last four values				average	std dev
1st	5	32.21	32.36	31.99	32.44	32.25	0.20
	20	30.68	30.41	30.36	30.74	30.55	0.19
	40	24.48	24.81	24.39	24.59	24.57	0.18
	60	34.47	34.58	34.63	34.18	34.47	0.20
	80	34.24	34.31	34.73	34.34	34.41	0.22
2nd	5	34.31	33.94	34.41	34.43	34.27	0.23
	20	29.23	28.88	28.85	29.19	29.04	0.20
	40	24.49	24.83	24.77	24.46	24.64	0.19
	60	20.58	20.43	20.64	20.5	20.54	0.09
	80	21.76	21.93	21.75	21.94	21.85	0.10

Applying the Bingham model to the obtained results for experiment F we obtain the flow curves presented in Figure F.2. These curves represent the ratio between the shear stress measured in the rheometer at each time stamp by the shear rate measured in a set of curves, and by the shear rate computed using the Bingham model. Table F.2 presents the numerical values for the Bingham model computation.

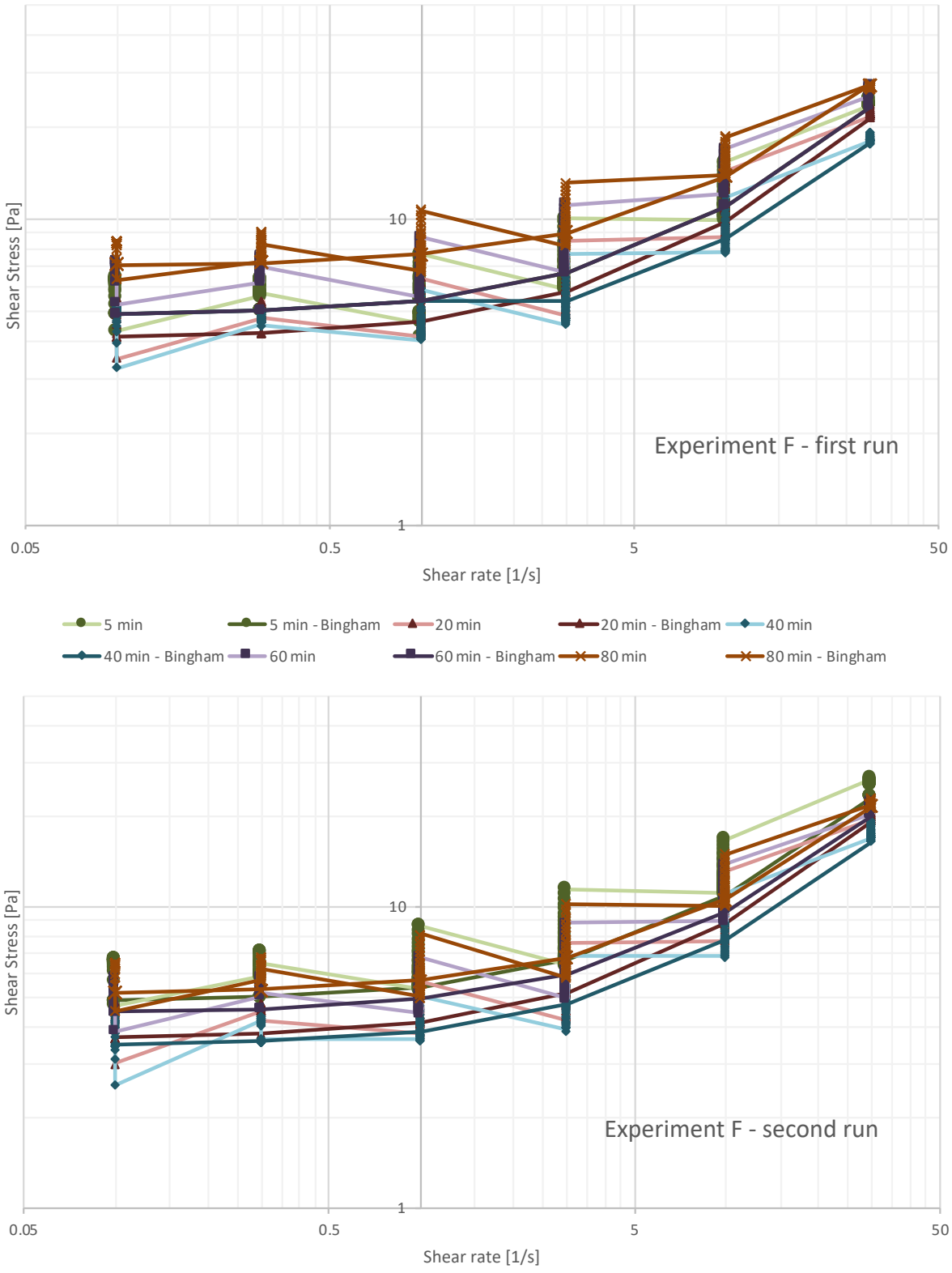

Fig. F.2. Flow curves (shear rate and shear stress ratio) for both runs of Experiment F.

Tab. F.2. Numerical values of Bingham model for both runs of Experiment F.

time stamp	1st run dynamic yield stress (τ_0)	2nd run dynamic yield stress (τ_0)	1st run plastic viscosity (μ)	2nd run plastic viscosity (μ)
5	4.826	5.173	0.616	0.698
20	4.056	3.627	0.580	0.521
40	4.005	3.439	0.456	0.439
60	5.757	4.431	0.641	0.526
80	7.006	5.149	0.679	0.549

Carrying on, Figure F.3 shows the viscosity versus the shear rate and Table F.3 presents the numeric values plotted in Figure F.3 for both runs of Experiment F.

Tab. F.3. Viscosity over shear rate values for both runs of Experiment F.

Shear rate	1st run 5 m.	2nd run 5 m.	1st run 20 m.	2nd run 20 m.	1st run 40 m.	2nd run 40 m.	1st run 60 m.	2nd run 60 m.	1st run 80 m.	2nd run 80 m.
30	0.790	0.885	0.726	0.653	0.602	0.567	0.840	0.684	0.919	0.732
10	0.993	1.108	0.876	0.770	0.779	0.685	1.203	0.895	1.386	1.012
3	1.952	2.121	1.615	1.405	1.508	1.296	2.222	1.650	2.722	1.946
1	4.561	5.330	4.154	3.801	4.037	3.666	5.590	4.426	6.752	5.033
0.3	18.700	19.620	15.900	14.910	15.240	13.890	20.620	16.840	24.330	19.040
0.1	64.560	66.250	54.910	47.730	51.160	44.710	71.110	57.620	84.260	64.190

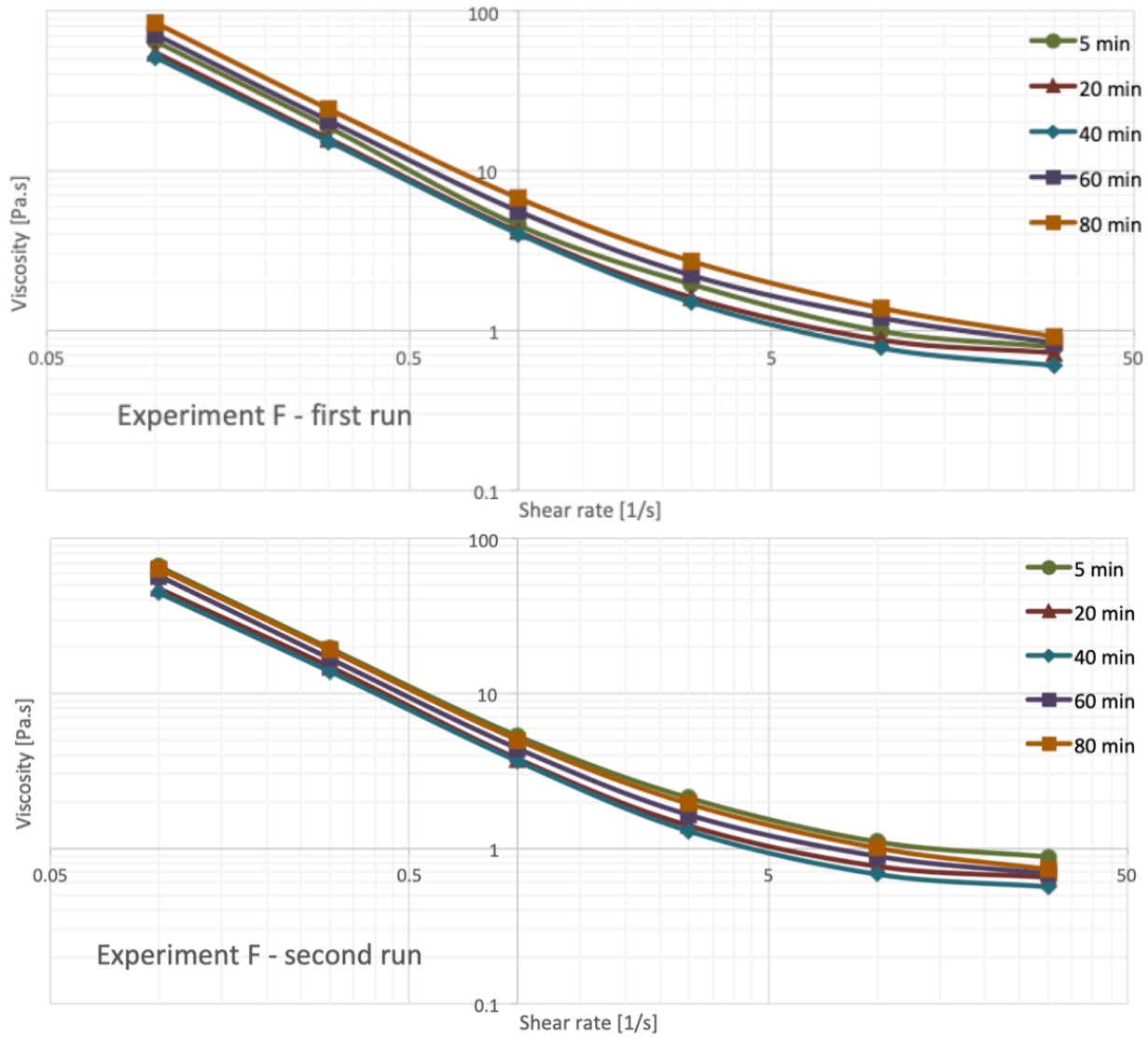

Fig. F.3. Viscosity over shear rate for both runs of Experiment F.

Figure F.4 presents the shear rate applied for almost eleven minutes (555 seconds) and the resulting viscosity at each time stamp for Experiment F. As expected, the viscosity increases as the shear rate drops for all time stamps. Tables F.4 presents the numerical values shown in Figure F.4 for the first and second runs.

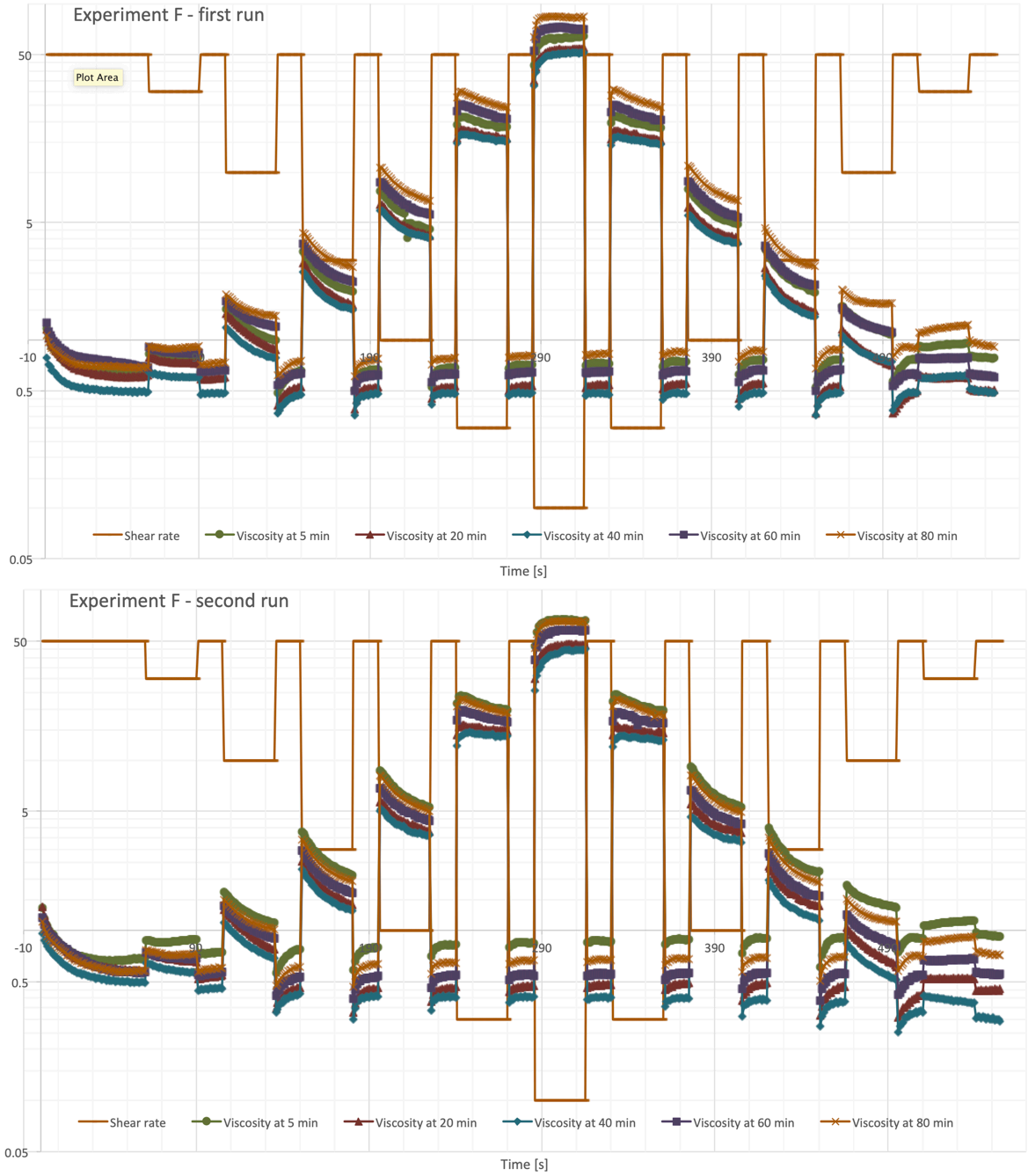

Fig. F.4. Shear rate and viscosity over time for both runs of Experiment F.

Tab. F.4. Shear rate and apparent viscosity over time values for both runs of Experiment F.

time (run)	shear rate	shear stress 5 m.	app. visc. 5 m.	shear stress 20 m.	app. visc. 20 m.	shear stress 40 m.	app. visc. 40 m.	shear stress 60 m.	app. visc. 60 m.	shear stress 80 m.	app. visc. 80 m.
60(1)	50.0	32.44	0.65	30.74	0.61	24.59	0.49	34.18	0.68	34.34	0.69
90(1)	30.0	23.70	0.79	21.78	0.73	18.04	0.60	25.18	0.84	27.56	0.92

time (run)	shear rate	shear stress 5 m.	app. visc. 5 m.	shear stress 20 m.	app. visc. 20 m.	shear stress 40 m.	app. visc. 40 m.	shear stress 60 m.	app. visc. 60 m.	shear stress 80 m.	app. visc. 80 m.
105(1)	50.0	33.59	0.67	30.10	0.60	24.12	0.48	32.97	0.66	36.51	0.73
135(1)	10.0	9.93	0.99	8.76	0.88	7.79	0.78	12.03	1.20	13.86	1.39
150(1)	50.0	32.83	0.66	26.33	0.53	23.53	0.47	31.73	0.63	37.72	0.75
180(1)	3.0	5.86	1.95	4.85	1.62	4.52	1.51	6.67	2.22	8.17	2.72
195(1)	50.0	33.54	0.67	26.27	0.53	23.78	0.48	30.90	0.62	38.47	0.77
225(1)	1.0	4.56	4.56	4.15	4.15	4.04	4.04	5.59	5.59	6.75	6.75
240(1)	50.0	34.41	0.69	26.51	0.53	23.89	0.48	31.21	0.62	39.03	0.78
270(1)	0.3	5.61	18.70	4.77	15.90	4.57	15.24	6.19	20.62	7.30	24.33
285(1)	50.0	35.54	0.71	26.65	0.53	24.15	0.48	32.12	0.64	40.31	0.81
315(1)	0.1	6.46	64.56	5.49	54.91	5.12	51.16	7.11	71.11	8.42	84.26
330(1)	50.0	35.98	0.72	26.94	0.54	23.70	0.47	32.59	0.65	41.52	0.83
360(1)	0.3	5.54	18.47	4.64	15.48	4.41	14.71	6.10	20.34	7.30	24.31
375(1)	50.0	37.21	0.74	27.61	0.55	24.04	0.48	32.61	0.65	41.90	0.84
405(1)	1.0	4.91	4.91	3.92	3.92	3.75	3.75	5.40	5.40	6.76	6.76
420(1)	50.0	37.96	0.76	27.53	0.55	24.23	0.48	32.91	0.66	42.68	0.85
450(1)	3.0	5.73	1.91	4.44	1.48	4.14	1.38	6.39	2.13	8.28	2.76
465(1)	50.0	38.22	0.76	26.27	0.53	24.39	0.49	33.25	0.67	43.90	0.88
495(1)	10.0	10.74	1.07	7.06	0.71	7.46	0.75	11.16	1.12	16.53	1.65
510(1)	50.0	38.28	0.77	24.91	0.50	24.39	0.49	31.01	0.62	44.30	0.89
540(1)	30.0	28.60	0.95	17.89	0.60	18.51	0.62	23.45	0.78	36.86	1.23
555(1)	50.0	39.19	0.78	25.14	0.50	24.19	0.48	30.06	0.60	45.69	0.91
60(2)	50.0	34.43	0.69	29.19	0.58	24.46	0.49	28.39	0.57	29.01	0.58
90(2)	30.0	26.54	0.88	19.58	0.65	17.01	0.57	20.50	0.68	21.94	0.73
105(2)	50.0	37.41	0.75	27.42	0.55	22.53	0.45	28.38	0.57	30.06	0.60
135(2)	10.0	11.08	1.11	7.70	0.77	6.85	0.68	8.95	0.90	10.12	1.01
150(2)	50.0	38.85	0.78	22.93	0.46	21.13	0.42	26.65	0.53	30.50	0.61
180(2)	3.0	6.36	2.12	4.22	1.41	3.89	1.30	4.95	1.65	5.84	1.95
195(2)	50.0	39.96	0.80	23.00	0.46	20.28	0.41	26.89	0.54	31.49	0.63
225(2)	1.0	5.33	5.33	3.80	3.80	3.67	3.67	4.43	4.43	5.03	5.03

time (run)	shear rate	shear stress 5 m.	app. visc. 5 m.	shear stress 20 m.	app. visc. 20 m.	shear stress 40 m.	app. visc. 40 m.	shear stress 60 m.	app. visc. 60 m.	shear stress 80 m.	app. visc. 80 m.
240(2)	50.0	41.15	0.82	23.26	0.47	20.06	0.40	27.22	0.54	32.24	0.65
270(2)	0.3	5.89	19.62	4.48	14.91	4.17	13.89	5.05	16.84	5.71	19.04
285(2)	50.0	41.80	0.84	23.51	0.47	20.33	0.41	27.07	0.54	33.22	0.66
315(2)	0.1	6.62	66.25	4.77	47.73	4.47	44.71	5.76	57.62	6.42	64.19
330(2)	50.0	43.17	0.86	24.04	0.48	20.12	0.40	27.80	0.56	33.27	0.67
360(2)	0.3	5.89	19.65	4.32	14.41	3.94	13.12	4.95	16.51	5.54	18.47
375(2)	50.0	44.02	0.88	24.64	0.49	19.71	0.39	27.93	0.56	33.98	0.68
405(2)	1.0	5.30	5.30	3.74	3.74	3.27	3.27	4.25	4.25	4.96	4.96
420(2)	50.0	44.63	0.89	24.43	0.49	19.39	0.39	27.95	0.56	34.47	0.69
450(2)	3.0	6.63	2.21	4.18	1.39	3.42	1.14	4.75	1.58	5.74	1.91
465(2)	50.0	45.07	0.90	23.30	0.47	19.10	0.38	27.68	0.55	34.87	0.70
495(2)	10.0	13.58	1.36	6.12	0.61	5.10	0.51	8.11	0.81	11.26	1.13
510(2)	50.0	44.76	0.90	21.35	0.43	16.50	0.33	27.40	0.55	34.95	0.70
540(2)	30.0	34.06	1.14	15.57	0.52	11.27	0.38	20.28	0.68	27.54	0.92
555(2)	50.0	46.28	0.93	22.68	0.45	14.63	0.29	27.58	0.55	35.50	0.71

For Experiment F, the paste footprint was analyzed with density analysis only at the 20 mins time stamp. Therefore, it was executed an analysis of the density and degased density, and an analysis of water quantity at all time stamps (5 to 80 mins). Figure F.5 depicts the results of such analysis and Table F.5 presents the numerical values observed.

Tab. F.5. Paste footprint values for both runs of Experiment F.

measure	1st run 5 m.	2nd run 5 m.	1st run 20 m.	2nd run 20 m.	1st run 40 m.	2nd run 40 m.	1st run 60 m.	2nd run 60 m.	1st run 80 m.	2nd run 80 m.
Quantity of water %	50%	50%	50%	50%	51%	51%	50%	50%	50%	51%
Density of Degased Sample [Mg/m3]			1.886	1.812						
Density Sample [Mg/m3]			1.796	1.784						

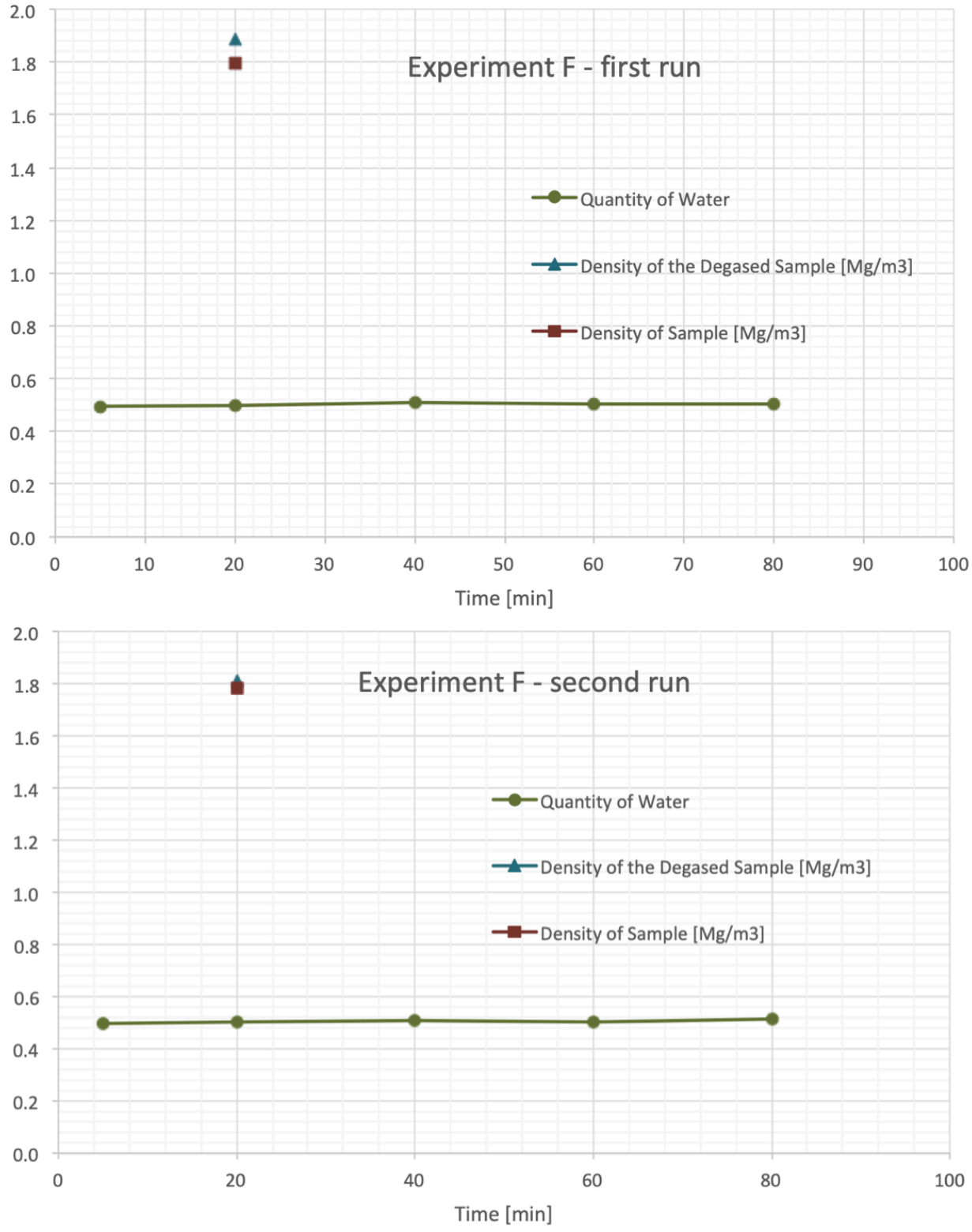

Fig. F.5. Paste footprint results for both runs of Experiment F.